REPUBLIQUE ALGERIENNE DEMOCRATIQUE ET POPULAIRE

MINISTERE DE L'ENSEIGNEMENT SUPERIEUR ET DE LA RECHERCHE SCIENTIFIQUE

UNIVERSITE YAHIA FARES DE MEDEA

FACULTE DE TECHNOLOGIE

THESE DE DOCTORAT

Présentée en vue de l'obtention du grade de DOCTEUR

Filière : Génie des Procédés

Spécialité : Génie des Procédés

Par : EULDJI Amel

THEME :

Modélisation des Comportements Physico-Chimiques et Rhéologiques des nano-fluides : Etude comparative

Soutenue publiquement devant le jury composé de :

ALI AGHA Hamza	MCA.	Université de Médéa	Président
LAIDI Maamar	Pr.	Université de Médéa	Encadrant
RAHAL Soufiane	MCA.	Université de Médéa	Examinateur
MOUSSAOUI Mohamed	MCA.	Université de Bouira	Examinateur
BENSEDIRA Sid Ali	MCA.	Université de Blida 1	Examinateur
DANOUNI Samir	MCA.	Université de Tipaza	Examinateur
HENTABLI Mohamed	MCB.	Université de Chlef	Invité

Année : 2024/2025

PEOPLE'S DEMOCRATIC REPUBLIC OF ALGERIA
MINISTRY OF HIGHER EDUCATION AND SCIENTIFIC RESEARCH
UNIVERSITY YAHIA FARES OF MEDEA



FACULTY OF TECHNOLOGY

DOCTORAL THESIS

To obtain the degree of DOCTOR

in: Process Engineering

Specialty: Process Engineering

Presented by: EULDJI Amel

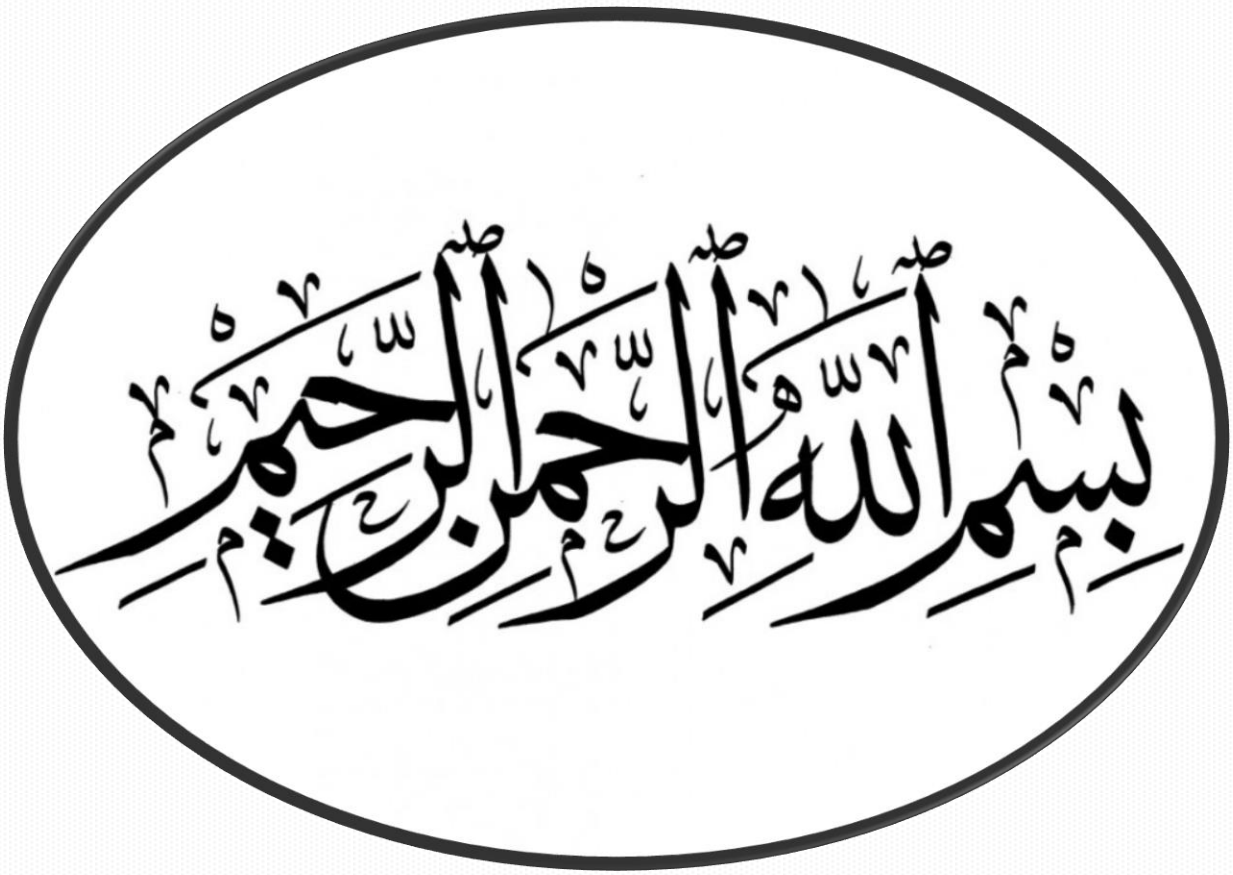
THESIS TITLE :

Modeling the Physico-Chemical and Rheological Behaviors of Nanofluids: A Comparative Study

Publicly defended before the jury composed of:

ALI AGHA Hamza	MCA.	University of Medea	President
LAIDI Maamar	Pr.	University of Medea	Supervisor
RAHAL Soufiane	MCA.	University of Medea	Examiner
MOUSSAOUI Mohamed	MCA.	University of Bouira	Examiner
BENSEDIRA Sid Ali	MCA.	University of Blida 1	Examiner
DANOUNI Samir	MCA.	University of Tipaza	Examiner
HENTABLI Mohamed	MCB.	University of Chlef	Guest

Année : 2024/2025


بسم الله الرحمن الرحيم

ACKNOWLEDGMENTS

First and foremost, I would like to express my heartfelt gratitude to ALLAH for granting me the courage and determination necessary to complete this research, which is vital for my intellectual and professional future.

I would like to take a moment to honor the memory of my parents, who passed away before seeing this chapter of my life come to fruition. Your encouragement and wisdom have been a constant source of inspiration, even in your absence. I wish you could be here to celebrate this achievement, but I know you are watching over me with pride.

I am deeply indebted to my thesis supervisor, Professor LAIDI Maamar, for his unwavering support during challenging times. His patience, insightful guidance, and valuable comments have been instrumental in shaping this work. Please accept my deepest respect and appreciation.

I would also like to extend my sincere thanks to Professor HANINI Salah for proposing this research topic, dedicating his time to mentoring me, and sharing his extensive knowledge about nanofluids. His contributions have greatly enriched my understanding of the subject. Please accept my heartfelt gratitude.

My profound thanks go to Mr. HENTABLI Mohamed, our guest of honor, for his invaluable support throughout my doctoral studies. His assistance, wise advice, and constant availability were essential pillars in the completion of this thesis.

I am honored by the presence of Mr. ALI AGHA Hamza and deeply grateful for his interest in this work by agreeing to chair the jury.

I also wish to express my gratitude to Mr. RAHAL Soufiane, Mr. MOUSSAOUI Mohamed, Mr. BENSEDIRA Sid Ali, and Mr. DANOUNI Samir for their valuable time and constructive feedback as members of the jury. Their critiques and suggestions will undoubtedly contribute to improving this work further.

Finally, I would be remiss not to thank all those who supported me throughout my studies, your encouragement and assistance have been invaluable in bringing this project to fruition.

DEDICATION

I dedicate this research to:

- The memory of my beloved parents. May Allah, the All-Merciful, grant them entry into His vast paradise.
- My dear fiancé Mustapha, whose love and support mean the world to me.
- My cherished brothers, Mohammed and Abderrahmane, and Nawel, my sister-in-law.
- My dear sister Touba, her husband Mounir, and my adorable nephew Karim.
- My friends and all those who hold a special place in my heart.

نمذجة السلوكيات الفيزيائية الكيميائية والانسيابية للموائع النانوية: دراسة مقارنة

تنقسم هذه الدراسة إلى مساهمتين:

تبحث المساهمة الأولى في الخصائص الحرارية والانسيابية للموائع النانوية الهجينة الثلاثية (THNFs) القائمة على الماء والمحتوية على جسيمات نانوية من $CuO-CaCO_3-SiO$، باستخدام نماذج انحدار متجه الدعم (SVR) المحسّنة باستخدام خوارزمية Dragonfly (DA) وخوارزمية FOX (FOA). استُخدمت بيانات تجريبية شملت درجات حرارة تتراوح بين 15 و60 درجة مئوية، وتركيزات حجمية لجسيمات نانوية تتراوح بين 0.1 و0.5 %، لتدريب النماذج والتحقق من صحتها. أظهر نموذج FOA-SVR أداءً تنبؤيًا متفوقًا، محققًا قيمة R^2 قدرها 0.9998 وخطأ جذر متوسط المربعات (RMSE) قدره 0.0044 للّزوجة الديناميكية، وقيمة R^2 قدرها 0.9997 وخطأ جذر متوسط مربعات (RMSE) قدره 0.0019 للتوصيل الحراري. أكدت النتائج المقارنة مع نموذج DA-SVR مع تقنيات التحقق المتبادل، بما في ذلك Holdout وLeave-M-Out، متانة هذا النموذج. تسلط النتائج الضوء على إمكانات التعلم الآلي في تحسين تركيبات الموائع النانوية، مع تطبيقات في أنظمة الإدارة الحرارية المتقدمة.

أما الدراسة الثانية، فتستخدم نموذج انحدار متجه الدعم محسن بخوارزمية Dragonfly (SVR-DA) للتنبؤ بإنتاجية المياه في جهاز تقطير شمسي أحادي المنحدر قائم على الموائع النانوية. باستخدام 251 نقطة بيانات تجريبية، تم تحليل معلمات رئيسية مثل الإشعاع الشمسي، درجات الحرارة المحيطة، درجات حرارة الحوض، عمق الماء وخصائص الجسيمات النانوية. حقق النموذج دقة تنبؤية عالية، حيث بلغت قيمة R^2 0.9999 للتدريب و0.9958 للاختبار، أما بالنسبة لـ RMSE فبلغت القيمتان 1.8987 و8.5100 على التوالي. عزز دمج السوائل النانوية الأداء الحراري، حيث زادت من إنتاجية السائل النانوي المركّب من Al_2O_3 والماء بنسبة 14.22% مقارنةً بأجهزة التقطير الشمسية التقليدية. أكد تحليل البقايا عدم وجود تحيز في التنبؤات، بينما أظهر تحليل التباين (ANOVA) (القيمة الاحتمالية = 0.7937) موثوقية إحصائية. يقدم نموذج SVR-DA المحسّن أداة فعّالة لتحسين كفاءة تحلية المياه بالطاقة الشمسية. تشير النتائج إلى إمكانات التعلم الآلي في تحسين تنقية المياه باستخدام الطاقة المتجددة. تُسهم الدراسة في الإدارة المستدامة للمياه في المناطق القاحلة، مع خطط مستقبلية لتوسيع نطاق التحقق واستكشاف تقنيات تحسين إضافية.

الكلمات المفتاحية: موائع نانوية هجينة ثلاثية، التوصيل الحراري، انحدار متجه الدعم، خوارزمية تحسين FOX، التعلم الآلي، خوارزمية Dragonfly، تحسين تحلية المياه بالطاقة الشمسية.

RÉSUMÉ

Modélisation des Comportements Physico-Chimiques et Rhéologiques des Nanofluides : Etude Comparative

Cette étude se divise en deux contributions :

La première examine les propriétés thermiques et rhéologiques de nanofluides tri-hybrides aqueux à base de CuO-$CaCO_3$-SiO_2 (THNFs) à l'aide de modèles de régression à vecteurs de support (SVR) optimisés par l'algorithme Dragonfly (DA) et l'algorithme d'optimisation FOX (FOA). Des données expérimentales couvrant des températures de 15 à 60 °C et des concentrations de nanoparticules de 0.1 à 0.5 % en volume, ont été utilisées pour entraîner et valider les modèles. Le modèle FOA-SVR a démontré des performances prédictives supérieures, atteignant une valeur R^2 de 0.9998 et une erreur quadratique moyenne (RMSE) de 0.0044 pour la viscosité dynamique, et une valeur R^2 de 0.9997 avec une RMSE de 0.0019 pour la conductivité thermique. Des résultats comparatifs avec les techniques DA-SVR et de validation croisée, notamment Holdout et Leave-M-Out, ont confirmé la robustesse du modèle FOA-SVR. Ces résultats soulignent le potentiel de l'apprentissage automatique pour l'optimisation des formulations de nanofluides, avec des applications dans les systèmes de gestion thermique avancés.

Dans sa deuxième étude, un modèle de régression à vecteurs de support optimisé par l'algorithme Dragonfly (SVR-DA) est utilisé pour prédire la productivité en eau d'un distillateur solaire à simple pente utilisant des nanofluides. Sur la base de 251 points de données expérimentales, des paramètres clés tels que le rayonnement solaire, les températures, ambiante et du bassin, la profondeur de l'eau et les propriétés des nanoparticules ont été analysés. Le modèle a atteint une précision élevée prédictive avec un R^2 de 0.9999 pour l'apprentissage et de 0.9958 pour les tests, ainsi qu'un RMSE de 1.8987 et 8.5100, respectivement. L'intégration de nanofluides à base d'Al_2O_3/eau a amélioré la performance thermique, augmentant la productivité de 14,22 % par rapport aux distillateurs solaires conventionnels. L'analyse résiduelle a confirmé l'absence de biais dans les prédictions, tandis que la validation ANOVA (valeur p = 0.7937) a démontré la fiabilité statistique. Le modèle SVR-DA optimisé offre un outil robuste pour améliorer l'efficacité de la désalinisation solaire. Les résultats suggèrent le potentiel de l'apprentissage automatique pour optimiser la purification de l'eau basée sur les énergies renouvelables. L'étude contribue à la gestion durable de l'eau dans les régions arides. Les travaux futurs viseront à étendre la validation et à explorer des techniques d'optimisation supplémentaires.

Mots-clés : Nanofluides trihybrides, Conductivité thermique, Régression par vecteurs de support, Algorithme d'optimisation FOX, Apprentissage automatique, Algorithme Dragonfly, Optimisation de la désalinisation solaire.

Modeling the Physico-Chemical and Rheological Behaviors of Nanofluids: A Comparative Study

This study is divided into two contributions:

The first one investigates the thermal and rheological properties of water-based CuO-$CaCO_3$-SiO_2 tri-hybrid nanofluids (THNFs) using Support Vector Regression (SVR) models optimized with the Dragonfly Algorithm (DA) and the FOX Optimization Algorithm (FOA). Experimental data covering temperatures from 15 to 60 °C and nanoparticle concentrations of 0.1–0.5 vol% were used to train and validate the models. The FOA-SVR model demonstrated superior predictive performance, achieving an R^2 value of 0.9998 and a root mean square error (RMSE) of 0.0044 for dynamic viscosity, and an R^2 of 0.9997 with an RMSE of 0.0019 for thermal conductivity. Comparative results with DA-SVR and cross-validation techniques, including Holdout and Leave-M-Out, confirmed the robustness of the FOA-SVR model. The findings highlight the potential of machine learning for optimizing nanofluid formulations, with applications in advanced thermal management systems.

The second one, his study employs a Dragonfly Algorithm-optimized Support Vector Regression (SVR-DA) model to predict the water productivity of a nanofluid-based single-slope solar still. Using 251 experimental data points, key parameters such as solar radiation, ambient and basin temperatures, water depth, and nanoparticle properties were analyzed. The model achieved high predictive accuracy with an R^2 of 0.9999 for training and 0.9958 for testing, and an RMSE of 1.8987 and 8.5100, respectively. The integration of nanofluids enhanced thermal performance, with Al_2O_3-water nanofluid increasing productivity by 14.22% over conventional solar stills. Residual analysis confirmed unbiased predictions, while ANOVA validation (p-value = 0.7937) demonstrated statistical reliability. The optimized SVR-DA model provides a robust tool for improving solar desalination efficiency. Findings suggest the potential for machine learning in optimizing renewable energy-based water purification. The study contributes to sustainable water management in arid regions. Future work will extend validation and explore additional optimization techniques.

Keywords: Trihybrid nanofluids, Thermal conductivity, Support Vector Regression, FOX Optimization Algorithm, Machine learning, Dragonfly Algorithm, Solar desalination optimization.

AARD	Average Absolute Relative Deviation
AI	Artificial Intelligence
ANFIS	Adaptive Network-based Fuzzy Inference System
ANN	Artificial Neural Network
ANOVA	ANalysis Of VAriance
b	Intercept of the regression function
C	penalty parameter
CFD	Computational Fluid Dynamics
CNNs	Convolutional Neural Networks
CNTs	Carbon NanoTubes
Cp	Heat capacity
CSS	Conventional Solar Stills
CVD	Chemical Vapor Deposition
DA	Dragonfly Algorithm
DBSCAN	Density-Based Spatial Clustering of Applications with Noise
DL	Deep Learning
DQNs	Deep Q-Networks
DW	Distilled Water
EG	Ethylene Glycol
F	Ficher test statistics
f	Fluid
FOA	Fox Optimization Algorithm
H_CV	Holdout Cross-Validation
H_0	Null hypothesis

HSS	Hemispherical Solar Stills
IQR	InterQuartile Range
K	kernel function
k	Thermal conductivity
KDE	Kernel Density Estimate
LMO_CV	Leave-M-Out Cross-Validation
MAE	Mean Absolute Error
ML	Machine Learning
MRPE	Mean Relative Percentage Error
MSE	Mean Square Error
NF	NanoFluid
NLP	Natural Language Processing
PCA	Principal Component Analysis
PINNs	Physics-Informed Neural Networks
PSO	Particle Swarm Optimization
PTC	Parabolic Trough Collectors
PVD	Physical Vapor Deposition
PVT	PhotoVoltaic Thermal
R	Correlation coefficient
R^2	Determination coefficient
RBF	Gaussian Radial Basis kernel Function
RL	Reinforcement Learning
RMSE	Root Mean Square Error
RNNs	Recurrent Neural Networks

RSD	Relative Standard Deviation
S	Solid
SSs	Solar Stills
Std	Standard Deviation
SVM	Support Vector Machines
SVR	Support Vector Regression
T	temperature
TEM	Transmission Electron Microscopy
THNFs	Ternary Hybrid NanoFluids
t-SNE	t-distributed Stochastic Neighbor Embedding
VR	Volume Ratio
α	Significance level
$\boldsymbol{\alpha_i}$	Lagrange multipliers
$\boldsymbol{\alpha_i^*}$	Optimal desired weight vector
ε	Insensitive parameter
λ	Weight vector
$\boldsymbol{\mu}$	Dynamic viscosity
$\boldsymbol{\xi}$	Deviation of training samples outside ε-insensitive zone
ρ	Density
σ	Kernel parameter
φ	Volume fraction

Acknowledgments

Dedication

ملخص/Résumé/Abstract

Glossary

Index

List of figures

List of tables

GENERAL INTRODUCTION

1. Background to the study 01

2. Objectives of the thesis and organization of the manuscript 02

PART I. THEORITICAL FRAMEWORK

CHAPTER I: OVERVIEW OF NANOFLUIDS

1. Introduction 06

2. Types of Nanofluids 07

3. Properties of nanofluids 09

3.1. Volume Fraction 10

3.2. Density 10

3.3. Thermal Conductivity 10

3.4. Viscosity 14

3.5. Specific Heat 16

3.6. Colloidal Stability 16

4. Preparation of mono nanofluids 17

4.1. One-step method 17

4.2. Two-Step Method 18

5. Applications of Nanofluids 21
6. Advantages of nanofluids 24
7. Disadvantages of nanofluids 24
8. Environmental impacts of nanofluids 24
9. Conclusions 25

CHAPTER II. OVERVIEW OF MACHINE LEARNING

1. Introduction 28
2. Real-world applications of ML 30
3. Types of machine learning 32
   3.1. Supervised Learning 32
   3.2. Unsupervised Learning 33
   3.3. Semi-supervised learning 34
   3.4. Reinforcement Learning 34
4. Popular Machine Learning Algorithms 36
5. Support vector machine 37
6. Machine Learning Workflow 40
7. Overfitting and Underfitting 40
8. Tools for Machine Learning 41
9. Conclusions 41

PART II. MODELING PART

CHAPITRE III. CONTRIBUTION 01

FOX-Inspired Optimizer with Support Vector Regression Modelling of Water-Based $CaCO_3$-CuO-SiO_2 Trihybrid Nanofluids Thermal Properties: Comparative Study

1. Introduction 44

2. Methodology 44
2.1. Data description 44
2.2. Multicollinearity analysis 47
2.3. Integration of metaheuristic algorithms with support vector regression for predicting thermophysical properties 48
2.4. Cross-Validation Approach 51
A. Holdout Cross-Validation 51
B. Leave-M-Out Cross-Validation 51
C. Evaluation criteria 52
3. Results and Discussion 52
3.1. Dynamic Viscosity Model result 53
3.2. Thermal Conductivity Model result 55
3.3. Leave-M-Out Cross-Validation (LMO_CV) and Holdout Cross-Validation (H_CV): comparative Results 56
3.4. Comparison between FOA-SVR and DA-SVR models 57
4. Comparison with previously published models 61
5. Conclusion 62

CHAPITRE IV. CONTRIBUTION 02

Using Support vector machine optimized with Dragonfly Algorithm to predict water productivity of a nanofluid-based single-slope solar still

1. Introduction 65
2. Experimental setup and procedure 67
3. Data collection 69
4. Statistical description of the dataset 69
5. Dragonfly Algorithm Optimization 72

6. DA-SVM model training 73
7. Model evaluation and performance 73
8. Residual Error distribution Analysis for the DA-SVMr Model 75
9. Statistical Validation Using One-Way ANOVA 76
10. Comparative Analysis with Related Studies 77
11. Conclusions 79

GENERAL CONCLUSION

1. Conclusions of the thesis 83
2. Perspectives & Recommendations 85

PART I : THEORITICAL FRAMEWORK

CHAPTER I : OVERVIEW OF NANOFLUIDS

1	Displays the year-wise publication records on various areas of nanofluids, sourced from the Web of Science.	7
2	TEM image illustrating the morphology of TiO_2 nanoparticles in various shapes.	7
3	Illustrates a) The factors influencing the effectiveness of nanofluids, and b) The thermal conductivity values of various materials used in nanofluids, including base fluids like water and nanofluids containing materials such as carbon or aluminum.	11
4	Illustrates the comparison of thermal conductivity between commonly used liquids and solids	11
5	Factors influencing the effective thermal conductivity of nanofluids.	12
6	Composition of ternary hybrid nanofluid.	13
7	Factors influencing the viscosity of nanofluids.	15
8	Zeta Potential and Colloidal Stability.	17
9	Illustrates a schematic representation of the one-step process used for the preparation of nanofluids.	18
10	Illustrates a schematic representation of the two-step process for preparing nanofluids.	19
11	Illustrates nanofluid preparation techniques: (a) the one-step method and (b) the two-step method.	19
12	Displays: (a) the one-step method, (b) the advantages and disadvantages of the one-step method, (c) the two-step method, and (d) the advantages and disadvantages of the two-step method	20
13	Highlights some fundamental applications of nanofluids.	22
14	General applications of nanofluids.	22

15	Diagrammatic representation of the solar desalination system.	23
16	Environmental impacts of nanofluids.	25

CHAPTER II. OVERVIEW OF MACHINE LEARNING

1	Practical Applications of Machine Learning [1], a) Speech recognition and processing. b) Facial recognition technology, c) Predicting the three-dimensional structures of proteins. d) Cancer classification using DNA microarray analysis.	30
2	Evolution of Machine Learning Publications Over Time. a) Trends in the number of machine learning-related articles published over time; b) estimated relative percentages of these publications as of 2020.	31
3	Illustration of Supervised Learning.	32
4	Supervised Learning approach	33
5	Unsupervised Learning approach	33
6	Illustration of the Semi-supervised Learning Approach	34
7	Overview of the Reinforcement Learning Framework.	35
8	Machine Learning Popularity Index.	35
9	Classification of machine learning algorithms.	36
10	Types of Machine Learning	36
11	Nonlinear SVR with Vapnik's ε-insensitive loss function	38
12	Network architecture of SVM.	39
13	Machine Learning Workflow.	40
14	Overfitting & underfitting in machine learning	41

PART II. MODELING PART

CHAPTER III. CONTRIBUTION 01

FOX-Inspired Optimizer with Support Vector Regression Modelling of Water-Based $CaCO_3$-CuO-SiO_2 Trihybrid Nanofluids Thermal Properties: Comparative Study

1	Violin plots illustrating the distribution of the experimental dataset.	46
2	Correlation matrix showing the multicollinearity analysis among the key parameters of the dataset.	47
3	Five main factors controlling dragonflies' behavior.	49
4	Integration of Dragonfly Algorithm with SVM for Regression Optimization.	49
5	Red Fox hunting behavior: exploration and exploitation.	50
6	Integration DA and FOA with SVR.	50
7	Kernel Density Estimate (KDE) plots (a: thermal conductivity, b: dynamic viscosity).	56
8	Regression plot showing the predicted versus actual values of dynamic viscosity for the test dataset and the entire dataset using the FOA-SVR-LMO_CV model.	58
9	Regression plot showing the predicted versus actual values of the thermal conductivity for the test dataset and the entire dataset using the FOA-SVR-LMO_CV model.	59
10	Kernel Density Estimate (KDE) plot of the residuals for dynamic viscosity predictions ($mPa.s^{-1}$) using the FOA-SVR-LMO_CV model.	60
11	Kernel Density Estimate (KDE) plot of the residual values between the predicted and actual thermal conductivity using the FOA-SVR-LMO_CV model.	61

CHAPITRE IV. CONTRIBUTION 02

Using Support vector machine optimized with Dragonfly Algorithm to predict water productivity of a nanofluid-based single-slope solar still

1	The number of research papers published between 2011 and 2020 according Google Scholar search containing the terms "solar still" and "nanofluid".	66
2	Experimental setup of single slope solar still.	68
3	(a) Diagram illustrating the operation of a solar water desalination system, and (b) schematic representation of a solar still integrated with a heat exchanger.	68
4	Visualization using violin plots to represent the distribution of various experimental parameters influencing the performance of a solar still.	72
5	Comparison of Experimental and Predicted Productivity with Linear Fit Analysis	74
6	(a) Residual error distribution, (b) Normal distribution residual error.	76

PART I. THEORITICAL FRAMEWORK

CHAPTER I. OVERVIEW OF NANOFLUIDS

1	Some theoretical models for binary hybrid nanofluid.	12
2	An example of numerical values for base water and ternary hybrid nanoparticles.	12
3	Thermal properties calculation models for ternary hybrid nanofluids.	14
4	Conventional models for viscosity of nanofluids calculation	14
5	Viscosity of various common liquids at a temperature of 30°C.	15
6	Presents the theoretical models for hybrid nanofluids.	16
7	Thermal conductivity of nanoparticles and base fluids used in the nanofluids.	21

PART II. MODELING PART

CHAPTER III. CONTRIBUTION 01

FOX-Inspired Optimizer with Support Vector Regression Modelling of Water-Based $CaCO_3$-CuO-SiO_2 Trihybrid Nanofluids Thermal Properties: Comparative Study

1	Summary of data extracted from previous experimental study on aqueous trihybrid nanofluids with SDS as Surfactant at various parameters.	44
2	Statistical analysis data.	45
3	Hyperparameters results	53
4	Evaluation of statistical metrics and uncertainty for DA-SVR and FOA-SVR models using global data	54
5	Comparison of the Predictive Accuracy of the Developed DA-SVR Model for THNFs with Previously Published Models.	62

CHAPITRE IV. CONTRIBUTION 02

Using Support vector machine optimized with Dragonfly Algorithm to predict water productivity of a nanofluid-based single-slope solar still

1	Statistical analysis data	70
2	Optimization Parameters for DA-SVMr Model	73
3	Statistical metrics for training, testing, and combined data sets in solar still productivity analysis	75
4	One-way ANOVA test between the actual and predicted values.	77
5	Performance comparison of DA-SVMr model and recent modeling studies for solar still productivity prediction.	79

GENERAL INTRODUCTION

Nanofluids represent an innovative advancement in materials science and engineering, offering enhanced thermal and physical properties that have captured significant attention in recent years. These engineered fluids are created by dispersing nanometer-sized particles, typically ranging from 1 to 100 nanometers, into base fluids such as water, oil, or ethylene glycol. The concept of nanofluids, introduced in the mid-1990s by Choi [1,2], was developed to address the limitations of traditional heat transfer fluids in meeting the growing demands of modern industrial and technological systems.

By incorporating nanoparticles, nanofluids exhibit significantly enhanced thermal properties, enabling more efficient heat dissipation and temperature regulation [3]. This makes them particularly valuable in industries such as energy [4,5], electronics cooling [6,7], automotive [8,9], aerospace [10,11], and biomedical engineering [12,13]. Beyond their thermal advantages [14], nanofluids demonstrate unique rheological [15], optical [16], and magnetic properties [17]. These characteristics can be tailored by adjusting the type [18,19], size [20], concentration [21], and surface properties [22] of the nanoparticles, opening up new possibilities for innovation in fields such as solar energy harvesting [23], drug delivery [24], and advanced manufacturing [25].

An innovative advancement in nanofluid technology is the development of hybrid nanofluids. These fluids incorporate composite nanoparticles or two different types of nanoparticles in the base fluid, resulting in exceptional physicochemical characteristics that surpass those of single-component nanofluids [26]. Hybrid nanofluids have shown promising results in photovoltaic thermal (PVT) systems [27], solar collectors [28], and energy storage applications [29]. The synergistic effects arising from the interaction between different types of nanoparticles contribute to the remarkable performance of hybrid nanofluids.

In the field of solar desalination, nanofluids have shown remarkable potential for improving the efficiency of solar stills. The integration of nanofluids in solar stills has demonstrated several key benefits, including enhanced thermal properties, increased evaporation rates, and improved overall thermal efficiency. Studies have shown significant improvements in freshwater production, with some nanofluid-enhanced solar stills achieving productivity increases of up to 57.9% compared to conventional systems [30].

The application of machine learning (ML) and deep learning (DL) methods in modeling and predicting the properties of nanofluids has emerged as a transformative approach in materials science and engineering [31,32]. These techniques, combined with advanced optimization algorithms, offer a powerful framework for exploring the vast design space of nanofluids more efficiently [33]. Recent studies have employed computational intelligence and

machine learning techniques to optimize complex nanofluid systems, such as ternary hybrid nanofluids, aiming to maximize thermal conductivity while minimizing viscosity by adjusting various parameters like volume fractions, temperatures, and mixing ratios [34].

This research addresses a significant gap in the field by utilizing advanced machine-learning techniques, specifically Support Vector Regression (SVR) optimized with the Dragonfly Algorithm (DA) and the Fox Optimization Algorithm (FOA), to model the thermophysical properties of trihybrid nanofluids. The Dragonfly Algorithm, inspired by the static and dynamic swarming behaviors of dragonflies in nature, has shown excellent performance in solving optimization problems [35]. Similarly, the Fox Optimization Algorithm, which mimics the intelligent hunting behavior of foxes, has demonstrated effectiveness in various optimization tasks [36]. By combining these nature-inspired optimization techniques with SVR, researchers can create more robust and accurate predictive models for nanofluid properties.

The integration of these advanced algorithms allows for the efficient handling of non-linear relationships and provides more accurate predictions compared to traditional models. This approach not only enhances the understanding of complex nanofluid systems but also lays the groundwork for their practical application in advanced thermal systems, such as solar collectors [37] and heat exchangers [38], where enhanced heat transfer efficiency is crucial. Furthermore, the use of these optimization algorithms can significantly improve the efficiency and accuracy of predictive models, making them more reliable for industrial applications and accelerating the development of novel nanofluids with tailored properties for specific use cases [39].

Building upon the introduction to nanofluids and their applications, it's important to outline the structure of this thesis, which delves deeper into the intersection of nanofluids, artificial intelligence, and solar desalination technologies. The thesis is organized into four main chapters, each focusing on a critical aspect of this interdisciplinary research:

The first chapter provides a comprehensive overview of nanofluids, exploring their fundamental properties, synthesis methods, and applications across various industries. This chapter lays the foundation for understanding the unique characteristics of nanofluids that make them particularly valuable in heat transfer applications, including their enhanced thermal conductivity and the challenges associated with their development and implementation.

The second chapter provides a comprehensive overview of machine learning (ML) and its applications. It covers the history of ML, types of algorithms, popular techniques like Support Vector Machines, and the ML workflow. The chapter highlights the tools commonly

used in ML, emphasizing how these computational methods can accelerate innovation in materials science and fluid dynamics.

The third chapter presents a comparative study on modeling trihybrid nanofluids using Support Vector Regression (SVR) optimized with both the Dragonfly Algorithm (DA) and the Fox Optimization Algorithm (FOA). This innovative approach addresses the challenges of predicting the complex properties of multi-component nanofluids, showcasing the power of combining advanced machine learning techniques with nature-inspired optimization algorithms to enhance predictive accuracy and efficiency.

The final chapter focuses on the practical application of these advanced modeling techniques to a single-slope solar still desalination system. By integrating the insights gained from nanofluid modeling and AI optimization, this chapter demonstrates how these cutting-edge approaches can be used to improve the efficiency and productivity of solar desalination technologies, addressing one of the most pressing global challenges: water scarcity.

Deep learning models can also aid in designing novel nanofluid compositions with improved thermal conductivity and stability, reducing energy consumption and scaling issues. By integrating AI and nanotechnology, future desalination plants can achieve higher efficiency, lower costs, and improved sustainability, addressing global water scarcity challenges.

PART I:

THEORITICAL FRAMEWORK

CHAPTER I:

OVERVIEW OF NANOFLUIDS

1. Introduction

Nanofluids are a revolutionary class of engineered fluids that have garnered significant attention in recent years due to their enhanced thermal and physical properties. These fluids are created by dispersing nanometer-sized particles, typically ranging from 1 to 100 nanometers, into a base fluid such as water, oil, or ethylene glycol.

The concept of nanofluids was first introduced in the mid-1990s (Introduced by Choi in 1995) as a means to address the limitations of traditional heat transfer fluids, which often struggle to meet the growing demands of modern industrial and technological systems. By incorporating nanoparticles, the thermal properties of the base fluid are significantly enhanced, enabling more efficient heat dissipation and temperature regulation. This makes nanofluids particularly valuable in industries such as energy, electronics cooling, automotive, aerospace, and biomedical engineering.

In addition to their thermal advantages, nanofluids also demonstrate unique rheological, optical, and magnetic properties, which can be tailored by adjusting the type, size, concentration, and surface characteristics of the nanoparticles. This versatility has opened up new possibilities for innovation in fields like solar energy harvesting, drug delivery, and advanced manufacturing.

Despite their immense potential, the development and application of nanofluids also present challenges, including issues related to nanoparticle stability, aggregation, and potential environmental or health impacts. Ongoing research aims to address these concerns while further optimizing the performance and scalability of nanofluids for real-world applications.

In summary, nanofluids represent a cutting-edge advancement in fluid engineering, offering unprecedented opportunities to enhance heat transfer and energy efficiency across a multitude of industries. As research and technology continue to evolve, nanofluids are poised to play a pivotal role in shaping the future of thermal management and beyond [40].

However, in comparison to the extensive research on thermal conductivity, the viscosity of nanofluids has received significantly less attention from researchers. This is demonstrated by the recent growth in annual publications on nanofluids, as shown in Figure 1. The data was sourced from the Web of Science on November 24, 2015, by searching the topic “nanofluids” and refining the results with the terms “thermal conductivity” and “viscosity.” The publications encompass journal articles, conference papers, patents, news articles, letters, and other records. Figure 1 indicates that the majority of publications focus on thermal conductivity (56%), followed by viscosity (24%). However, there has been a slight rise in research on the viscosity of nanofluids in recent years, as shown in Figure 1.

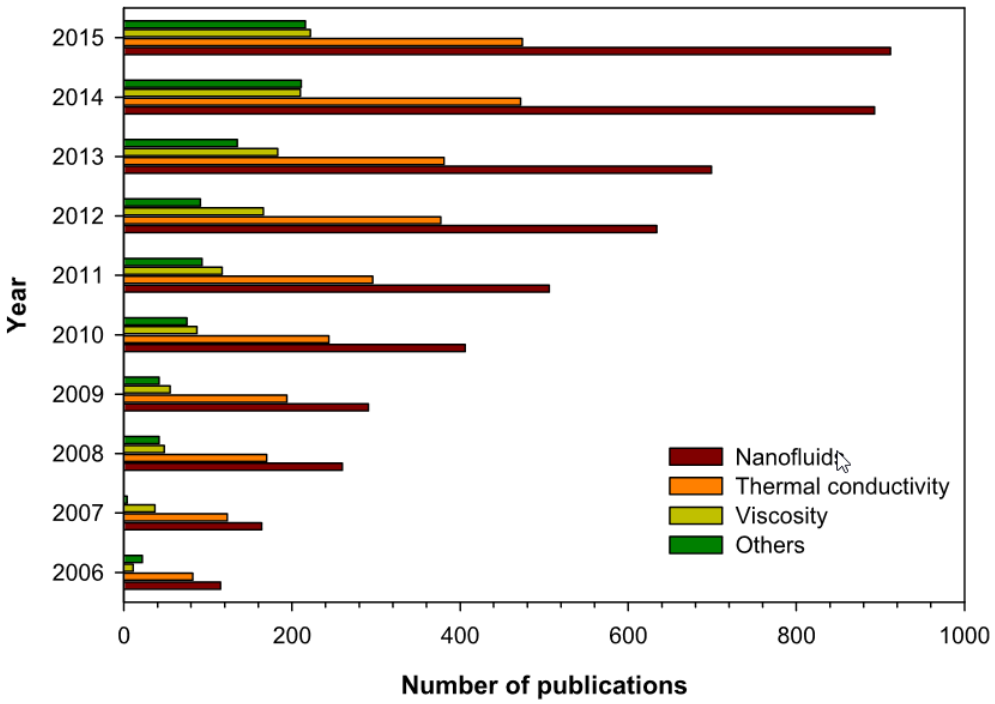


Figure 1. displays the year-wise publication records on various areas of nanofluids, sourced from the Web of Science [41].

The shapes of nanoparticles frequently used in base fluids are shown in Figure 2.

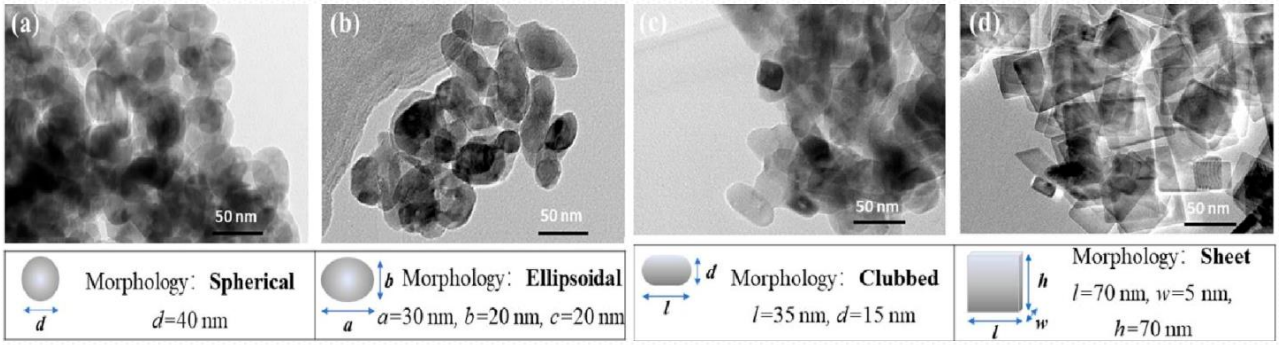


Figure 2. TEM image illustrating the morphology of TiO2 nanoparticles in various shapes [42].

2. Types of Nanofluids

Nanofluids are advanced fluids that contain suspended nanoparticles, enhancing their thermal and rheological properties. They can be categorized based on the material and the shape and concentration used of the nanoparticles dispersed in the base fluid, base fluid, application and the composition [43].

- The nanoparticles used can be made of metals (e.g., Copper: Cu, Aluminum: Al), metal oxides (e.g., Aluminum Oxide: Al_2O_3, Titanium Dioxide: TiO_2), they are widely used due to their stability, affordability, and good thermal properties. Carbides (Silicon Carbide (SiC) and Titanium Carbide (TiC)), they are known for their high thermal

conductivity and mechanical strength. Nitrides like Boron Nitride (BN) which can be used in high-temperature applications due to their thermal stability. The carbon-based materials like graphene or carbon nanotubes (CNTs) have exceptional thermal and electrical properties, making them suitable for advanced applications. Finally, composite Nanofluids, which are hybrid nanoparticles made by combining two or more materials, such as Al_2O_3-CuO, TiO_2-SiO_2 and Graphene-Cu, they are designed to enhance multiple properties simultaneously.

The shape of nanoparticles can also influence the properties of nanofluids, they can base spherical, cylindrical (e.g., carbon nanotubes), platelet (e.g., graphene), rod-shaped and irregular shapes.

Nanofluids can be classified based on the volume or weight fraction of nanoparticles, low-concentration nanofluids (e.g., <1%), medium-concentration nanofluids (e.g., 1–5%) and high-concentration nanofluids (e.g., >5%).

- The base fluid determines the application and performance of the nanofluid. Common base fluids include water which is the most common base fluid due to its availability, low cost, and high heat capacity. It is used in cooling systems, heat exchangers, and electronic cooling.

  The second base fluid is Ethylene Glycol (EG) which is used as a base fluid for its antifreeze properties in automotive cooling systems and cold regions.

  The Oil-Based Nanofluids includes Mineral oils, silicone oils, or engine oils are suitable for high-temperature applications and lubrication.

  The Bio-Based Nanofluids are derived from natural sources, such as vegetable oils or bio-glycols and considered as environmentally friendly and used in green technologies.

  The Refrigerant-Based Nanofluids like R134a or R600a are used in refrigeration and air conditioning systems.

- Nanofluids can also be classified based on their intended application such as in Heat Transfer Nanofluids which are designed to enhance thermal conductivity and heat transfer efficiency and they find their applications in heat exchangers, solar collectors, and cooling systems.

  They can used in Biomedical Nanofluids especially in drug delivery, hyperthermia treatment, and bioimaging. They are often made with biocompatible nanoparticles like gold or iron oxide.

  They find application in optical nanofluids like in optical filters, sensors, and solar absorption. They often contain metallic nanoparticles like gold or silver.

They can used for Lubrication to reduce friction and wear in mechanical systems. They commonly contain nanoparticles like graphene, MoS_2, or CuO.

And finally, they can be used in thermal energy storage systems and batteries. They often contain carbon-based nanoparticles or metal oxides.

- Nanofluids can be categorized according to the number of different types of nanoparticles dispersed in the base fluid.

  Mono-Nanofluids: Contain only one type of nanoparticle dispersed in the base fluid (Example: Al_2O_3 (aluminum oxide) nanoparticles in water (Al_2O_3/Water)). They commonly used in basic heat transfer and cooling systems due to their simplicity and ease of preparation.

  Binary Nanofluids: Contain two types of nanoparticles dispersed in the base fluid (Example: A mixture of Al_2O_3 and CuO (copper oxide) nanoparticles in water (Al_2O_3-CuO/Water)). They are used to enhance thermal and mechanical properties compared to mono-nanofluids, making them suitable for more demanding applications.

  Ternary Nanofluids: Contain three types of nanoparticles dispersed in the base fluid (Example: A mixture of Al_2O_3, CuO, and TiO_2 nanoparticles in water (Al_2O_3-CuO-TiO_2/Water)). They offer improved thermal conductivity, stability, and multifunctional properties, making them ideal for advanced heat transfer and energy systems.

  Quaternary Nanofluids: Contain four types of nanoparticles dispersed in the base fluid (Example: A mixture of Al_2O_3, CuO, TiO_2, and Fe_3O_4 (iron oxide) nanoparticles in water (Al_2O_3-CuO-TiO_2-Fe_3O_4/Water)). They are designed for highly specialized applications where multiple properties (thermal, magnetic, optical, etc.) are required simultaneously.

The resulting nanofluids exhibit superior thermal conductivity, heat transfer efficiency, and stability compared to conventional fluids, making them highly promising for a wide range of applications. Researchers continue to explore new combinations and applications to optimize their efficiency and sustainability.

3. Properties of nanofluids

Nanofluids are characterized by their enhanced thermophysical properties compared to traditional base fluids. These properties, such as density, heat capacity, thermal conductivity, and dynamic and kinematic viscosity, are significantly altered by the addition of nanoparticles. Numerous parameters, including the nature of the nanoparticles, their size, volume fraction, the conductivity of the base fluid and the nanoparticles, and the temperature of the medium, can

have a notable effect on the resulting nanofluid's characteristics. These enhanced properties are crucial for their performance in various applications, ranging from thermal management to energy systems. Given the complexity and importance of these properties, it is essential to review and analyze the main theoretical and experimental approaches developed in the literature for evaluating these characteristics. This will help optimize nanofluid performance and expand their applications across industries.

3.1. Volume Fraction

It refers to the ratio of the volume of nanoparticles (solid) to the total volume (solid + fluid) [43].

$$\varphi = \frac{\text{Volume of solid}}{\text{Total volume}} = \frac{V_s}{V_s+V_f}$$

3.2. Density

To determine the density of a nanofluid as a function of the volume fraction (φ) at a given temperature, provided that the resulting suspension is perfectly homogeneous [43].

$$\rho_{nf} = \left(\frac{m}{V}\right)_{nf} = \frac{m_f + m_s}{V_f + V_s} = \frac{\rho_f V_f + \rho_s V_s}{V_f + V_s}$$

$$\rho_{nf} = (1-\varphi)\rho_f + \varphi\rho_s$$

3.3. Thermal Conductivity

refers to a material's ability to conduct heat. In nanofluids, it is significantly enhanced by the addition of nanoparticles. The thermal conductivity of nanofluids is a key thermophysical property that significantly impacts their thermal performance. The factors governing the thermal conductivity of nanofluids include nanoparticle concentration, size, shape, the thermal conductivity of the base fluid, stabilization techniques, and the methods used to measure thermal conductivity. Understanding the trends in the effective thermal conductivity (k_{nf}) of nanofluids requires examining the individual and combined effects of these factors. This section outlines the general trends observed in the effective thermal conductivity of nanofluids, which are influenced by parameters such as nanoparticle concentration, shape, thermal conductivity, base fluid properties, operating temperature, and the techniques employed for stabilization and thermal conductivity measurement. Figure 3 highlights the factors affecting the effective thermal conductivity of nanofluids, as described by Ambreen and Kim [44].

Figure 4 presents a comparison of thermal conductivity between commonly used liquids and solids. In contrast to metallic solids and carbon, the thermal conductivity of typical working

fluids is significantly lower. This disparity suggests that incorporating solid particles into the working fluid can potentially enhance thermal conductivity [45].

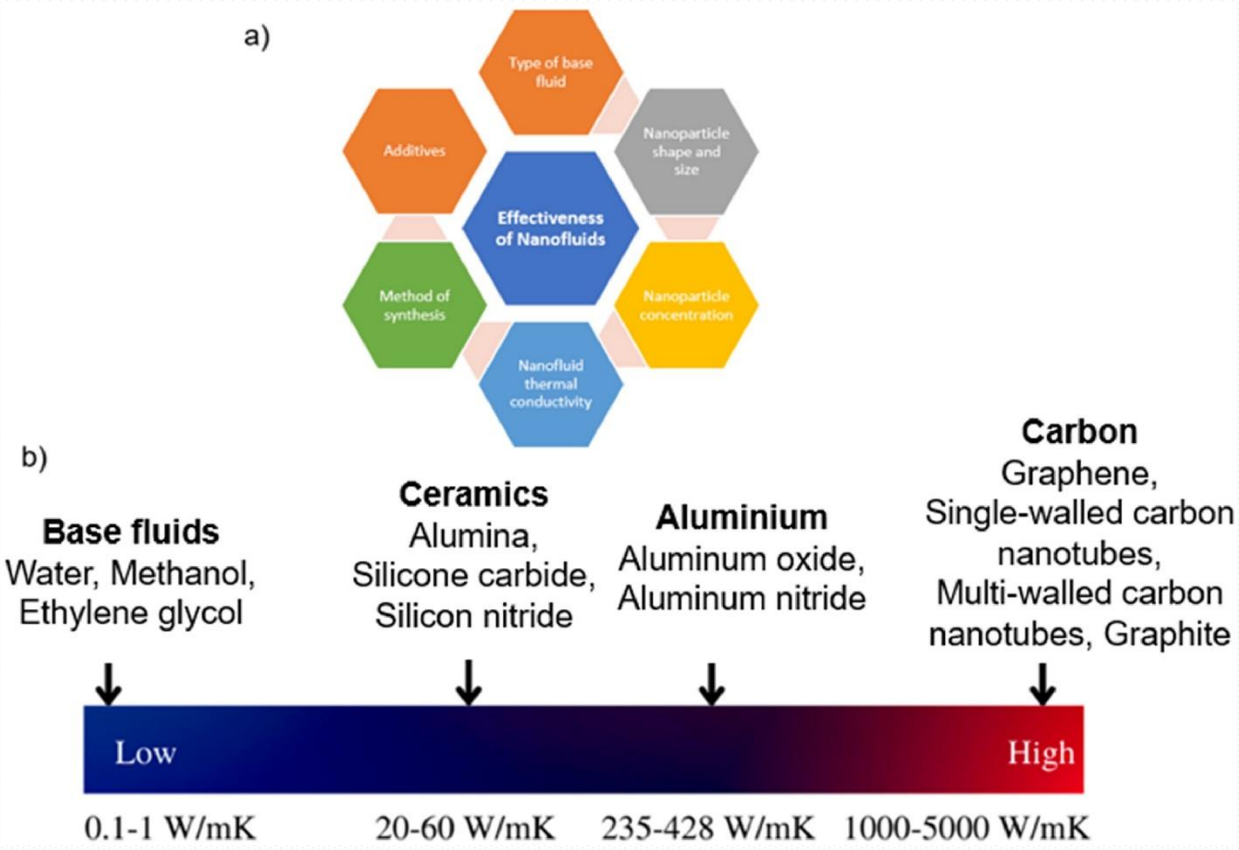


Figure 3. illustrates a) The factors influencing the effectiveness of nanofluids, and b) The thermal conductivity values of various materials used in nanofluids, including base fluids like water and nanofluids containing materials such as carbon or aluminum [46].

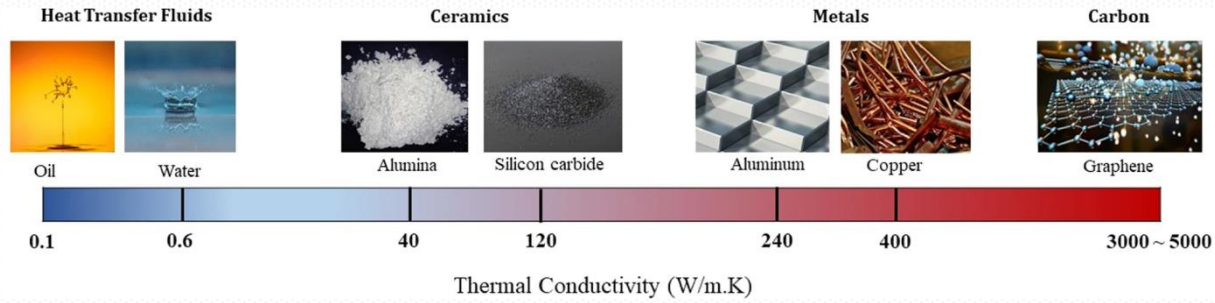


Figure 4. illustrates the comparison of thermal conductivity between commonly used liquids and solids [45].

- **Influencing Factors**
  - Nanoparticle concentration: Higher nanoparticle concentrations generally lead to increased thermal conductivity.

- Type of nanoparticles: Metallic nanoparticles (e.g., Cu, Ag) and carbon nanotubes (CNTs) offer higher thermal conductivity compared to metal oxides (e.g., Al_2O_3, TiO_2).
- Shape and size of nanoparticles: Cylindrical (e.g., CNTs) or platelet-shaped (e.g., graphene) nanoparticles enhance thermal conductivity more than spherical particles (Figure 5).

This property is exploited in cooling systems, heat exchangers, and solar collectors.

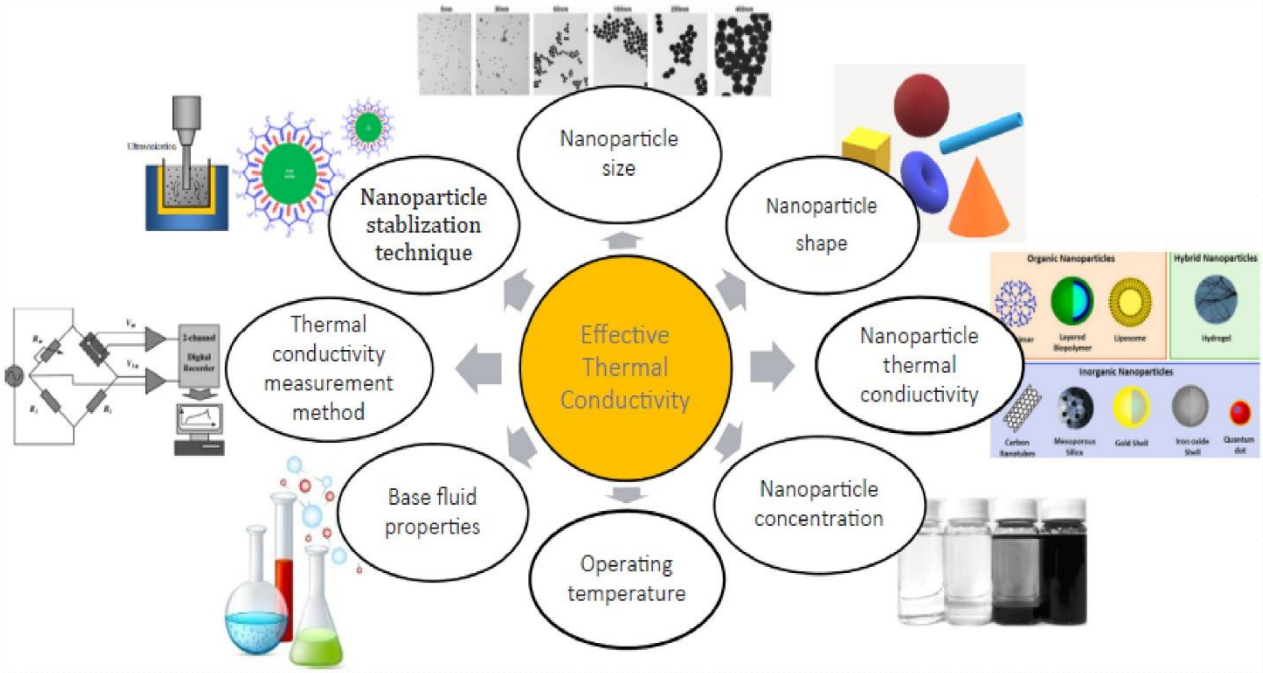


Figure 5. Factors influencing the effective thermal conductivity of nanofluids [44].

In earlier studies, attempts were made to estimate the thermal conductivity of hybrid or more nanofluids by modifying models originally developed for single nanofluids, as shown in Table 1.

Table 1. Some theoretical models for binary hybrid nanofluid.

Thermal conductivity of hybrid Nanofluid	Maxwell model (1881) [47]	$\frac{k_{nf}}{k_{bf}} = 1 + \frac{3\left(\frac{k_{np}}{k_{bf}} - 1\right)\varphi}{\left(\frac{k_{np}}{k_{bf}} + 2\right) - \left(\frac{k_{np}}{k_{bf}} - 1\right)\varphi}$ $\frac{k_{hnf}}{k_{bf}} = \frac{(1+2\varphi)\left(\varphi_{np1}k_{np1} + \varphi_{np2}k_{np2}\right) + 2\varphi_{bf}(1-\varphi)}{(1-\varphi)\left(\varphi_{np1}k_{np1} + \varphi_{np2}k_{np2}\right) + k_{bf}\varphi(2+\varphi)}$ ϕ: Volume fraction
	Yu-Choi model (2003) [48]	$\frac{k_{hnf}}{k_{bf}} = \frac{k_{np2} + 2k_{bf} - 2\varphi(k_{bf} - k_{np1})(1+\beta)^3}{k_{np2} + 2k_{bf} - \varphi(k_{bf} - k_{np1})(1+\beta)^3}$ β: the ratio of the nanolayer thickness to the original particle radius
	Hamilton- Crosser model (1962) [49]	$\frac{k_{hnf}}{k_{bf}} = \frac{k_{np2} + (n-1)k_{nf} - \varphi_{np2}(n-1)\left(k_{nf} - k_{np2}\right)}{k_{np2} + (n-1)k_{nf} - \varphi_{np2}\left(k_{nf} - k_{np2}\right)}$ Spherical particles (n = 3), Cylindrical particles (n = 6)

This complex approach considers various factors, such as particle volume fraction (φ), temperature, particle shape (e.g., cylindrical, spherical), pH value, nanoparticle diameter, and the impact of Brownian motion due to the random movement of particles [50]. A thorough understanding of these interrelated factors is crucial for accurately modeling and predicting the thermal conductivity of hybrid nanofluids, thereby improving the efficiency of thermal systems [51].

Tri-hybrid nanofluids, also referred to as ternary hybrid nanofluids, represent an advanced evolution of hybrid nanofluids, involving the suspension of three distinct nanomaterials within a base fluid [52]. Researchers have found that tri-hybrid nanofluids offer superior improvements in thermophysical properties, heat transfer efficiency, biomedical applications, and other areas compared to both traditional and hybrid nanofluids [53–55].

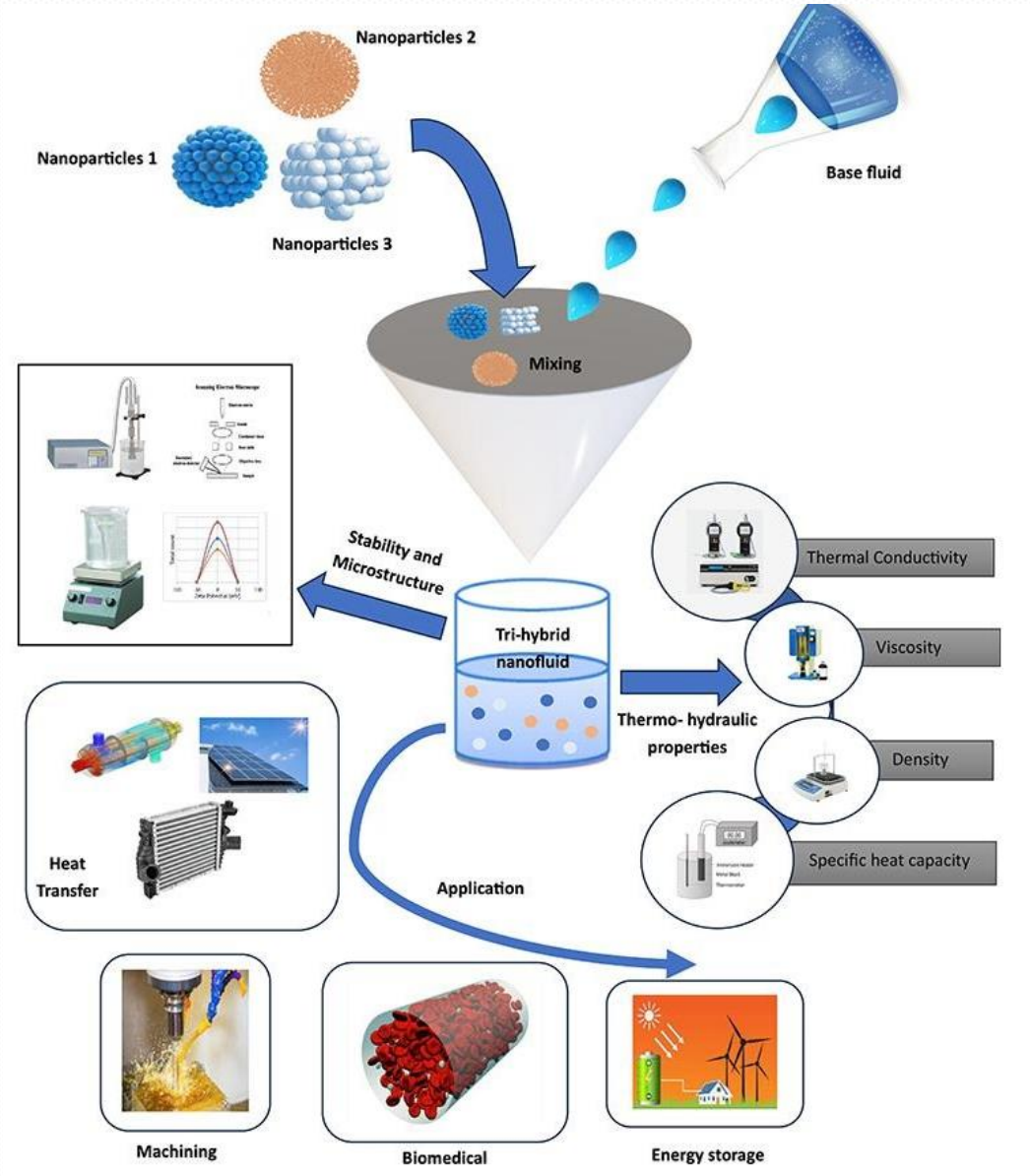


Figure 6. Composition of ternary hybrid nanofluid.

Table 2. An example of numerical values for base water and ternary hybrid nanoparticles [52].

Properties	$Al_2O_3(\emptyset_1)$	$Cu(\emptyset_2)$	$TiO_2(\emptyset_3)$	H_2O
$\rho(kg/m^3)$	3970	8933	4250	997.1
$Cp(J/KgK)$	765	385	686.2	4179
$k(W/mK)$	0.40	400	8.538	0.613
$\sigma(W/m)$	35×10^6	59.6×10^6	2.352×10^{-4}	0.05

Table 3. Thermal properties calculation models for ternary hybrid nanofluids [52].

Density	$\rho_{mnf} = (1-\emptyset_3)\left\{(1-\emptyset_2)\left[(1-\emptyset_1)\rho_f + \emptyset_1\rho_{s1}\right] + \emptyset_2\rho_{s2}\right\} + \emptyset_3\rho_{s3}$
Dynamic Viscosity	$\mu_{mnf} = \frac{\mu_f}{(1-\emptyset_3)^{2.5}(1-\emptyset_2)^{2.5}(1-\emptyset_1)^{2.5}}$
Thermal Conductivity	$\frac{k_{mnf}}{k_{hnf}} = \frac{k_{s3}+(m-1)k_{hnf}-(m-1)\phi_3(k_{hnf}-k_{s3})}{k_{s3}+(m-1)k_{hnf}+\phi_3(k_{hnf}-k_{s3})}$ where $\frac{k_{hnf}}{k_{nf}} = \frac{k_{s2}+(m-1)k_{nf}-(m-1)\phi_2(k_{nf}-k_{s2})}{k_{s2}+(m-1)k_{nf}+\phi_2(k_{nf}-k_{s2})}$ and $\frac{k_{nf}}{k_f} = \frac{k_{s1}+(m-1)k_f-(m-1)\phi_1(k_f-k_{s1})}{k_{s1}+(m-1)k_f+\phi_1(k_f-k_{s1})}$
Heat capacity	$(\rho C_p)_{mnf} = (1-\emptyset_3)\left\{(1-\emptyset_2)\left[(1-\emptyset_1)(\rho C_p)_f + \emptyset_1(\rho C_p)_{s1}\right] + \emptyset_2(\rho C_p)_{s2}\right\} + \emptyset_3(\rho C_p)_{s3}$
Electrical Conductivity	$\frac{\sigma_{mnf}}{\sigma_{hnf}} = \frac{\sigma_{s3}+2\sigma_{hnf}-2\phi_3(\sigma_{hnf}-\sigma_{s3})}{\sigma_{s3}+2\sigma_{hnf}+\phi_3(\sigma_{hnf}-\sigma_{s3})}$, Where $\frac{\sigma_{hnf}}{\sigma_{nf}} = \frac{\sigma_{s2}+2\sigma_{nf}-2\phi_2(\sigma_{nf}-\sigma_{s2})}{\sigma_{s2}+2\sigma_{nf}+\phi_2(\sigma_{nf}-\sigma_{s2})}$ and $\frac{\sigma_{nf}}{\sigma_f} = \frac{\sigma_{s1}+2\sigma_f-2\phi_1(\sigma_f-\sigma_{s1})}{\sigma_{s1}+2\sigma_f+\phi_1(\sigma_f-\sigma_{s1})}$

mnf: ternary hybrid nanofluids, S1: Solid component 1, ϕ: Nanoparticle volume fraction, nf: nanofluid, hnf: Hybrid nanofluid

3.4. Viscosity

Is a measure of a fluid's resistance to flow. It is affected by the presence of nanoparticles. The prediction of nanofluid viscosity using theoretical models is crucial for optimizing their performance in various applications, such as heat transfer systems and advanced cooling technologies.

Table 4. conventional models for viscosity of nanofluids calculation

Viscosity of nanofluids	Einstein [56]	$\mu_{nf} = \mu_{bf}(1+2.5\varphi)$ Applicable for low (less than 2%) concentration of nanoparticle
	Brinkma [57]	$\mu_{nf} = \mu_{bf}(1-\varphi)^{-2.5}$ The equation was developed for 4 vol% concentrations of particles. It is a modified version of Einstein's model
	Thomas et al. [58]	$\frac{\mu_{nf}}{\mu_{bf}} = 1 + 2.5\varphi + 10.5\varphi^2 + 0.00273e^{16.6\varphi}$
	Krieger and Dougherty [59]	$\mu_{nf} = \mu_f\left(1-(\varphi/\varphi_m)\right)^{[\eta]\varphi_m}$
	Chen et al. [60]	$\mu_{nf} = \mu_f\left(1-(\varphi_{cl}/\varphi_m)\right)^{[\eta]\varphi_m}$
	Kitano et al. [56]	$\frac{\mu_{nf}}{\mu_{bf}} = \frac{1}{\left(1-(\varphi/\varphi_m)\right)^2}$

The viscosity of nanofluids is influenced by several factors, including particle size, shape, volume fraction, temperature, and the nature of the base fluid (Figure 7).

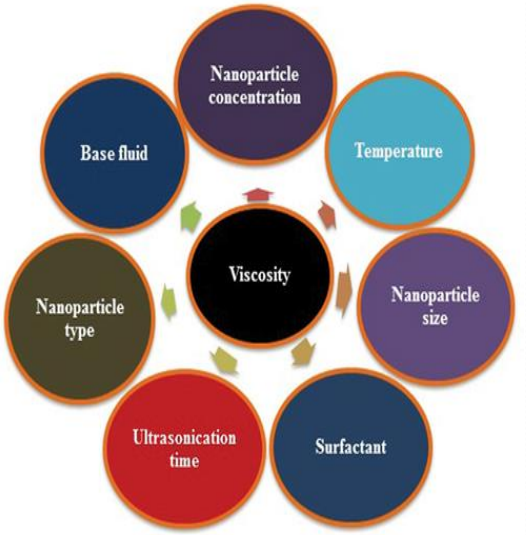


Figure 7. Factors influencing the viscosity of nanofluids [61].

Researchers have developed various theoretical models, such as the Einstein and Brinkman models, to estimate the viscosity of nanofluids. However, these models often require modifications to account for the unique interactions between nanoparticles and the base fluid, as well as the effects of particle clustering and Brownian motion. Accurate viscosity prediction is essential for enhancing the efficiency and stability of nanofluids in practical applications (Table 4). The absolute viscosities of various commonly used fluids are presented in Table 5.

Table 5. Viscosity of various common liquids at a temperature of 30°C [62].

Fluid	**Absolute viscosity, (Pa s)**	**Fluid**	**Absolute viscosity, (Pa s)**
Acetic acid	0.001155	Hexane	0.000297
Acetone	0.000316	Kerosene	0.00164
Alcohol, propyl	0.00192	Linseed oil	0.0331
Benzene	0.000601	Methanol	0.00056
Bromine	0.00095	Mercury	0.0015
Carbon disulfide	0.00036	Octane	0.00051
Carbon tetrachloride	0.00091	Phenol	0.0080
Castor oil	0.650	Propane	0.00011
Chloroform	0.00053	Propylene	0.00009
Decane	0.000859	Propylene glycol	0.042
Dodecane	0.00134	Toluene	0.000550
Ethanol	0.001095	Turpentine	0.001375
Ether	0.000223	Water, Fresh	0.00089
Ethylene glycol	0.0162	20:80% EG/W	0.0013
Freon refrigerant R-11	0.00042	40:60% EG/W	0.00226
Glycerin	0.950	60:40% EG/W	0.00384
Heptane	0.000376	30:70% PG/W	0.00219

3.5. Specific Heat

are modified by the addition of nanoparticles.

a) Influencing Factors

- Density: The density of the nanofluid increases with nanoparticle concentration, as nanoparticles are generally denser than the base fluid.
- Specific Heat: Specific heat often decreases with the addition of nanoparticles, as nanoparticles typically have lower heat capacities than the base fluid.

b) Impact: These properties influence the thermal storage capacity and energy efficiency of systems using nanofluids.

These properties are important in thermal energy storage systems and solar power plants.

Table 6. Presents the theoretical models for hybrid nanofluids.

Specific heat of hybrid Nanofluid	Pak et al. (1998) [63]	$Cp_{hnf} = (1 - \varphi_{np1} - \varphi_{np2})Cp_{bf} + \varphi_{np1}Cp_{np1} + \varphi_{np2}Cp_{np2}$
	Xuan et al. (2000) [64]	$(\rho Cp)_{hnf} = (1 - \varphi_{np1} - \varphi_{np2})(\rho Cp)_{bf} + \varphi_{np1}(\rho Cp)_{np1} + \varphi_{np2}(\rho Cp)_{np2}$

3.6. Colloidal Stability

It refers to the ability of nanoparticles to remain uniformly dispersed in the base fluid without sedimentation or aggregation.

a) Influencing Factors:

- Nanoparticle Size: Smaller nanoparticles are more stable as they are less prone to sedimentation.
- pH of the Fluid: An appropriate pH can enhance stability by modifying the surface charges of nanoparticles.
- Use of Surfactants: Surfactants are often added to prevent nanoparticle aggregation.
- Dispersion Techniques: Ultrasonication and milling are commonly used to improve nanoparticle dispersion.

b) Impact:

Poor colloidal stability reduces the efficiency of nanofluids and can clog circulation systems.

Figure 7 illustrates the relationship between zeta potential and colloidal stability. In the first image, a stable colloid with a high zeta potential shows well-dispersed particles due to strong electrostatic repulsion, preventing aggregation and sedimentation. In contrast, an

unstable colloid with a low zeta potential experiences weak repulsion, leading to particle aggregation and settling. The second image highlights the electric double layer around a colloidal particle, where the tightly bound Stern layer and the diffuse layer of counter-ions create an electrostatic environment. The zeta potential, measured at the boundary of the diffuse layer, is crucial in determining whether particles remain stable or aggregate.

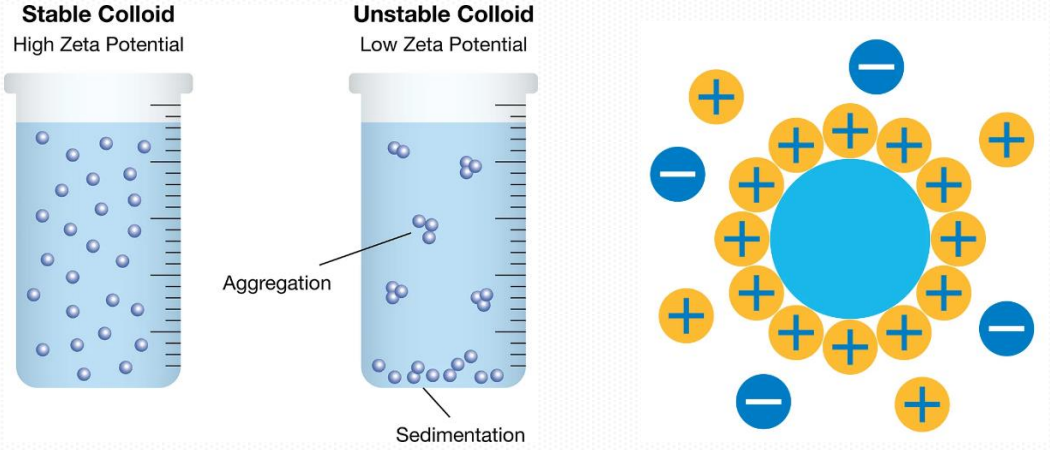


Figure 8. Zeta Potential and Colloidal Stability.

4. Preparation of mono nanofluids

4.1. One-step method

In general, as noted by Animasaun et al. [65,66], the thermophysical properties of solids typically exceed those of liquids, as demonstrated in Table 5.

The preparation of nanofluids is a critical step in leveraging nanoparticles to enhance the thermal conductivity of fluids. Two primary methodologies are employed in the production of nanofluids: (1) the one-step approach and (2) the two-step approach. The one-step method integrates the synthesis of nanoparticles with the preparation of nanofluids in a single process. In this technique, nanoparticles are directly generated using either physical vapor deposition (PVD) or chemical vapor deposition (CVD). This approach eliminates the need for intermediate steps such as drying, storage, transportation, and dispersion of nanoparticles, thereby reducing nanoparticle agglomeration and enhancing fluid stability. However, a significant limitation of this method is its compatibility only with low-vapor-pressure fluids, as well as the difficulty in producing large quantities of nanofluids. Additionally, residual reactants often remain in the nanofluids, and the high cost of the process makes it challenging to scale up for industrial applications. These drawbacks restrict the widespread use of the one-step method.

Figure 9 provides a schematic diagram of the one-step process for preparing nanofluids, as described by Pereira et al. [67].

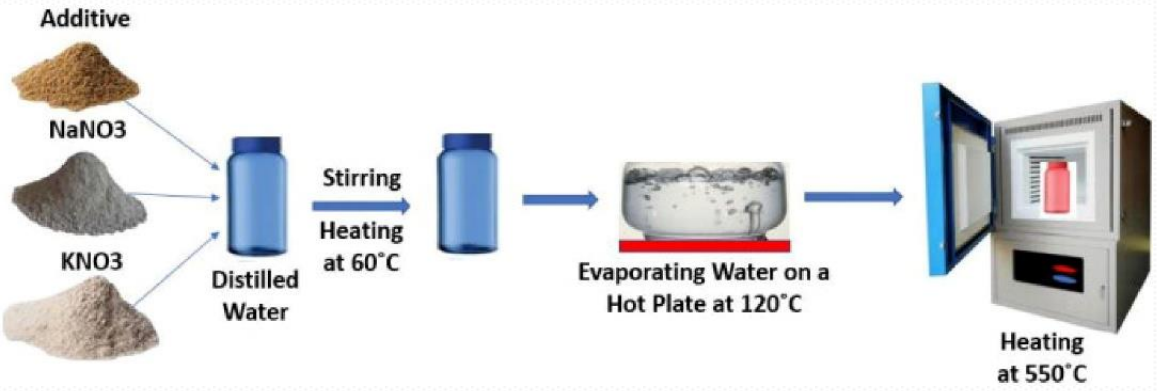


Figure 9. Illustrates a schematic representation of the one-step process used for the preparation of nanofluids [67].

2.2. Two-Step Method

The two-step method for preparing nanofluids involves dispersing pre-synthesized nanoparticles, nanofibers, or nanotubes into a base fluid. In this approach, nanoparticles are first produced as dry powders using techniques such as inert gas condensation, chemical vapor deposition (CVD), mechanical alloying, or other suitable methods. The nanoscale powder is then dispersed into the base fluid in a subsequent step. This method separates the synthesis of nanoparticles from the preparation of nanofluids, which can lead to nanoparticle agglomeration during drying, storage, and transportation. Such agglomeration can cause clogging of microchannels and reduce thermal conductivity. To mitigate these issues, techniques like ultrasonic agitation or the addition of surfactants are commonly employed to improve nanoparticle dispersion and reduce aggregation [68,69]. Ultrasonic agitation uses sound waves with frequencies above 20 kHz to generate intense mechanical vibrations and acoustic cavitation, breaking down larger droplets and ensuring uniform dispersion of nanoparticles in the base fluid. The stability of the nanofluid is often assessed using the zeta potential, which measures the potential difference between the bulk fluid and the charged layer around the nanoparticles. A zeta potential greater than ±30 mV indicates a stable nanofluid [66].

The two-step method offers potential cost advantages, as industrial-scale nanopowder synthesis is already well-established in various industries. However, achieving long-term stability of the nanofluid suspension remains a critical challenge. Techniques such as pH adjustment or the use of polymeric stabilizers can be employed to enhance stability. Figure 10 provides a schematic diagram of the two-step process for preparing nanofluids [70].

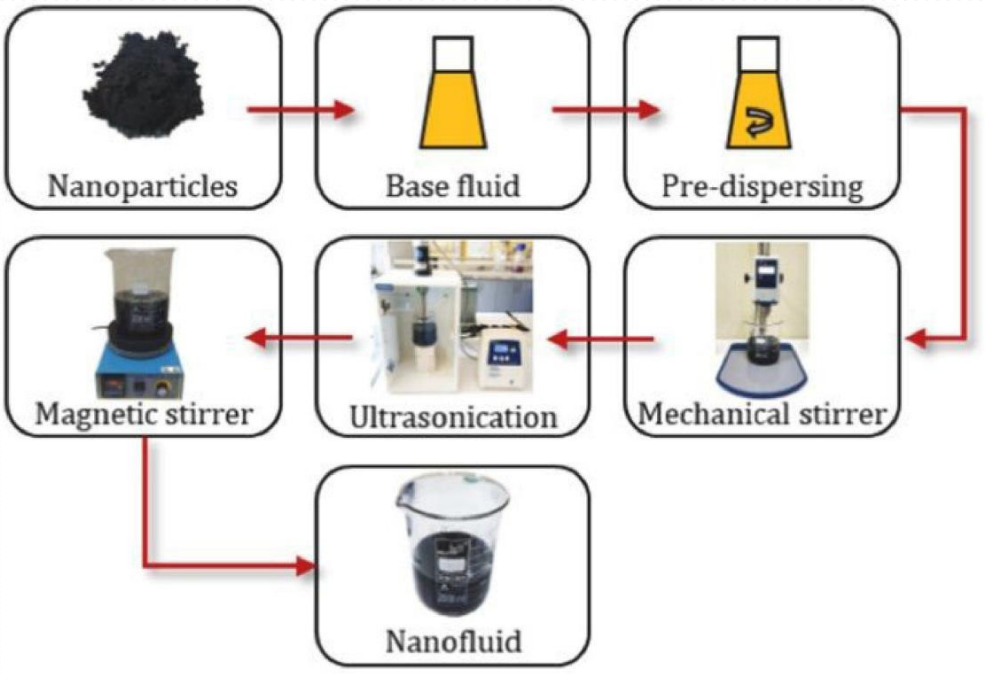


Figure 10. illustrates a schematic representation of the two-step process for preparing nanofluids, [43]

Figures 11 and 12 provide a clear depiction of the one-step and two-step methods, respectively. Additionally, they offer a comparison of the advantages and disadvantages associated with both methods.

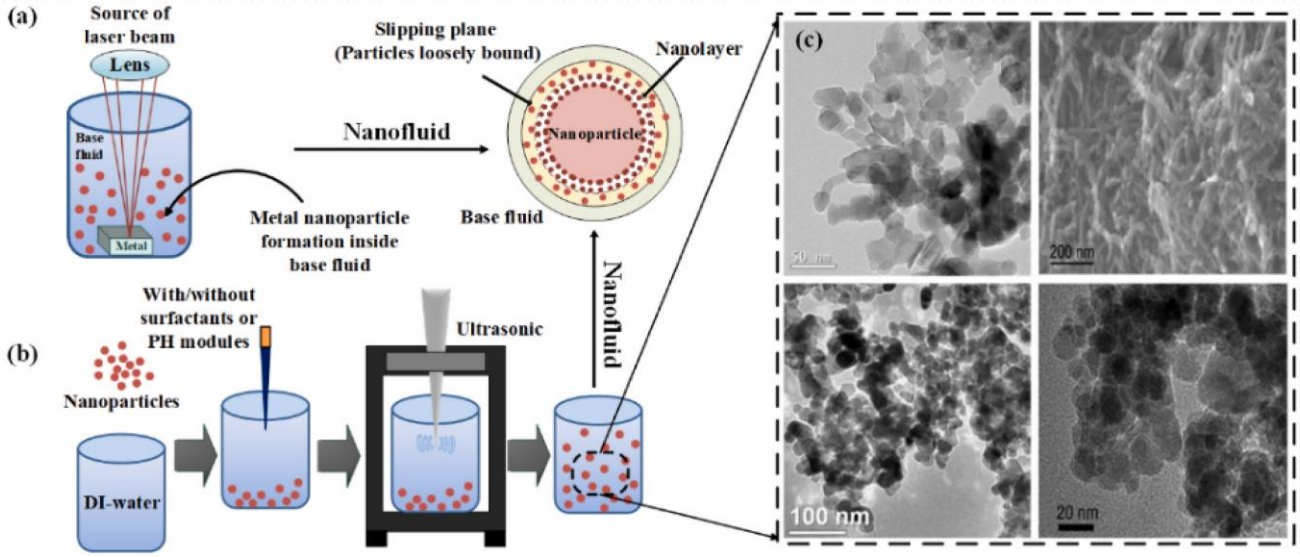


Figure 11. Illustrates nanofluid preparation techniques: (a) the one-step method and (b) the two-step method [71].

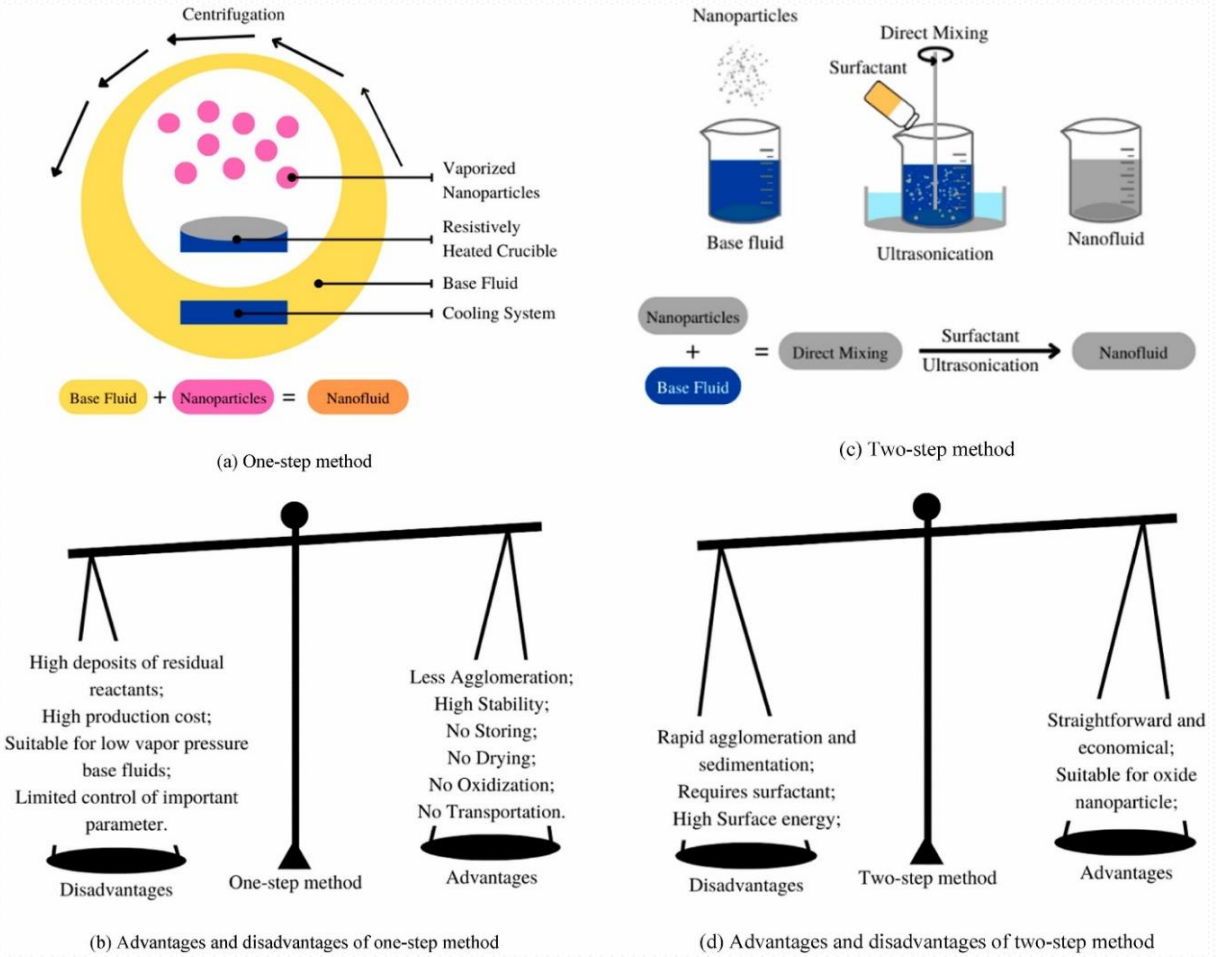


Figure 12. displays: (a) the one-step method, (b) the advantages and disadvantages of the one-step method, (c) the two-step method, and (d) the advantages and disadvantages of the two-step method [72].

Graphically, the one-step technique is illustrated in Figure 12a. This method typically involves physical synthesis, where nanoparticles are vaporized and directly condensed into a liquid state under low pressure, allowing for the direct synthesis of nanoparticles into the base fluid [73,74]. Figure 12b highlights the advantages and disadvantages of the one-step method. In contrast, the two-step technique, depicted in Figure 12c, is a more common and cost-effective approach for nanofluid production. Its simplicity makes it particularly suitable for producing oxide-based nanofluids.

However, the two-step method, as shown in Figure 12d, has notable drawbacks, including rapid sedimentation, the necessity for additional steps, and high surface energy [75].

Table 7. Thermal conductivity of nanoparticles and base fluids used in the nanofluids [66].

Substance	Density (kg/m^3)	Specific heat (J/kg K)	Thermal conductivity (W/m K)
Al	2710	900	237
Ag	10,490	429	429
Au	19,300	128	318
Fe	7874	451	83.5
CuO	6000	551	33
MgO	3560	955	45
Fe_3O_4	5200	670	6.0
SiO_2	2330	765	36
CeO_2	7220	460	16
SWCNT	1400	1380	3500
MWCNT	2600	710	3000
Ethylene glycol	1110	2347	0.253
SAE 30 Engine Oil	840	1760	0.145
Propylene glycol	1040	2507	0.147

5. Applications of Nanofluids

Nanofluids have revolutionized various fields due to their unique properties. In energy and thermal transport, they are extensively used in heat exchangers to enhance heat transfer efficiency and in solar panels to improve energy absorption. In the automotive industry, nanofluids play a crucial role in engine cooling systems, ensuring better thermal management and improved engine performance. In medicine, they are utilized as contrast agents for advanced imaging techniques and enable targeted drug delivery and hyperthermia treatments for cancer therapy. In water treatment, nanofluids enhance filtration processes, effectively removing contaminants and improving water quality. In the aerospace sector, they provide thermal protection for critical components, ensuring stability and performance under extreme conditions. Additionally, nanofluids are used in electronics cooling to manage heat in high-performance devices.



Figure 13. Highlights some fundamental applications of nanofluids [40,76].



Figure 14. General applications of nanofluids [40].

They also find applications in lubrication, reducing friction and wear in mechanical systems. In renewable energy, nanofluids improve the efficiency of geothermal systems and thermal energy storage. Their use in industrial processes enhances heat transfer in manufacturing and chemical processing. In biomedical engineering, nanofluids enable innovative solutions for diagnostics and therapy. Their versatility and effectiveness make nanofluids a key material in advancing technology and addressing critical challenges across industries. Figure 13 and 14 illustrates several fundamental applications of nanofluids.

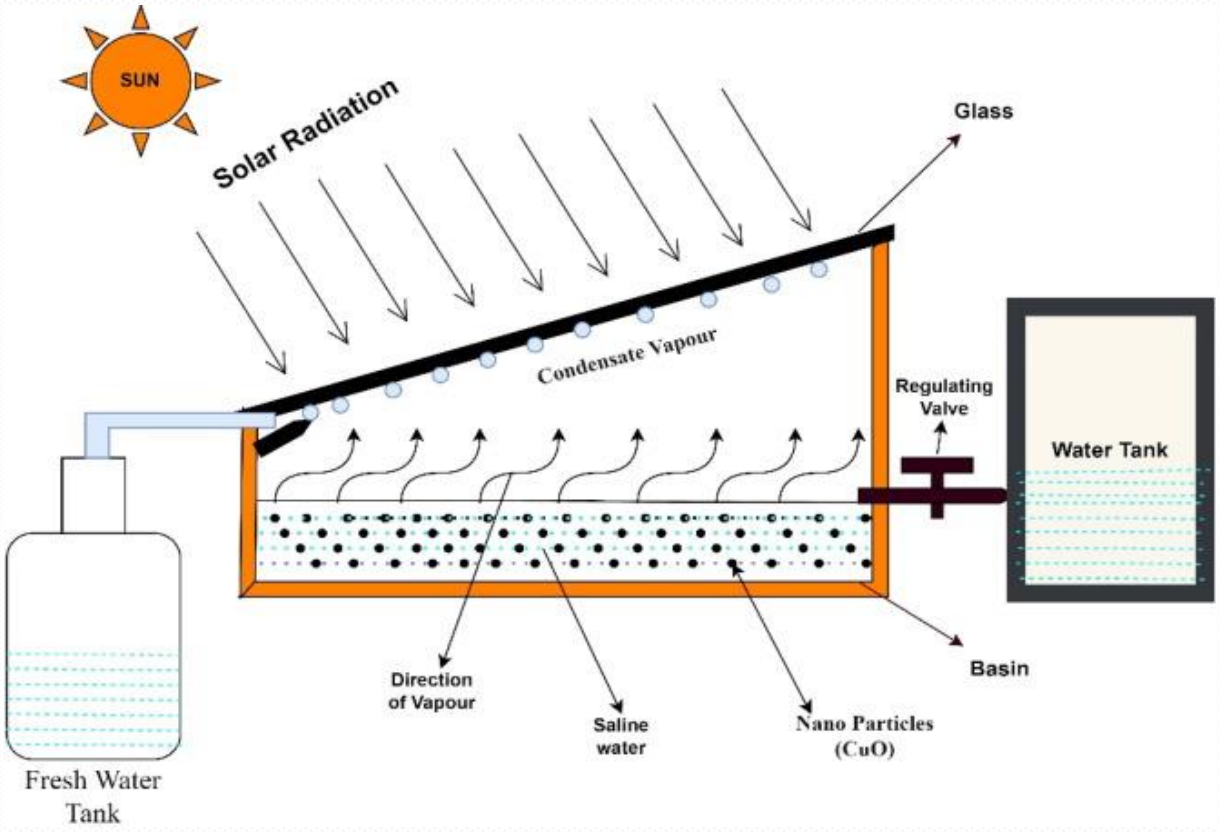


Figure 15. Diagrammatic representation of the solar desalination system [77].

Nanofluids present a promising solution for enhancing heat transfer rates in desalination processes and boosting freshwater production. This approach is vital for meeting the growing demand for freshwater. While various techniques have been proposed to improve freshwater production, they often lead to higher energy consumption. However, researchers have focused on solar energy-driven desalination systems to generate clean water. The incorporation of nanofluids has shown significant improvements in system performance. The design of this desalination system is illustrated in Figure 14 [77].

6. Advantages of nanofluids

Nanofluids offer several significant advantages, making them highly valuable in various applications. One of their key benefits is enhanced thermal efficiency, as they significantly improve heat dissipation compared to traditional fluids. This leads to reduced energy consumption, making systems more energy-efficient and cost-effective. Additionally, nanofluids exhibit anti-corrosive properties, which help protect equipment and extend its lifespan. Their adaptability to diverse applications is another major advantage, as they can be tailored for use in fields such as energy, automotive, medicine, and aerospace. These advantages make nanofluids a versatile and innovative solution for improving performance and sustainability across industries.

7. Disadvantages of nanofluids

Nanofluids offer remarkable enhancements in thermal conductivity and heat transfer efficiency. However, they also come with several disadvantages:

1. Agglomeration and Sedimentation: Nanoparticles tend to cluster together and settle over time, leading to instability and reduced efficiency.
2. High Production Cost: The synthesis and dispersion of nanoparticles can be expensive, limiting large-scale applications.
3. Corrosion and Erosion: Nanoparticles can cause wear and tear on pipelines and equipment, leading to potential damage and maintenance issues.
4. Health and Environmental Concerns: The small size of nanoparticles raises concerns about their potential toxicity and environmental impact.
5. Viscosity Increase: Adding nanoparticles to the base fluid can significantly increase viscosity, leading to higher pumping power requirements.
6. Limited Compatibility: Nanoparticles may not be compatible with certain base fluids, affecting stability and performance.
7. Measurement Challenges: Accurate characterization and measurement of nanofluid properties can be complex and require advanced equipment.

Despite these challenges, ongoing research aims to optimize nanofluids for practical applications.

8. Environmental impacts of nanofluids

Nanofluids offer significant advancements in thermal management and energy efficiency, but their environmental impacts raise concerns that need careful consideration:

1. Toxicity to Living Organisms: Nanoparticles can enter ecosystems through wastewater and industrial discharge, posing risks to aquatic life and potentially affecting the food chain.
2. Airborne Pollution: During manufacturing and handling, nanoparticles can become airborne, leading to respiratory issues and other health hazards for workers and nearby communities.
3. Soil Contamination: Accidental spills or improper disposal can lead to nanoparticle accumulation in soil, affecting microbial activity and plant growth.
4. Non-Biodegradability: Some nanoparticles are non-biodegradable and can persist in the environment for extended periods, leading to long-term ecological damage.
5. Energy-Intensive Production: The synthesis of nanofluids often requires significant energy and chemical usage, contributing to carbon emissions and resource depletion.
6. Water Contamination: Nanoparticles can infiltrate water sources, affecting water quality and posing potential risks to human health.

Addressing these concerns through proper regulation, waste management, and eco-friendly nanomaterial development is essential for sustainable nanofluid applications.

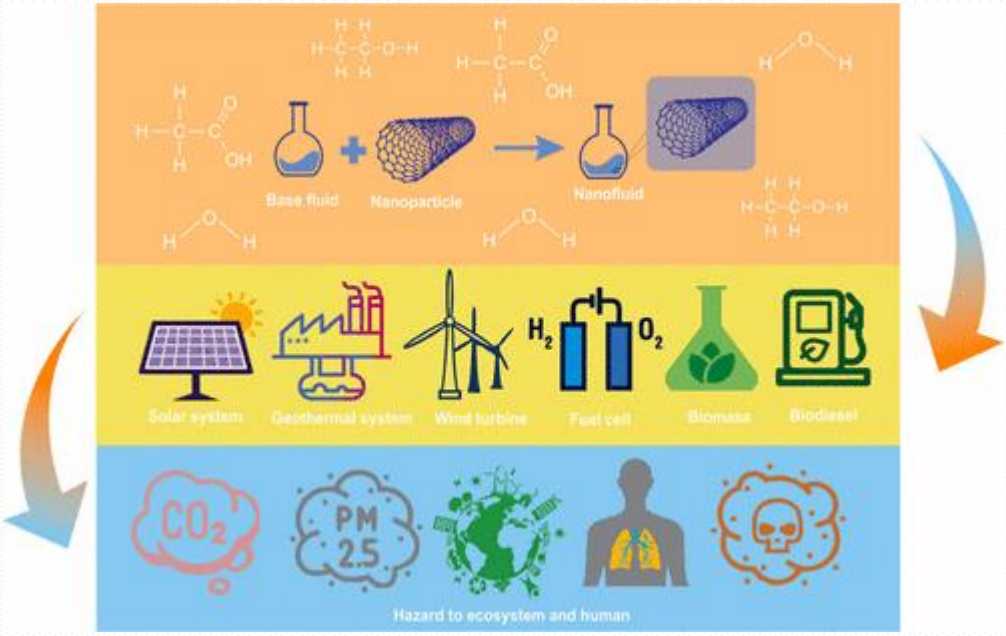


Figure 16. Environmental impacts of nanofluids.

9. Conclusions

Based on this part, some conclusions can be drawn in the following bullets:

- Nanofluids represent a major advancement in improving thermal and energy transport systems, offering enhanced performance and better stability.

- Their ability to deliver superior efficiency opens up applications across various industrial sectors.
- However, further research is needed to optimize their stability, cost, and environmental impact.
- Future prospects focus on hybrid nanofluids and multi-component mixtures (ternary and quaternary), which promise even greater performance.
- These innovations highlight the potential of nanofluids to revolutionize energy and thermal management technologies.
- The use of nanofluids as solar collectors is gaining traction as an appealing research area. Numerous studies on parabolic trough collectors (PTC) utilizing nanofluids have been published. However, these studies mainly focus on nanofluids with water as the base fluid and operate at temperatures below 100°C.

CHAPITRE II:

OVERVIEW OF MACHINE LEARNING

CHAPTER II : *Overview of Machine learning*

1. Introduction

The application of machine learning (ML) and deep learning (DL) methods in modeling and predicting the properties of nanofluids has emerged as a transformative approach in materials science and engineering. Nanofluids, which are colloidal suspensions of nanoparticles in base fluids, exhibit enhanced thermophysical, optical, and electrical properties compared to conventional fluids. These unique characteristics make them highly desirable for applications in heat transfer, energy storage, biomedical systems, and advanced cooling technologies. However, accurately predicting and optimizing the properties of nanofluids, such as thermal conductivity, viscosity, specific heat, and heat transfer coefficients, remains a significant challenge due to the complex interactions between nanoparticles and base fluids, as well as the influence of factors like particle size, concentration, and temperature [78].

Traditional methods for characterizing nanofluids rely heavily on experimental measurements and numerical simulations, which are often time-consuming, expensive, and limited in scope. Machine learning and deep learning techniques, on the other hand, provide a data-driven alternative that can efficiently model the nonlinear relationships and intricate dependencies inherent in nanofluid systems. By leveraging large datasets from experimental studies, molecular dynamics simulations, or computational fluid dynamics (CFD) models, ML and DL algorithms can identify patterns and correlations that are difficult to capture using conventional methods [79].

Recent advancements in optimization techniques have further enhanced the performance of ML and DL models in this domain. Optimization methods such as Bayesian optimization, genetic algorithms, particle swarm optimization, and gradient-based approaches (e.g., Adam, RMSprop) are being employed to fine-tune hyperparameters, improve model accuracy, and reduce computational costs. These methods enable the development of robust predictive models that can generalize well across diverse datasets and experimental conditions. For instance, Bayesian optimization has been used to optimize the architecture of neural networks, while genetic algorithms have been applied to select the most relevant features for predicting nanofluid properties [80].

Deep learning models, particularly convolutional neural networks (CNNs) and recurrent neural networks (RNNs), have shown remarkable success in handling high-dimensional data and capturing temporal or spatial dependencies in nanofluid systems. For example, CNNs can be used to analyze microscopy images of nanofluids to predict particle dispersion and stability, while RNNs are well-suited for modeling time-dependent properties such as heat transfer performance under dynamic conditions. Additionally, transfer learning techniques allow pre-

trained models to be adapted for specific nanofluid applications, reducing the need for extensive datasets and training time [81].

The integration of ML and DL with recent optimization methods has also facilitated the discovery of novel nanofluids with tailored properties. By combining predictive models with optimization algorithms, researchers can identify optimal nanoparticle compositions, concentrations, and operating conditions to achieve desired performance metrics. This approach not only accelerates the design and development of nanofluids but also minimizes the reliance on trial-and-error experimentation, leading to cost savings and faster innovation [81].

Despite these advancements, challenges remain in ensuring the reliability and interpretability of ML and DL models for nanofluid applications. Issues such as data scarcity, model overfitting, and the need for explainable AI (XAI) techniques must be addressed to build trust in these predictive tools. Furthermore, the integration of physics-based constraints into ML models, known as physics-informed neural networks (PINNs), is an emerging trend that promises to enhance the accuracy and generalizability of predictions by incorporating domain knowledge [81].

In conclusion, the use of machine learning and deep learning methods, combined with recent optimization techniques, offers a powerful framework for modeling and predicting the properties of nanofluids. These approaches enable researchers to explore the vast design space of nanofluids more efficiently, paving the way for the development of advanced materials with superior performance. As the field continues to evolve, interdisciplinary collaboration between data scientists, material scientists, and engineers will be essential to unlock the full potential of these technologies and drive innovation in nanofluid research and applications [82].

The history of machine learning (ML) dates back to the mid-20th century, with its roots in artificial intelligence (AI) and statistics. In the 1950s, Alan Turing proposed the idea of machines that could learn, laying the foundation for ML. The 1950s and 1960s saw the development of early algorithms like the perceptron, a simple neural network model. However, progress slowed due to limited computational power and data. The 1980s marked a resurgence with the advent of decision trees and backpropagation, enabling more complex neural networks. The 1990s introduced Support Vector Machines (SVM) and ensemble methods like Random Forests, which improved model accuracy [83].

The 2000s brought a data explosion and advancements in computing, leading to the rise of deep learning. Breakthroughs in neural networks, such as convolutional neural networks (CNNs) and recurrent neural networks (RNNs), revolutionized fields like image and speech recognition [83].

2. Real-world applications of ML

Artificial Intelligence (AI), particularly Machine Learning (ML), has advanced significantly in recent years, becoming essential for intelligently analyzing data and creating real-world applications [84,85]. For example, ML has become the preferred approach for developing practical software solutions.

Machine learning has found applications in diverse fields, including healthcare (diagnosis and drug discovery), finance (fraud detection and algorithmic trading), natural language processing (NLP), computer vision, and materials science. In the context of nanofluids, ML techniques are increasingly being used to model and predict thermophysical properties, optimize nanoparticle compositions, and design advanced fluids for specific applications [86,87] (Figure 1).

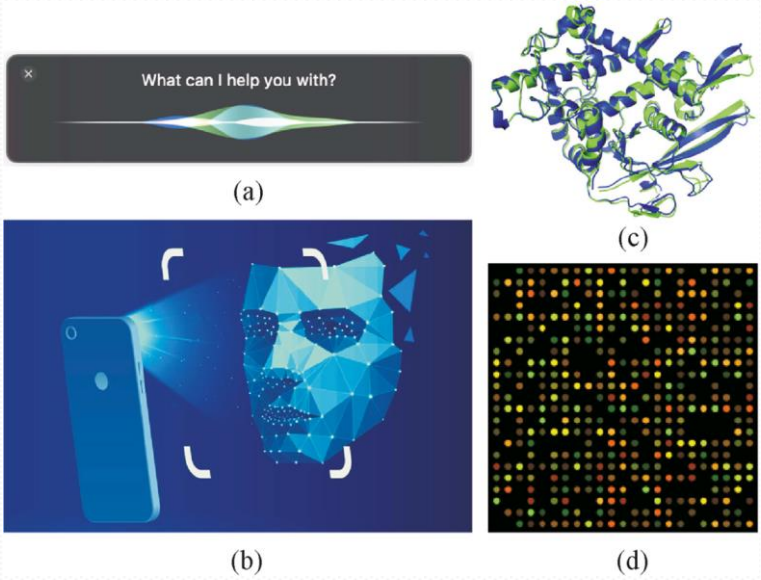


Figure 1. Practical Applications of Machine Learning [1], a) Speech recognition and processing. b) Facial recognition technology, c) Predicting the three-dimensional structures of proteins. d) Cancer classification using DNA microarray analysis.

The influence of machine learning has been equally widespread across scientific disciplines, enabling researchers to advance in areas such as cancer classification through DNA microarray analysis [88] and addressing one of biology's most significant challenges: predicting the three-dimensional structure of proteins from amino acid sequences [89]. Additionally, the COVID-19 pandemic has accelerated the adoption of ML for predicting SARS-CoV-2 diagnoses based on symptoms and for identifying potential drugs and vaccines through computational methods [90]. The effectiveness and efficiency of a machine learning solution largely depend on the nature and characteristics of the data, as well as the performance of the learning algorithms. To address the diverse challenges posed by various types of data and

problems, a wide range of ML algorithms such as supervised, unsupervised, semi-supervised, and reinforcement learning has been developed [91,92].

Some gaps in AI research have been addressed in recent years. Previously, studies were split between technological aspects (linked to natural sciences and engineering) and social aspects (linked to social sciences and humanities). These two perspectives have now been integrated, recognizing that AI cannot be treated as neutral or detached from societal contexts. As Emma Dahlin noted, understanding AI and ML requires acknowledging their inseparable connection to social concerns, and improving human-AI interaction demands greater focus on explainability, transparency, and reducing the "black-box" nature of these systems [1]. Figure 2a illustrates the annual count of ML-related publications since 1990, highlighting a stagnant phase in the 1990s when ML was primarily applied in logistics, medical diagnostics, and industry, followed by a surge in research output starting in the early 2000s, peaking in 2016. Figure 2b shows the application of ML in percentage.

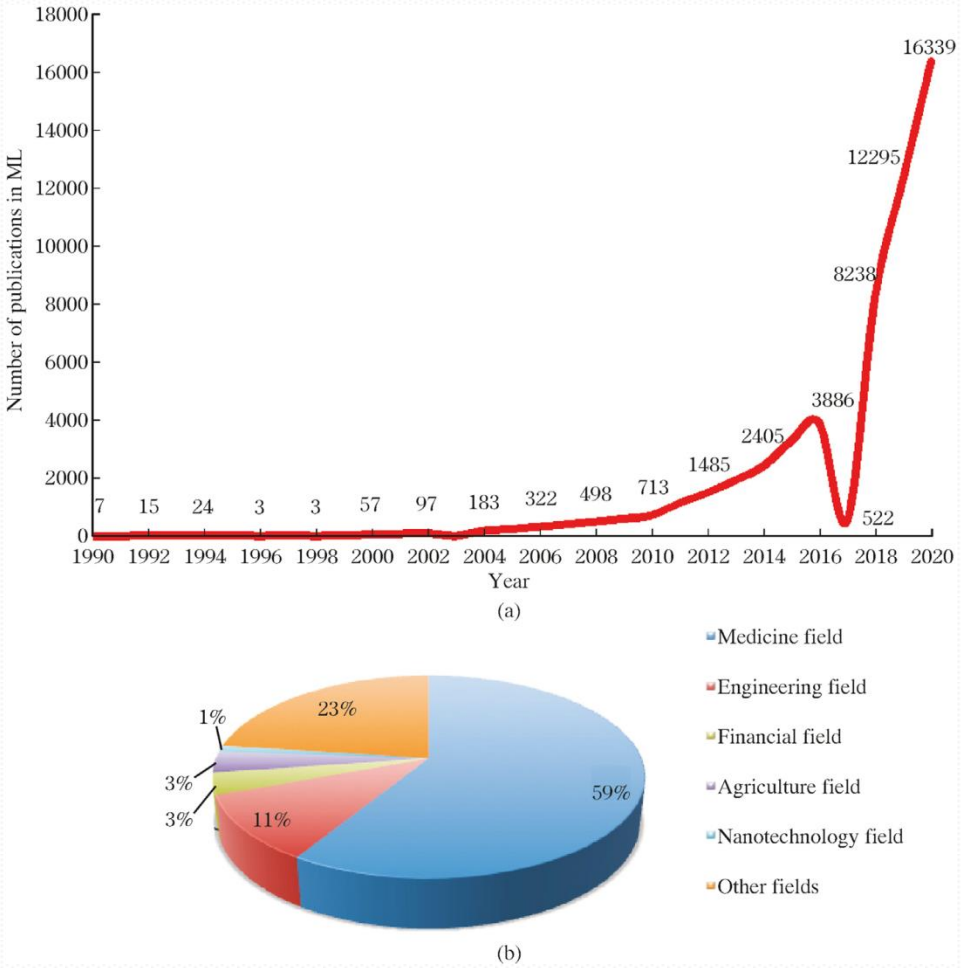


Figure 2. Evolution of Machine Learning Publications Over Time. a) Trends in the number of machine learning-related articles published over time; b) estimated relative percentages of these publications as of 2020 [1].

3. Types of machine learning

Machine learning (ML) is a transformative branch of artificial intelligence (AI) that empowers systems to learn from data, identify patterns, and make decisions with minimal human intervention. By leveraging statistical techniques and computational algorithms, ML enables the development of models that can generalize from existing data to make accurate predictions or decisions on new, unseen data. This chapter provides a comprehensive introduction to the fundamental concepts, types, and applications of machine learning, setting the stage for its integration into advanced fields such as nanofluid research.

Machine learning is broadly categorized into three main paradigms: supervised learning, unsupervised learning, and reinforcement learning. Each paradigm addresses different types of problems and employs distinct methodologies to extract insights from data.

3.1. Supervised Learning

This approach involves training models on labeled datasets, where each input data point is associated with a corresponding output label. The goal is to learn a mapping between inputs and outputs, enabling the model to predict outcomes for new data. Supervised learning is widely used for tasks such as classification (e.g., spam detection, image recognition) and regression (e.g., predicting house prices, temperature forecasting). Popular algorithms in this category include linear regression, logistic regression, support vector machines (SVMs), and neural networks. Classification algorithms and regression methods (refer to Figure 3) are two common forms of supervised learning used extensively for building predictive models.

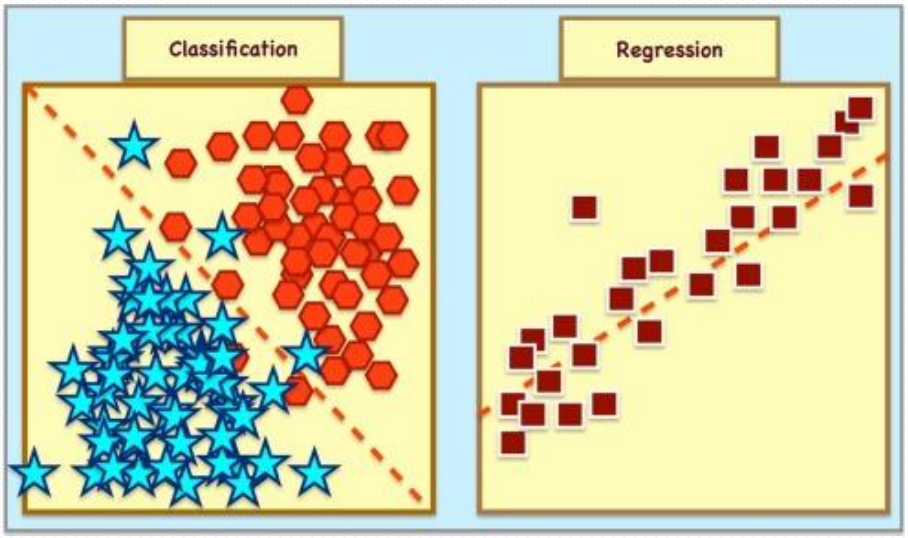


Figure 3: Illustration of Supervised Learning [93].

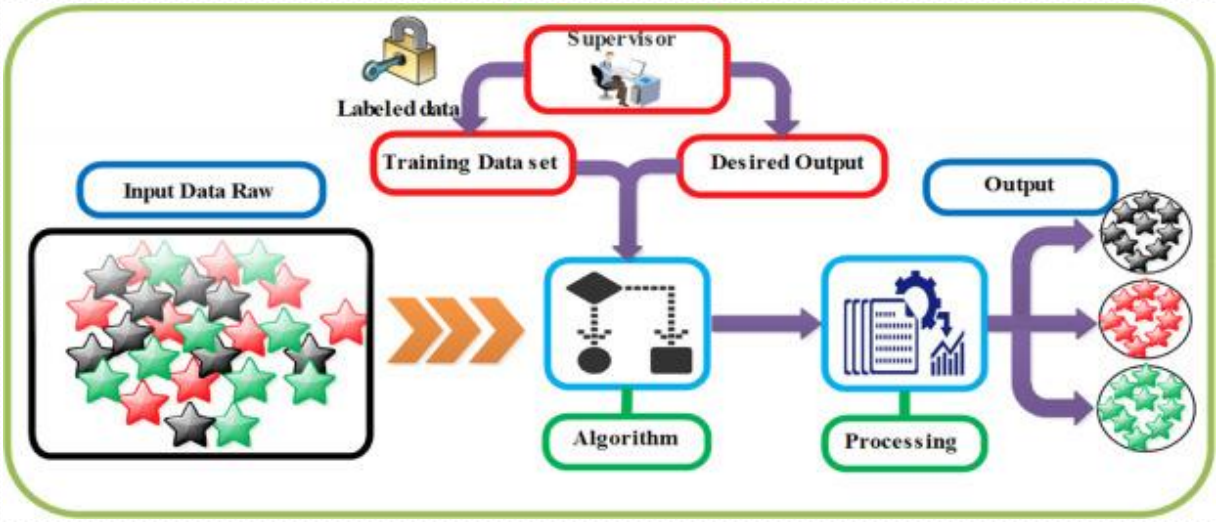


Figure 4. Supervised Learning approach [94].

3.2. Unsupervised Learning:

In unsupervised learning, the model is trained on unlabeled data, with the objective of identifying hidden patterns or structures within the dataset. Common tasks include clustering (grouping similar data points) and dimensionality reduction (simplifying data while retaining essential information). Algorithms such as k-means clustering, hierarchical clustering, principal component analysis (PCA), and t-distributed stochastic neighbor embedding (t-SNE) are frequently used in this domain. Unsupervised learning is particularly useful for exploratory data analysis, anomaly detection, and customer segmentation.

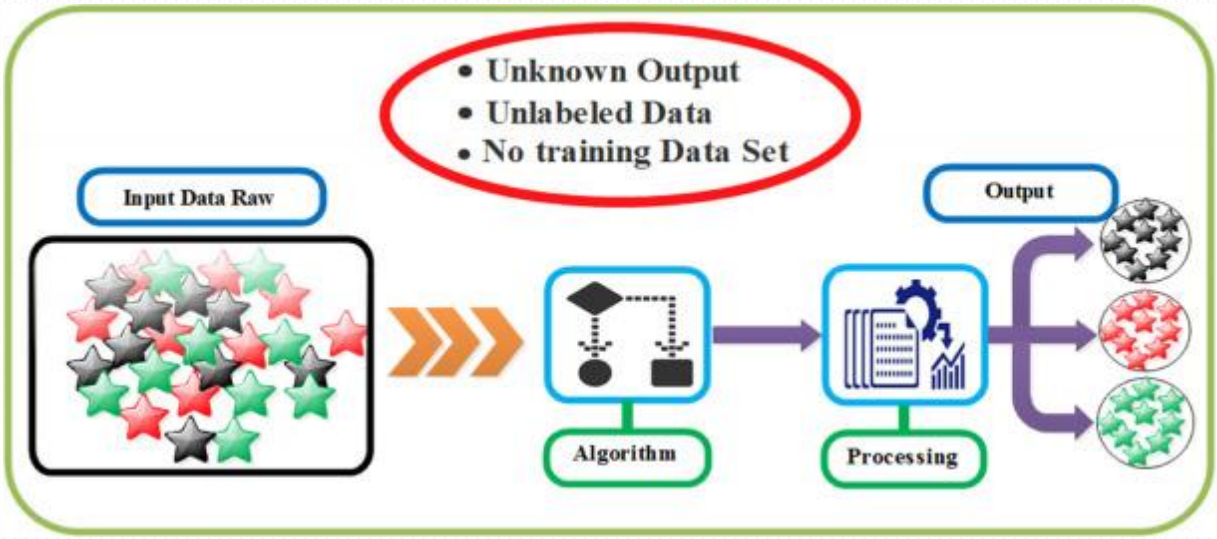


Figure 5. Unsupervised Learning approach [94].

3.3. Semi-supervised learning

It combines elements of supervised and unsupervised learning by utilizing both labeled and unlabeled data (Zhou and Belkin, 2014). Its primary objective is to enhance prediction accuracy beyond what can be achieved using only labeled data. This approach is particularly effective in applications such as machine translation, fraud detection, data labeling, and text classification. By leveraging the strengths of both labeled and unlabeled datasets, semi-supervised learning offers improved performance in various machine learning tasks.

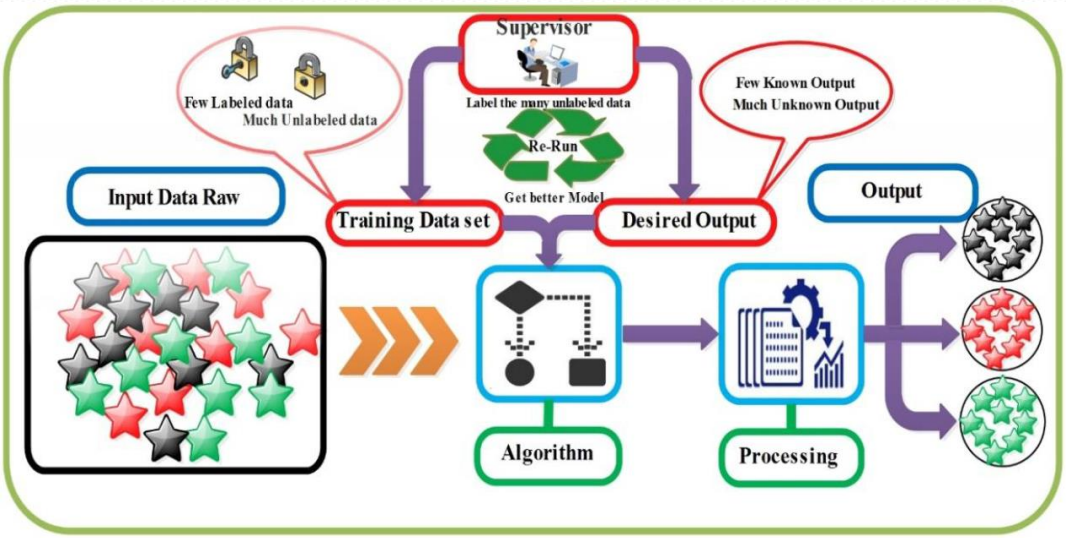


Figure 6. Illustration of the Semi-supervised Learning Approach [94].

3.4. Reinforcement Learning

Reinforcement learning (RL) focuses on training an agent to make sequential decisions by interacting with an environment. The agent learns through trial and error, receiving rewards or penalties based on its actions, and aims to maximize cumulative rewards over time. RL has been successfully applied in areas such as game playing (e.g., AlphaGo), robotics, and autonomous systems. Key algorithms in this category include Q-learning, deep Q-networks (DQNs), and policy gradient methods.

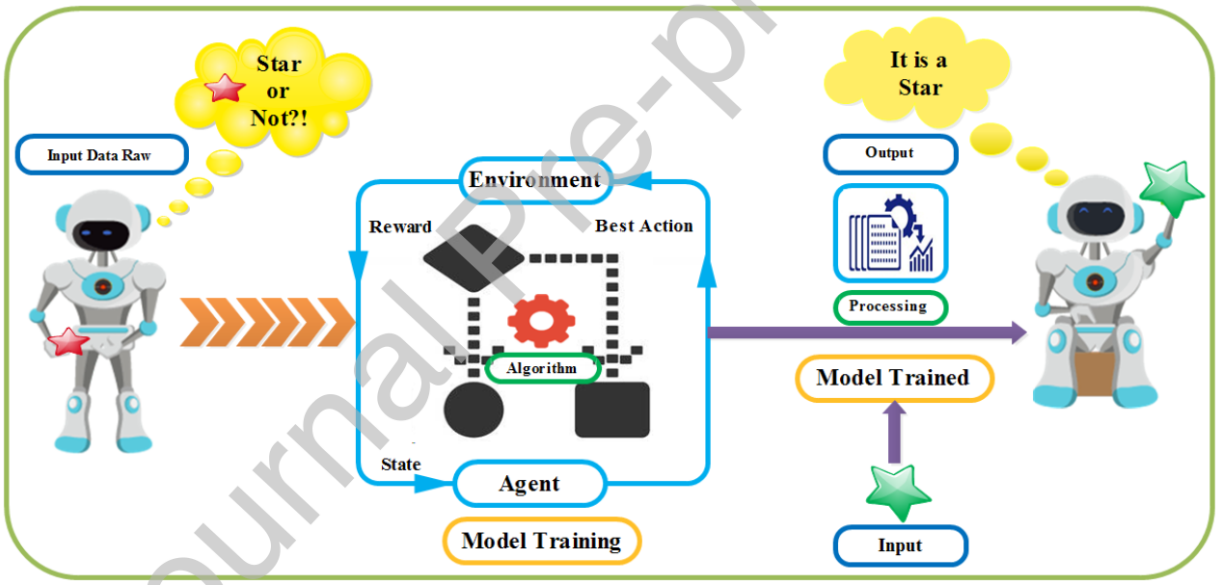


Figure 7. Overview of the Reinforcement Learning Framework [94].

Analysis of global data from Google Trends over the past five years reveals a significant rise in interest and application of reinforcement learning, peaking at a popularity index of 63.5 in 2019, surpassing supervised (30.13) and unsupervised learning (36.75). In contrast, semi-supervised learning, which utilizes both labeled and unlabeled data, has remained stagnant with a low popularity index of 5.6 (Figure 7).

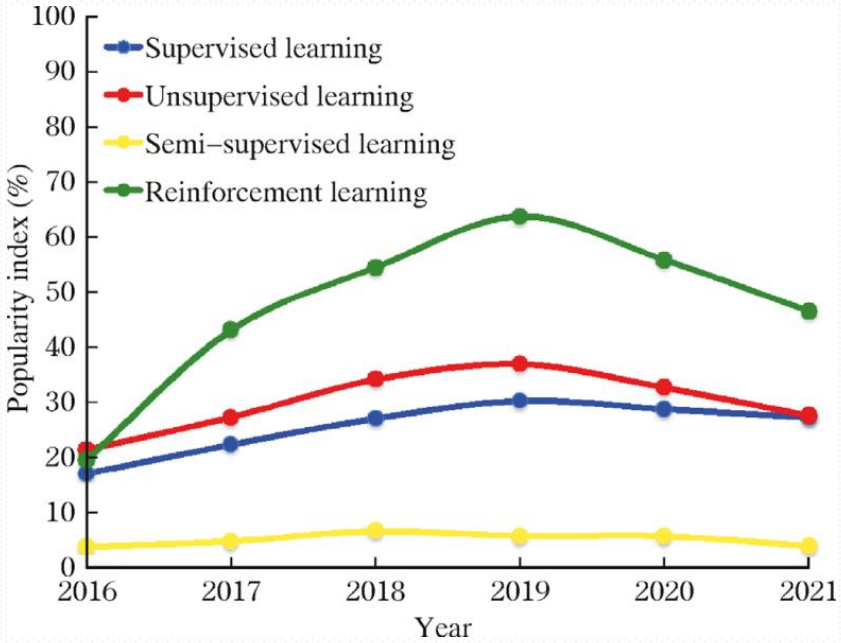


Figure 8. Machine Learning Popularity Index [1].

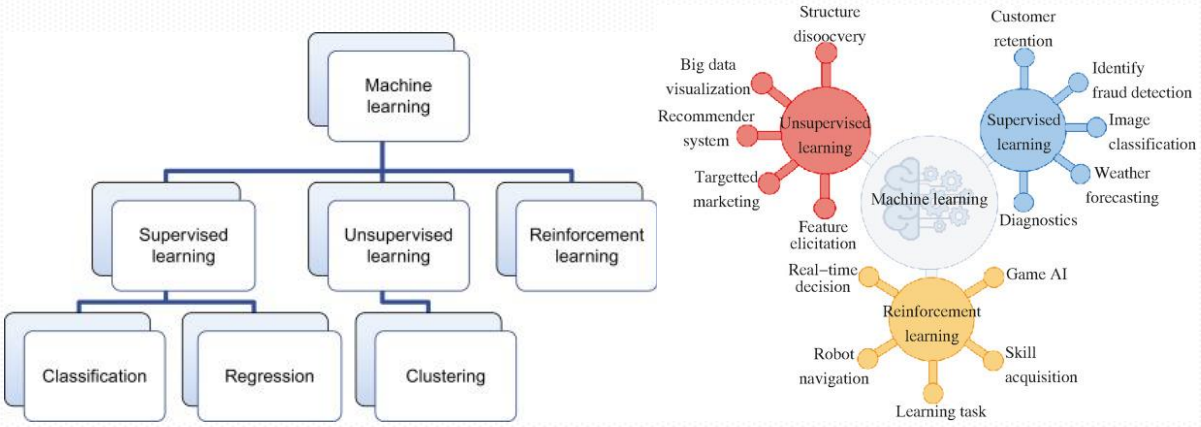


Figure 9. Classification of machine learning algorithms [1].

4. Popular Machine Learning Algorithms

Popular machine learning algorithms form the backbone of many data-driven solutions. Linear Regression predicts continuous outcomes by modeling relationships between variables, while Logistic Regression is used for binary classification tasks. Decision Trees split data into branches to make decisions, and Random Forests combine multiple trees to improve accuracy and reduce overfitting. Neural Networks, inspired by the human brain, power Deep Learning and are ideal for complex tasks like image and speech recognition. Clustering algorithms, such as K-Means and DBSCAN, group similar data points, uncovering hidden patterns in unsupervised learning. Support Vector Machines (SVM) excel in classification by finding optimal boundaries between classes. These algorithms cater to diverse problems, making them essential tools in the machine learning toolkit. the choice of algorithm depends on the nature of the problem, the available data, and the desired outcome.

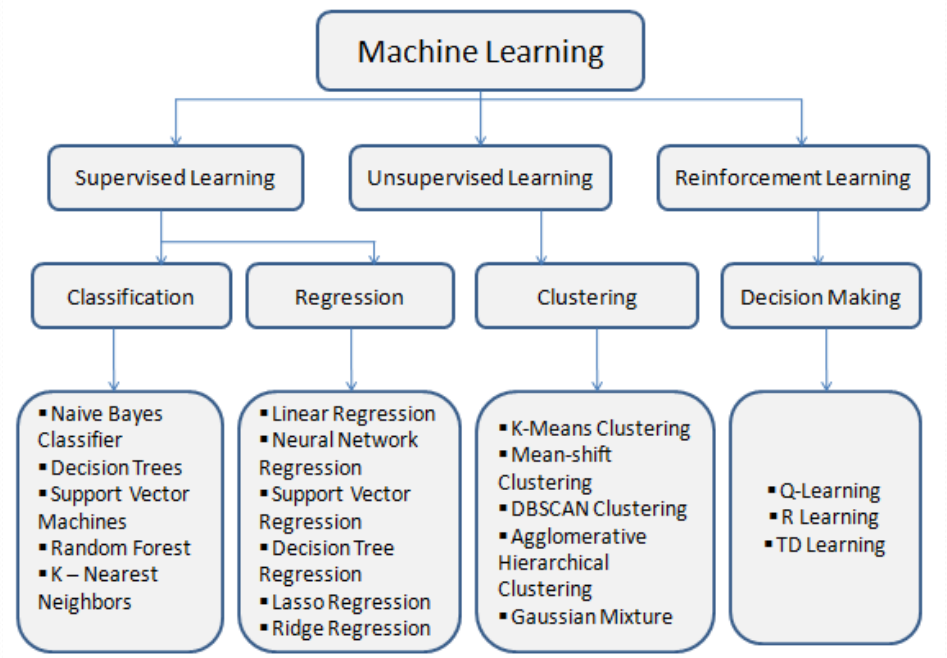


Figure 10. Types of Machine Learning [95].

5. Support vector machine

Support Vector Machines (SVMs) emerged from statistical learning theory, specifically leveraging the structural risk minimization principle. This framework balances two key objectives: minimizing empirical error while controlling the confidence boundary of the learning model, ensuring strong generalization performance [96].

SVMs prove effectiveness by demonstrating exceptional robustness in both classification [97] and regression modeling [98,99], often outperforming methods like neural networks, decision trees, and k-nearest neighbors. While mathematically sophisticated (building on Fermat's Principle (1638), Lagrange Multipliers (1788), and Kuhn-Tucker conditions (1951)) [100], the core idea remains accessible to practitioners. Cortes & Vapnik's [101] foundational work established its modern form. SVMs transform input data into a higher-dimensional feature space through kernel functions. This mapping simplifies complex classification boundaries by making them linearly separable in the transformed space.

The kernel trick allows SVMs to implicitly encode domain-specific knowledge without explicitly calculating high-dimensional transformations. This dual optimization minimizes both model complexity and prediction error simultaneously, enabling SVMs to uncover intricate relationships between input variables and system outputs. This formulation combines theoretical rigor with practical effectiveness, explaining SVMs' enduring popularity in machine learning [96].

Support Vector Machine (SVM) [102] is a statistical learning technique that transforms input data from its original low-dimensional space into a higher-dimensional feature space. It then utilizes a kernel function to derive a linear regression model in this new space.

The input data set is as follows: $\left\{\left(x_i^{(m)}, y_i\right), i = 1,2,\dots,N; m = 1,2,\dots,n\right\}$

Herein: $x_i^{(m)}$ represents the *i*-th element in *m*-th dimensional space, y_i denotes the scalar output, and *N* refers to the number of data sets.

The regression function of SVM is expressed as follows:

$$f(x) = (\lambda, x) + b$$

Here, λ represents the weight vector, and b is the intercept of the regression function, also referred to as the bias term.

SVM regression involves minimizing the following regularized risk function:

$$R_{emp}(f) = \frac{1}{N}\sum_{i=1}^{n} L_\varepsilon\left(y_i - f(\lambda, x_i)\right) + \frac{1}{2}\|\lambda\|^2$$

Where:

$$L_\varepsilon(y - f(\lambda, x)) = \begin{cases} 0 \; if \; |y - f(\lambda, x)| \leq \varepsilon \\ |y - f(\lambda, x)| - \varepsilon \quad otherwise \end{cases}$$

This equation represents the ε-insensitive loss function [103], where the ε-value determines the permissible error margin for the regression function f(x). The optimal solution is obtained by minimizing the following expression:

Minimize : $\frac{1}{2}\|\lambda\|^2 + C\sum_{i=1}^{n}(\xi + \xi^*)$

subject to $\begin{cases} y_i - f(x_i, \lambda) - b \leq \varepsilon + \xi_i^* \\ f(x_i, \lambda) + b - y_i \leq \varepsilon + \xi_i \\ \xi_i^*, \xi_i \geq 0 \end{cases}$

In this model, C is the penalty factor, ξ_i, ξ^* i ($i = 1, \ldots n$) represent (non-negative) slack variables quantifying the deviation of training samples outside ε-insensitive zone.

This nonlinear regression problem can be expressed as the following optimization problem depicted in Figure 11:

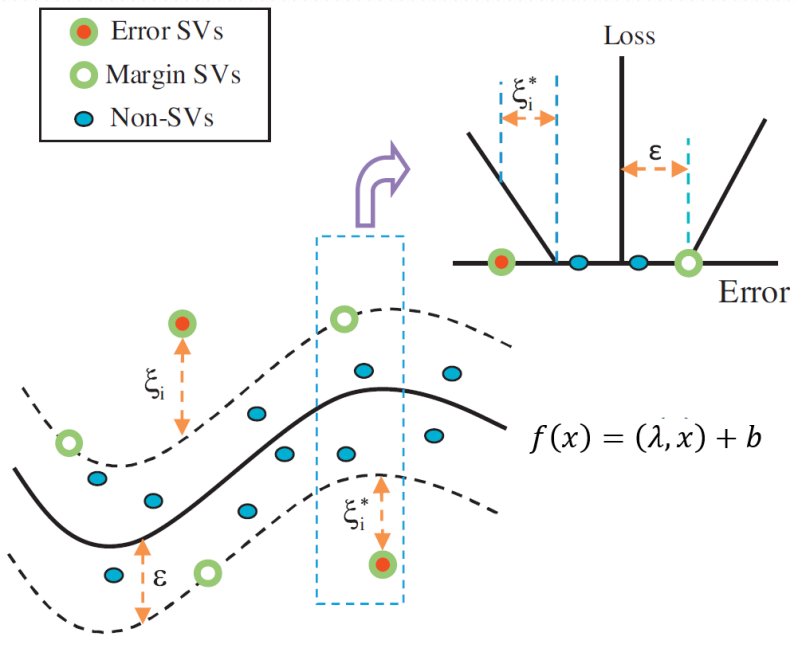


Figure 11. Nonlinear SVR with Vapnik's ε-insensitive loss function [104].

Maximize:

$$-\frac{1}{2}\sum_{i,j=1}^{n}(\alpha_i - \alpha_i^*)(\alpha_j - \alpha_j^*)(x_i - x_j) - \varepsilon\sum_{i=1}^{n}(\alpha_i - \alpha_i^*) + \sum_{i=1}^{n} y_i(\alpha_i - \alpha_i^*)$$

subject to $\begin{cases} \sum_{i=1}^{n}(\alpha_i - \alpha_i^*) = 0 \\ 0 \leq \alpha_i, \alpha_i^* \leq C \end{cases}$

where α_i and α_i^* denote respectively Lagrange multipliers and an optimal desired weight vector of the regression hyper-plane as mathematically defined in the following equation:

$$f(x) = \sum_{i=1}^{n} (\alpha_i - \alpha_i^*)\,(x_i, x_j) + b$$

The final regression function is listed as follows:

$$f(x) = \sum_{i=1}^{n} (\alpha_i - \alpha_i^*) K\,(x_i, x_j) + b$$

The kernel function $K(x_i, x_j)$ is equivalent to the inner product of two vectors in the high-dimensional feature space $\varphi(x_i)$ and $\varphi(x_j)$. That is, $K(x_i, x_j) = \langle \phi(x_i), \phi(x_j) \rangle$. In nonlinear regression problems, the general kernel function is the Gaussian radial basis kernel function (RBF) defined in the next equation:

$$K(x_i, x_j) = exp(-\gamma \|x_i, x_j\|)(\gamma > 0)$$

C, ε and γ in the SVM model have synergetic impact on the accuracy of training and estimated data. The performance of nonlinear Support Vector Regression (SVR) hinges on these three interdependent parameters: C governs the trade-off between model simplicity and training data fidelity, lower values risk underfitting by oversmoothing approximations, while higher values promote overfitting by prioritizing empirical error minimization. ε regulates regression precision via the ε-tube's width: narrower margins (small ε) increase support vector counts and model complexity, whereas wider margins (large ε) yield flatter functions with enhanced generalization. Both parameters co-influence the learning machine's behavior, as adjusting one necessitates recalibrating others to balance sparsity, accuracy, and computational efficiency. Kernel parameters further modulate these dynamics by defining implicit feature-space mappings. Optimizing these values typically requires iterative heuristic tuning rather than analytical solutions, as depicted in the architectural framework of Figure 11.

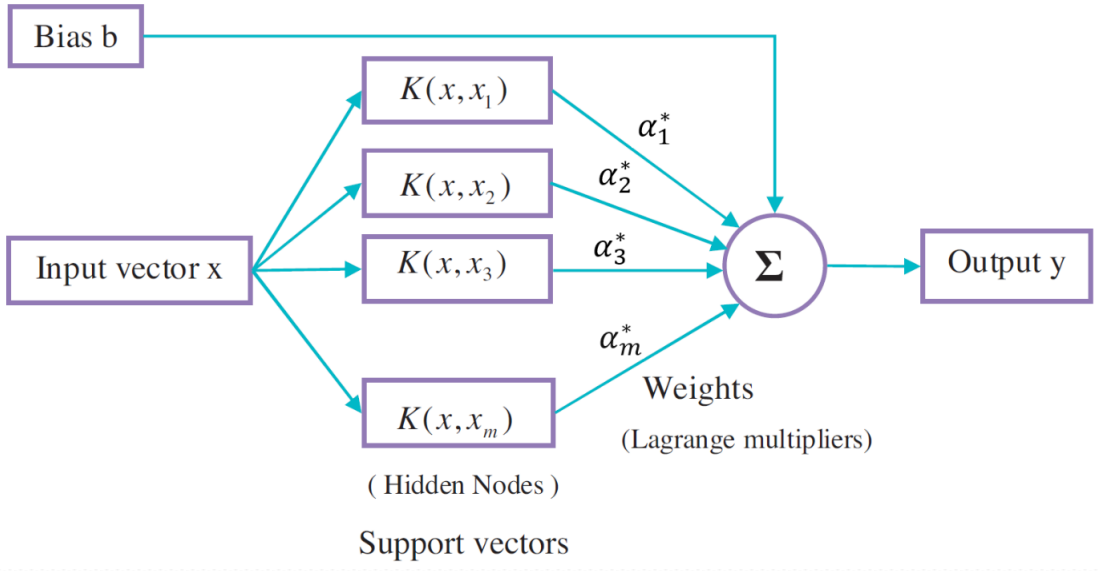


Figure 12. Network architecture of SVM [105].

6. Machine Learning Workflow

The machine learning workflow is a structured process that transforms raw data into actionable insights. It begins with data collection and preprocessing, where relevant data is gathered and cleaned to ensure quality and consistency. Next, feature engineering and selection involves identifying and creating meaningful input variables to improve model performance. Once the data is ready, model selection and training takes place, where an appropriate algorithm is chosen and trained on the dataset. Hyperparameter tuning follows, optimizing the model's parameters to enhance accuracy and efficiency. Finally, the model undergoes evaluation using metrics like accuracy or precision, and if satisfactory, it is deployed for real-world use. This iterative workflow ensures robust and reliable machine learning solutions (Figure 13).

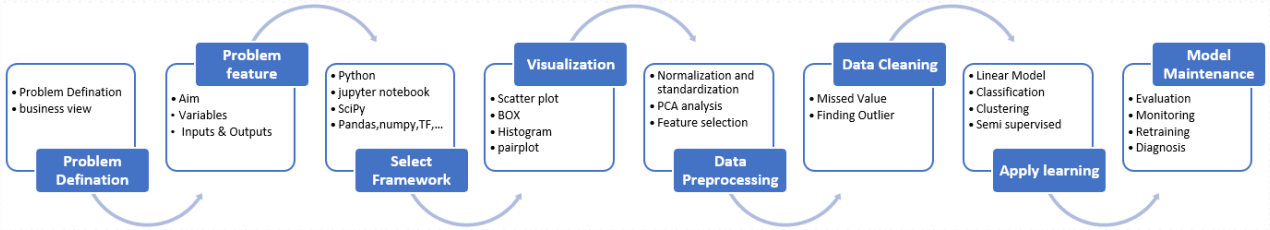


Figure 13. Machine Learning Workflow [106].

7. Overfitting and Underfitting

Overfitting and underfitting are two critical challenges in machine learning that impact a model's ability to generalize to new data. Overfitting occurs when a model learns the training data too well, capturing not only the underlying patterns but also noise and irrelevant details. This results in excellent performance on the training data but poor performance on unseen or test data. Overfitting is often caused by overly complex models, such as deep neural networks or decision trees with too many branches. To combat overfitting, techniques like regularization (e.g., L1/L2 regularization), dropout in neural networks, pruning in decision trees, and early stopping are commonly used. Additionally, increasing the amount of training data or simplifying the model can help reduce overfitting.

On the other hand, underfitting happens when a model is too simple to capture the underlying patterns in the data. This leads to poor performance on both the training and test datasets, as the model fails to learn the necessary relationships. Underfitting often occurs with overly simplistic models, such as linear regression applied to non-linear data, or when key features are missing. To address underfitting, increasing model complexity, adding more relevant features, or using more advanced algorithms can be effective. Balancing the tradeoff between overfitting and underfitting is essential for building models that generalize well. Techniques like cross-validation, hyperparameter tuning, and ensemble methods can help strike

this balance, ensuring the model performs well on both seen and unseen data. Understanding and addressing these concepts is crucial for developing reliable and accurate machine learning solutions.

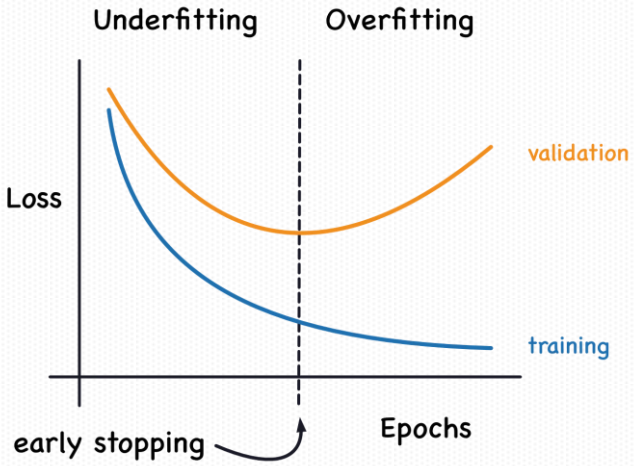


Figure 14. Overfitting & underfitting in machine learning [107].

8. Tools for Machine Learning

Machine learning is powered by a variety of popular libraries and tools that streamline development and analysis. Scikit-learn is a versatile library for traditional ML algorithms, offering tools for classification, regression, and clustering. TensorFlow and PyTorch are leading frameworks for deep learning, enabling the creation of complex neural networks with flexibility and scalability. For data processing, Pandas provides powerful data manipulation capabilities, while NumPy excels in numerical computations and array operations. Visualization is made easy with Matplotlib, a foundational plotting library, and Seaborn, which offers high-level, aesthetically pleasing statistical graphics. Together, these tools form a robust ecosystem for building, analyzing, and visualizing machine learning models efficiently.

9. Conclusions

This chapter provides an overview of machine learning algorithms for intelligent data analysis and their applications. It briefly explores how different ML methods can address real-world challenges, emphasizing that the success of an ML approach relies on both the quality of data and the effectiveness of the learning algorithms. This chapter lays the foundation for understanding how machine learning can be harnessed to address complex challenges in nanofluid research. By combining data-driven approaches with domain-specific knowledge, researchers can unlock new insights and accelerate the development of innovative solutions in this rapidly evolving field.

PART II :

MODELING PART

CHAPTER III :

CONTRIBUTION 01

FOX-Inspired Optimizer with Support Vector Regression Modelling of Water-Based $CaCO_3$-CuO-SiO_2 Trihybrid Nanofluids Thermal Properties: Comparative Study

CHAPITRE III: *Contribution 01 /FOX-Inspired Optimizer with Support Vector Regression Modelling of Water-Based $CaCO_3$-CuO-SiO_2 Trihybrid Nanofluids Thermal Properties: Comparative Study*

1. Introduction

Ternary hybrid nanofluids represent an advanced evolution of hybrid nanofluids, offering significant enhancements in thermophysical properties compared to both traditional and hybrid nanofluids. However, to the best of the authors' knowledge, only a few studies have addressed tri-hybrid nanofluids, whether through experimental investigations or modeling approaches. Therefore, the novelty of this chapter lies in utilizing a support vector machine (SVM) model, enhanced by recent and effective optimization techniques such as the dragonfly and fox optimization algorithms. These algorithms are employed to fine-tune the model's hyperparameters and address the complex nonlinear relationships between two key parameters and their influencing features in tri-hybrid nanofluids, using previously published data from the literature.

2. Methodology

2.1. Data description

The data used in this study were collected from previously published experimental research on CuO-CaCO3-SiO2 in an aqueous solution [25]. These tri-hybrid nanofluids were prepared using SDS as an anionic surfactant and subjected to ultrasonication. The study examined the effects of key parameters, including temperature, volume fraction, and nanoparticle concentration, on the rheological and thermal properties, specifically viscosity and thermal conductivity. Experiments were conducted at temperatures ranging from 15 to 60 °C, with nanoparticle concentrations varying from 0.1 to 0.5 vol%. A summary of the dataset is provided in Table 1 [25].

Table 1. Summary of data extracted from previous experimental study on aqueous trihybrid nanofluids with SDS as Surfactant at various parameters [108] .

Nanoparticles/Base Fluid	Solid Volume Concentration Range (%)	T(°C)	Trihybrid Combination (Vol Ratios)	Data points	References
CuO-$CaCO_3$-SiO_2 / DW	0.1-0.5	15-60	A (0.33, 0.33, 0.33) B (0.50, 0.25, 0.25) C (0.60, 0.30, 0.10) D (0.25, 0.50, 0.25) E (0.25, 0.25, 0.50)	360	[108]

The statistical analysis presented in Table 2 is essential for detecting outliers and errors within the dataset. This comprehensive overview provides detailed insights into the variability

and distribution of the measured properties. For instance, the VR_1 content varies between 0.25% and 0.60%, with a standard deviation of 0.15%, indicating moderate variability. The slight positive skewness of 0.0384 suggests that the distribution of VR_1 content is marginally biased towards higher values.

Table 2. Statistical analysis data.

Variables	VR_1 CuO	VR_2 $CaCO_3$	VR_3 SiO_2	VF (%)	T (°C)	μ (mPa s^{-1})	λ_{thnf} ($Wm^{-1}K^{-1}$)
Min	0.2500	0.2500	0.1000	0.0000	14.5893	0.4543	0.5764
Max	0.6000	0.5000	0.5000	0.5000	60.2995	1.7074	0.9495
Range	0.3500	0.2500	0.4000	0.5000	45.7102	1.2531	0.3731
Mean	0.4222	0.3222	0.2556	0.2500	37.4625	0.8797	0.7504
Geomean mean	0.3942	0.3128	0.2169	0.0000	34.3863	0.8383	0.7457
Harmmean mean	0.3673	0.3051	0.1818	0.0000	31.1419	0.8000	0.7408
Trimmean	0.4219	0.3164	0.2506	0.2500	37.4578	0.8653	0.7497
Kurtosis	1.2421	3.3966	2.1962	1.7314	1.7796	2.7378	2.4875
Moment	0.0001	0.0008	0.0013	0.0000	4.1921	0.0146	0.0000
Skewness	0.0384	1.3242	0.4788	0.0000	0.0014	0.6798	0.0234
Median Absolute Deviation	0.1445	0.0630	0.1074	0.1500	12.4916	0.2298	0.0680
Standard Deviation	0.1510	0.0849	0.1382	0.1710	14.3808	0.2784	0.0845
Interquartile range	0.3500	0.0833	0.2333	0.3000	24.9907	0.4199	0.1083
Variance	0.0228	0.0072	0.0191	0.0292	206.8068	0.0775	0.0071

Similarly, VR_2 and VR_3 exhibit more pronounced skewness, with values of 1.3242 and 0.4788, respectively, indicating distributions that are more significantly skewed towards higher values. The temperature range is extensive, spanning from 14.5893 °C to 60.2995 °C, with a mean of 37.4625 °C and a standard deviation of 14.3808 °C, highlighting substantial thermal variability.

The viscosity and thermal conductivity also display considerable variability, with standard deviations of 0.2784 mPa s^{-1} and 0.0845 $Wm^{-1}K^{-1}$, respectively. The kurtosis values for these properties suggest distributions with sharper peaks compared to a normal distribution, which can impact the accuracy of predictive models.

Understanding these statistical measures is crucial for analyzing the behavior of the ternary hybrid nanofluid under different conditions. For instance, the variability in viscosity

and thermal conductivity can significantly impact the nanofluid's performance in various applications. By leveraging these insights, researchers can optimize the composition and conditions for enhanced thermal and rheological management properties. Besides, this control is vital for effectively applying Support Vector Regression (SVR) models and interpreting the results. By recognizing the central tendency, dispersion, and skewness of the data, researchers can develop more robust models that account for potential outliers and errors, ultimately enhancing the reliability of the predictions.

Violin plots are an effective tool for visualizing data distributions and comparing them across different groups or categories within a dataset. Each plot includes a horizontal line indicating the median value, while the shaded area represents the density of the data. The interquartile range (IQR), which contains the middle 50% of the data, is highlighted within the plot, and the whiskers extend to the minimum and maximum values, excluding any outliers.

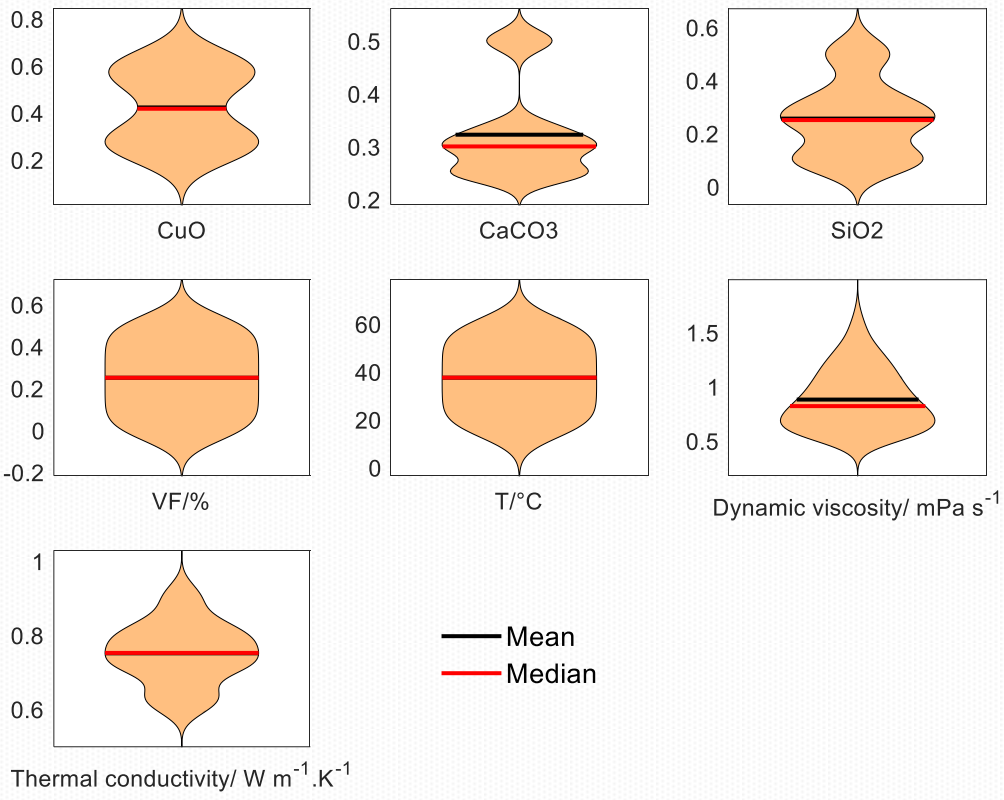


Figure 1. Violin plots illustrating the distribution of the experimental dataset.

The violin plots shown in Figure 1 provide a visual representation of the distribution and density of the dataset's variables, including CuO, $CaCO_3$, SiO_2 volume ratios, volume fraction (VF), temperature (T), dynamic viscosity, and thermal conductivity. CuO and VF exhibit symmetrical distributions centered around their mean and median values, while $CaCO_3$ shows a bimodal distribution with peaks near 0.25 and 0.4. SiO_2 demonstrates slight skewness toward

higher values. Temperature spans a broad range, with most values concentrated between 20 °C and 50 °C. Dynamic viscosity is right-skewed, with most values below 1 mPa s^{-1} but a long tail extending to higher values. Thermal conductivity has a relatively narrow distribution centered around 0.75 $Wm^{-1}K^{-1}$. These plots highlight the variability and central tendencies of the dataset, offering insights into its structure and potential outliers.

2.2. Multicollinearity analysis

Multicollinearity analysis is a statistical method used to evaluate the degree of linear association between two or more independent variables in a regression model. When multicollinearity is high, it can lead to several issues in regression analysis, such as inflated standard errors for regression coefficients, which reduce the precision of estimates and weaken the statistical power of the model. This makes it challenging to interpret the individual contributions of predictors, as their effects become intertwined, resulting in unreliable coefficient estimates and diminished significance. High multicollinearity can also cause instability in coefficient estimates, where small changes in data or model specification lead to large variations in results, further complicating interpretation and decision-making [109–111].

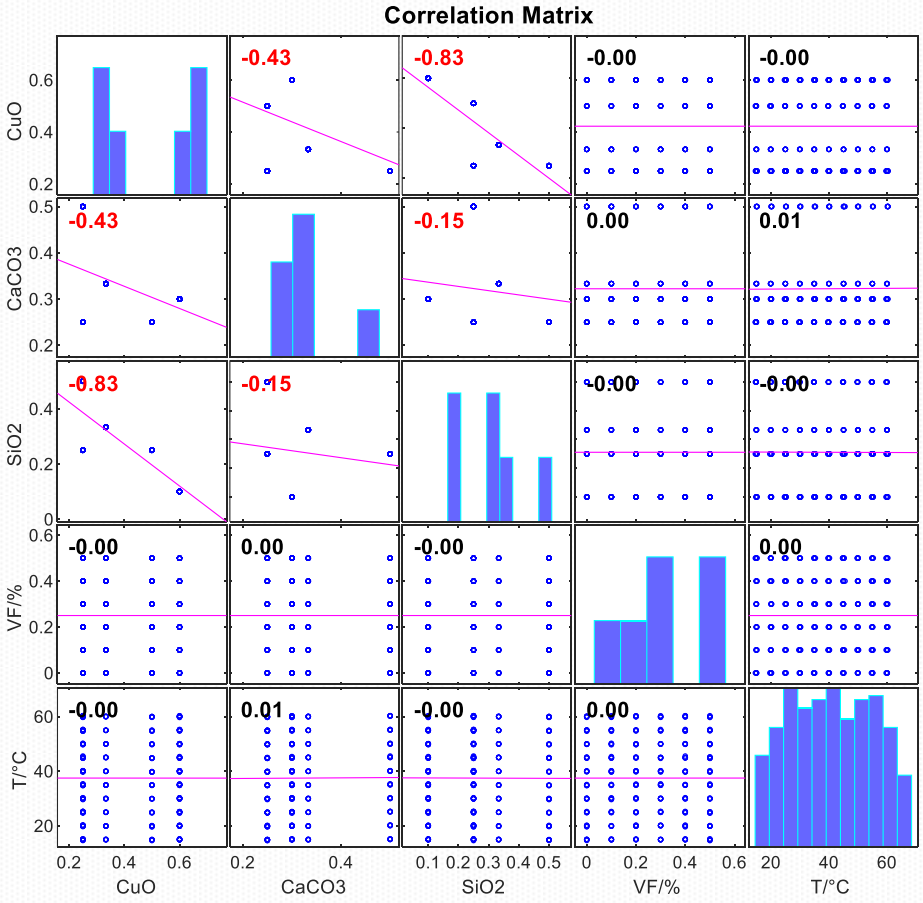


Figure 2. Correlation matrix showing the multicollinearity analysis among the key parameters of the dataset.

This correlation matrix shows the pairwise Pearson correlation coefficients among all the variables, which are likely input variables. The image is a correlation matrix plot that visually represents the relationships among five variables: volume ratios of CuO, $CaCO_3$, SiO_2, volume fraction of nanoparticles (VF) in the nanofluid, and the temperature (T), using a combination of histograms, scatter plots, and numerical correlation coefficients. The diagonal cells display histograms showing the distribution of each variable, such as CuO volume ratio's bimodal distribution and the temperature's uniform spread. The off-diagonal cells contain scatter plots illustrating pairwise relationships, with pink trend lines indicating the direction of any correlation. For instance, CuO and SiO_2 exhibit a strong negative correlation (-0.83), as seen in their downward-trending scatter plot, while CuO and $CaCO_3$ show a moderate negative correlation (-0.43). Conversely, VF and T have no significant relationships with other variables, as indicated by near-zero correlation coefficients and unstructured scatter plots. The red numerical values quantify these correlations, with values ranging from -1 (perfect negative correlation) to 1 (perfect positive correlation), while 0 indicates no relationship. This matrix highlights key insights, such as the inverse dependency between CuO and SiO_2 and the independence of VF and T from other variables, making it a powerful tool for understanding both individual distributions and inter-variable interactions in the dataset.

2.3. Integration of metaheuristic algorithms with support vector regression for predicting thermophysical properties

SVR is a powerful machine learning algorithm derived from the Support Vector Machine (SVM) framework. While SVM is often used for classification tasks, SVR extends its capabilities to regression problems, where the goal is to predict a continuous value instead of discrete classes [112]. SVR aims to find a function that best fits the data while maintaining a balance between prediction accuracy and model complexity. The key idea is to minimize the error within a specified margin (called the epsilon margin), while also ensuring that the function remains as flat as possible to avoid overfitting [113].

The accuracy and generalization capacity of SVR models heavily depend on selecting suitable hyperparameters, including the penalty parameter (C), the kernel parameter (σ), and the insensitive parameter (ε). These hyperparameters control the trade-off between model complexity and prediction error, the ability to capture nonlinear patterns, and tolerance to small deviations from observed data. However, finding the optimal combination of these parameters is challenging due to the high-dimensional search space involved. Traditional trial-and-error methods are inefficient and computationally expensive, making the integration of optimization

algorithms, particularly metaheuristic methods, a promising solution to enhance SVR's predictive performance [113,114].

Metaheuristic algorithms are indeed adaptive strategies inspired by natural processes, designed to efficiently solve complex optimization problems. They offer several advantages over conventional optimization techniques, including their ability to escape local optima and adapt to dynamic problem landscapes. This is because metaheuristics often incorporate stochastic elements, allowing them to explore solution spaces more expansively and avoid getting trapped in suboptimal solutions [115].

The DA mimics the swarming behavior of dragonflies, balancing exploration and exploitation [116]. It is based on five critical factors: separation, alignment, cohesion, attraction toward food sources, and distraction from predators. This allows the algorithm to dynamically adjust its search strategy, making it effective for high-dimensional optimization tasks [117].

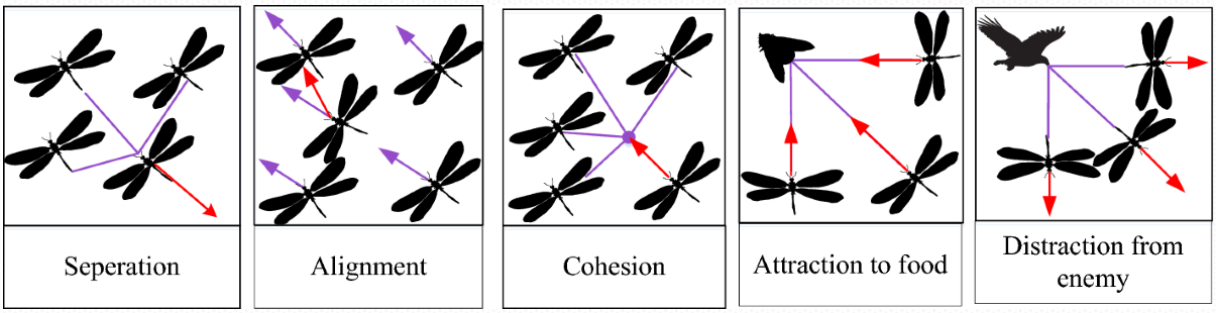


Figure 3. Five main factors controlling dragonflies' behavior [118].

Figure 4 illustrates a flowchart depicting the integration of the Dragonfly Algorithm with SVM for optimizing regression models.

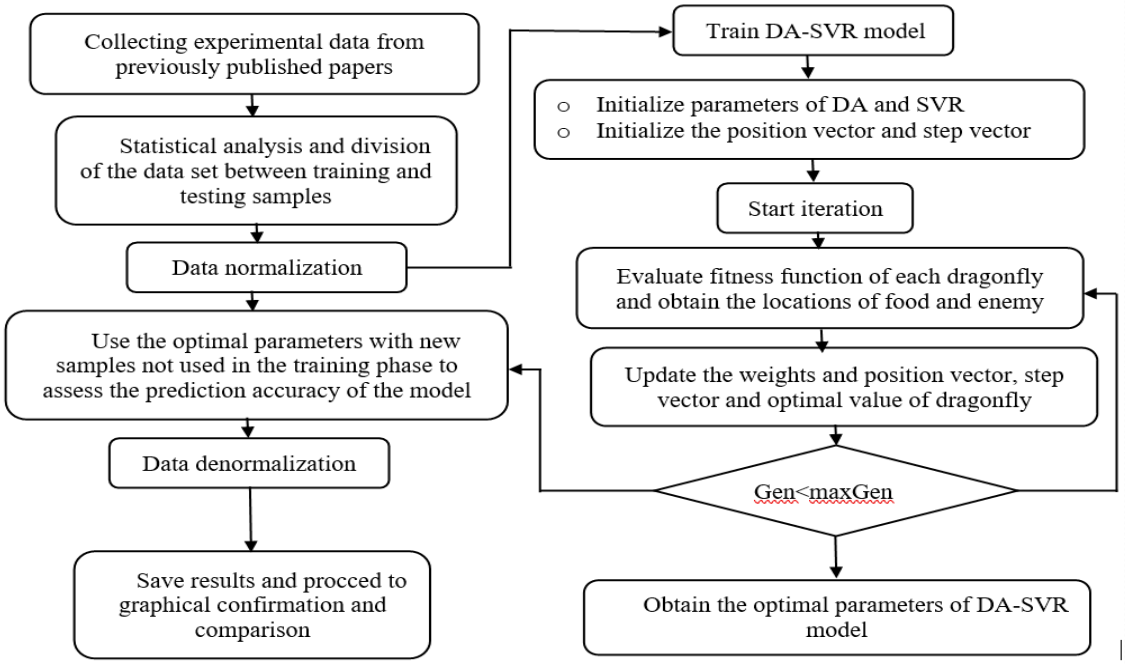


Figure 4. Integration of Dragonfly Algorithm with SVM for Regression Optimization.

The FOX-inspired algorithm simulates the adaptive hunting behavior of red foxes in snowy environments. It emulates two phases of hunting: exploration using ultrasound detection and exploitation by calculating the optimal jump to capture prey. The algorithm's strength lies in its balance between global search and local refinement, ensuring it efficiently converges toward the global solution without getting trapped in local optima [119].

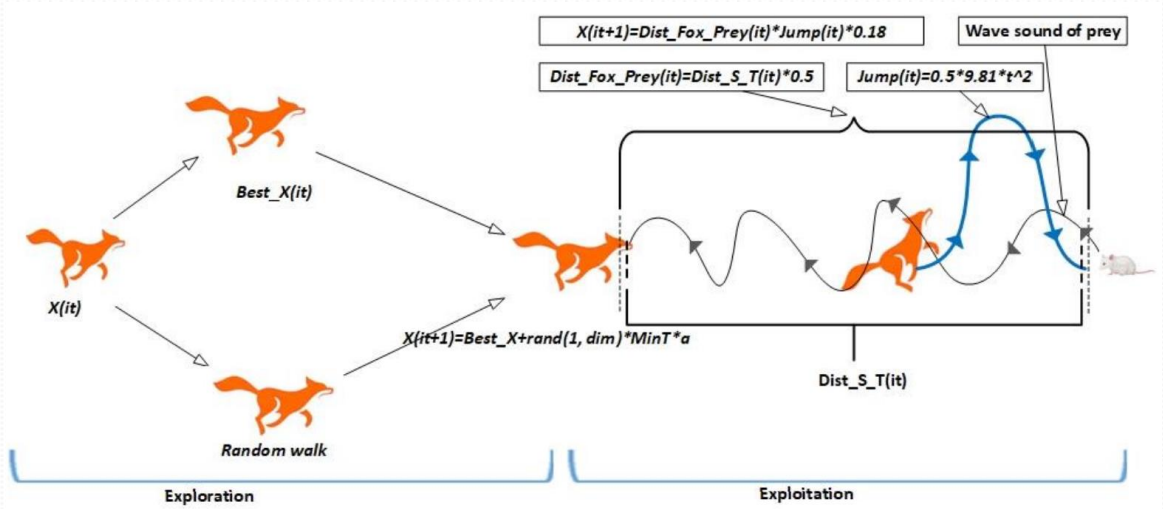


Figure 5. Red Fox hunting behavior: exploration and exploitation [119].

Combining SVR models with metaheuristic optimization algorithms has become a growing trend in machine learning research, especially for complex regression tasks. This hybrid approach leverages SVR's ability to model nonlinear relationships and the adaptive search capabilities of metaheuristic methods, resulting in more robust models capable of handling complex datasets [120].

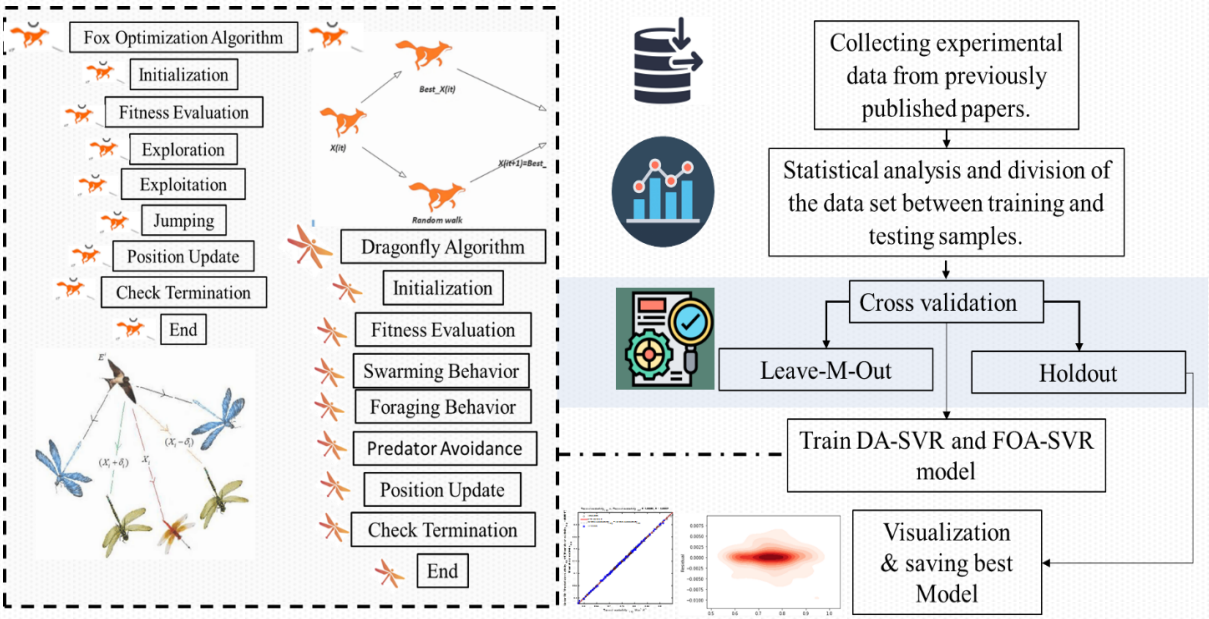


Figure 6. Integration DA and FOA with SVR [121].

Integrating DA and FOA algorithms highlights the potential of such hybrid approaches in achieving precise and reliable predictions for dynamic viscosity and thermal conductivity in hybrid nanofluids. These advancements contribute to developing more efficient predictive tools in engineering applications, reducing the need for expensive experimental measurements while ensuring accurate modeling of complex fluid behaviors.

The DA and FOA were used to randomly generate hyperparameters for the SVR within specified limits. These hyperparameters included the penalty parameter C (ranging from 0 to 10^6), sigma σ (from 10^{-3} to 10^2), the size of the insensitive zone (ε) (from 0 to 10^{-2}), and the kernel function (Gaussian RBF, linear, or polynomial) [121]. This process was repeated five times, with the error (such as the root mean squared error) calculated each time the test data was evaluated. The optimal number of search agents and iterations were determined by selecting the model that produced the lowest error.

2.4. Cross-Validation Approach

To ensure a comprehensive and robust evaluation of the model while minimizing the risk of overfitting, this study employed two cross-validation techniques: holdout cross-validation and Leave-M-Out cross-validation. Both methods were utilized to thoroughly assess the predictive performance of the SVR models, which were optimized using the DA and the FOA. By employing these approaches, the study aimed to provide a reliable and unbiased assessment of the models' ability to generalize well to unseen data, thereby ensuring the validity and reliability of the results.

E. Holdout Cross-Validation

In the holdout cross-validation approach, the dataset was divided into two subsets: 80% of the data was used for training the model, while the other 20% was kept for testing purposes. To ensure the robustness of the results and prevent any bias due to a specific data split, this partitioning process was repeated 100 times with random shuffling of the data. This extensive repetition allowed for a comprehensive evaluation of the model's performance, providing an initial assessment of its ability to generalize well to unseen data. By averaging the results across these multiple iterations, the holdout method offered a reliable estimate of the model's predictive capabilities.

F. Leave-M-Out Cross-Validation

To enhance the validation of the models' robustness, a Leave-M-Out cross-validation technique was used. During each iteration, 72 samples were withheld from the dataset, and the model was trained on the remaining data. These withheld samples were then used to assess the model's predictive performance. This process was repeated 100 times with varying

combinations of withheld samples. By doing so, the method offers a comprehensive assessment by evaluating the model across diverse subsets of the data, which aids in uncovering any potential limitations in the model's generalization capabilities.

G. Evaluation criteria

The model's accuracy was evaluated using a range of metrics to highlight the unique strengths of each predictive model. These metrics included mean square error (MSE), correlation coefficient (R), determination coefficient (R^2), Theil's U_2, relative standard deviation (RSD), mean absolute error (MAE), mean relative percentage error (MRPE), average absolute relative deviation (AARD), and root mean square error (RMSE) [122–125]. The mathematical formulations for these metrics are detailed in Equations (1) to (9) as follows:

$$R = \frac{\sum_{i=1}^{n}(y_{i,exp}-\bar{y}_{i,exp})(y_{i,pri}-\bar{y}_{i,pri})}{\sqrt{\sum_{i=1}^{n}(y_{i,exp}-\bar{y}_{i,exp})^2 \times \sum_{i=1}^{n}(y_{i,pri}-\bar{y}_{i,pri})^2}} \quad (1)$$

$$MAE = \frac{\sum_{i=1}^{n}|y_{i,pri-DA}-y_{i,exp}|}{n} \quad (2)$$

$$[U_2]_{Thei1} = \left[\frac{\sqrt{\sum_{i=1}^{n}(y_{i,exp}-y_{i,pri})^2}}{\sum_{i=1}^{n} y_{i,exp}^2}\right] \quad (3)$$

$$RSD = \frac{\sqrt{\frac{\sum_{i=1}^{n}(y_{i,exp}-y_{i,pri})^2}{n}}}{\bar{y}_{i,exp}} \times 100 \quad (4)$$

$$MAE = \frac{\sum_{i=1}^{n}|y_{i,exp}-y_{i,pri}|}{n} \quad (5)$$

$$AARD = 100 \times \frac{\sum_{i=1}^{n}\left(\frac{|y_{i,exp}-y_{i,pri}|}{y_{i,exp}}\right)}{n} \quad (6)$$

$$RMSE = \sqrt{\frac{\sum_{i=1}^{n}(y_{i,exp}-y_{i,pri})^2}{n}} \quad (7)$$

$$R^2 = 1 - \frac{\sum_{i=1}^{n}(y_{i,exp}-y_{i,pri})^2}{\sum_{i=1}^{n}(y_{i,exp}-\bar{y}_{i,exp})^2} \quad (8)$$

Where "n" represents the size of the dataset, the terms "$y_{i,exp}$" and "$y_{i,pri}$" denote the actual experimental and the predicted values, respectively. Additionally, "$\bar{y}_{i,exp}$" refers to the mean of the experimental values.

3. Results and Discussion

This section provides a comprehensive evaluation of how well two thermophysical properties, dynamic viscosity and thermal conductivity, can be predicted. The predictions were

made using Support Vector Regression (SVR) optimized by two different methods: the Dragonfly Algorithm (DA-SVR) and the FOX-inspired Optimization Algorithm (FOA-SVR). To ensure the robustness of the models, two cross-validation methods were used: Holdout Cross-Validation (H_CV) and Leave-M-Out Cross-Validation (LMO_CV).

Table 3. Hyperparameters results

Method	Model	Penalty parameter $C > 0$	Sigma σ	Size of the insensitive zone (ε)	Kernel function	Quantity of support vectors	Cross validation
DA-SVR	Dynamic viscosity	1.9817×10^{5}	2.9371	1.2686×10^{-4}	Gaussian RBF	288	Holdout 20%
	Thermal conductivity	1.2648×10^{5}	4,6032	6.4220×10^{-6}			
FOA-SVR	Dynamic viscosity	1.8269	1.2971	3.2490×10^{-5}			
	Thermal conductivity	2.8950	1.5342	3.6100×10^{-6}			
DA-SVR	Dynamic viscosity	1.0735×10^{3}	1.6403	3.3924×10^{-4}			LMO 72
	Thermal conductivity	729.9910	2.6356	3.8428×10^{-6}			
FOA-SVR	Dynamic viscosity	2.8313	1.1793	2.8090×10^{-5}			
	Thermal conductivity	17.2937	1.6752	3.7636×10^{-6}			

The models' performance was evaluated using several statistical metrics, including the above cited metrics. The hyperparameter results for both optimized models, using the two algorithms and cross-validation methods, are detailed in Table 3.

Table 4 outlines the performance metrics for the DA-SVR and FOA-SVR models when predicting dynamic viscosity and thermal conductivity. Overall, the results show that both models perform exceptionally well on training data and demonstrate good ability to generalize to new, unseen test data for both properties.

3.1. Dynamic Viscosity Model result

The DA-SVR model showed strong performance in predicting dynamic viscosity under both cross-validation methods, as shown in Tables 3 and 4.

Using the H_CV method, it achieved an RMSE of 0.0113 and an R^2 of 0.9984, indicating high accuracy. The model's hyperparameters suggested a rigid structure focused on minimizing errors. With LMO_CV, the model's performance improved significantly, with an RMSE of 0.0047 and an R^2 of 0.9997, using more flexible hyperparameters.

Table 4. Evaluation of statistical metrics and uncertainty for DA-SVR and FOA-SVR models using global data

Method	Dynamic viscosity evaluation Model										
	Data	**RMSE**	**R^2**	**r**	**b**	**slope**	**AARD**	**MRPE**	**MAE**	**STD**	**U^2**
DA-SVR Holdout_CV	Train	0.0046	0.9997	0.9999	0.0007	0.9991	0.2882	2.6980	0.0024	0.5254	2.50×10^{-5}
	Test	0.0113	0.9984	0.9993	0.0085	0.9907	1.0564	9.2069	0.0084	1.2671	1.44×10^{-4}
	All	0.0065	0.9995	0.9997	0.0023	0.9974	0.4418	9.2069	0.0036	0.7399	4.96×10^{-5}
DA-SVR LMO_CV	Train	0,0058	0,9996	0,9998	-0,0003	1,0010	0,3989	2,9194	0,0033	0,6743	$4,11\times10^{-5}$
	Test	0,0047	0,9997	0,9998	0,0011	0,9990	0,3358	2,8646	0,0026	0,5520	$2,75\times10^{-5}$
	All	0,0059	0,9996	0,9998	-0,0004	1,0010	0,4042	3,8344	0,0034	0,6713	$4,09\times10^{-5}$
FOA-SVR Holdout_CV	Train	0,0051	0,9997	0,9998	0,0004	0,9999	0,3247	2,6191	0,0027	0,5790	3.03×10^{-5}
	Test	0,0077	0,9992	0,9996	0,0043	0,9965	0,7226	2,8909	0,0060	0,8733	6.88×10^{-5}
	All	0,0057	0,9996	0,9998	0,0012	0,9992	0,4043	2,8909	0,0034	0,6491	3.82×10^{-5}
FOA-SVR LMO_CV	Train	0,0055	0,9996	0,9998	-0,0005	1,0006	0,3666	3,5994	0,0030	0,6410	$3,71\times10^{-5}$
	Test	0,0044	0,9997	0,9999	-0,0025	1,0020	0,3239	3,0708	0,0026	0,4758	$2,05\times10^{-5}$
	All	0,0053	0,9996	0,9998	-0,0008	1,0008	0,3581	3,5994	0,0029	0,6075	3,35×10-5
Method	**Thermal conductivity evaluation Model**										
	Data	**RMSE**	**R^2**	**r**	**b**	**slope**	**AARD**	**MRPE**	**MAE**	**STD**	**U^2**
DA-SVR Holdout_CV	Train	0,0020	0,9994	0,9997	0,0015	0,9978	0,1524	1,0197	0,0012	0,2647	$6,89\times10^{-6}$
	Test	0,0025	0,9991	0,9996	0,0025	0,9968	0,2700	1,1255	0,0020	0,3432	$1,15\times10^{-5}$
	All	0,0021	0,9994	0,9997	0,0017	0,9976	0,1759	1,1255	0,0013	0,2813	$7,79\times10^{-6}$
DA-SVR LMO_CV	Train	0,0019	0,9995	0,9997	0,0009	0,9988	0,1603	0,9802	0,0012	0,2614	$6,72\times10^{-6}$
	Test	0,0020	0,9993	0,9997	0,0005	0,9992	0,1672	0,8912	0,0013	0,2641	$6,80\times10^{-6}$
	All	0,0020	0,9995	0,9997	0,0008	0,9988	0,1617	0,9802	0,0012	0,2616	$6,74\times10^{-6}$
FOA-SVR Holdout_CV	Train	0.0018	0.9996	0.9998	0.0010	0.9986	0.1347	0.8730	0.0010	0.2354	$5,45\times10^{-6}$
	Test	0.0024	0.9991	0.9994	-0.0028	1.0038	0.2469	0.9356	0.0019	0.3161	$9,77\times10^{-6}$
	All	0.0019	0.9995	0.9997	0.0005	0.9993	0.1571	0.9356	0.0012	0.2533	$6,32\times10^{-6}$
FOA-SVR LMO_CV	Train	0,0019	0,9995	0,9997	0,0010	0,9987	0,1544	1,0643	0,0012	0,2607	$6,68\times10^{-6}$
	Test	0,0020	0,9993	0,9997	0,0006	0,9994	0,1673	0,8570	0,0012	0,2645	$6,83\times10^{-6}$
	All	0,0019	0,9995	0,9997	0,0012	0,9983	0,1553	1,0643	0,0012	0,2590	$6,60\times10^{-6}$

In comparison, the FOA-SVR model consistently outperformed DA-SVR in generalizing to test data. Under H_CV, FOA-SVR had an RMSE of 0.0077 and an R^2 of 0.9992, showing reduced error and improved correlation. Its hyperparameters indicated smoother decision boundaries. With LMO_CV, FOA-SVR delivered even better results, achieving an RMSE of 0.0044 and an R^2 of 0.9997. The hyperparameters highlighted the model's ability to generalize effectively while maintaining high precision.

3.2. Thermal Conductivity Model result

The DA-SVR model demonstrated robust performance in predicting thermal conductivity, though it exhibited moderately elevated error metrics compared to the FOA-SVR approach. Under the H_CV method, DA-SVR achieved a RMSE of 0.0025 and R^2 of 0.9991, reflecting strong predictive accuracy. However, its hyperparameter configuration, specifically a regularization parameter $C = 1.2648\times10^{5}$, kernel parameter $\sigma = 4.6032$, and epsilon tube $\varepsilon = 6.4220\times10^{-6}$, suggested a rigid model structure. This rigidity likely arose from the high C value (prioritizing minimizing training error over model simplicity) and the extremely low ε (enforcing a narrow error margin), which may limit adaptability to nuanced data patterns.

However, the LMO_CV method enhanced DA-SVR's performance, reducing the RMSE to 0.0020 and improving the R^2 to 0.9993. The revised hyperparameters ($C = 729.9910$, $\sigma = 2.6356$, $\varepsilon = 3.8428\times10^{-6}$) indicate a more balanced compromise between error reduction and model flexibility. The lower C value reduces overfitting risks, while the adjusted σ (kernel width) and slightly relaxed ε allow better generalization across diverse datasets. These refinements underscore the importance of cross-validation strategies and hyperparameter tuning in optimizing regression models for complex physical properties like thermal conductivity.

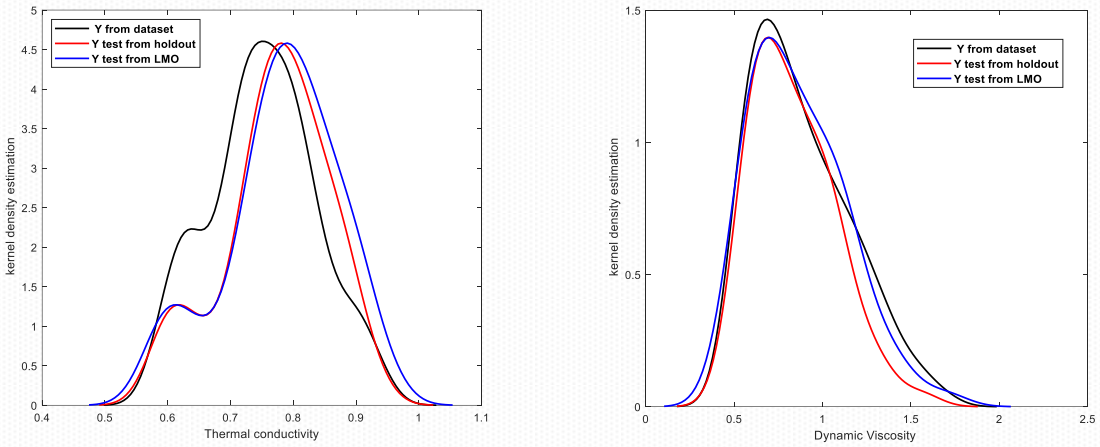
The FOA-SVR model demonstrated comparable error metrics to the DA-SVR approach while showcasing hyperparameters that highlight its efficiency and adaptability. Under Holdout Cross-Validation (H_CV), the FOA-SVR model achieved an RMSE of 0.0024 and a coefficient of determination ($R^2 = 0.9991$), reflecting strong predictive accuracy. Its hyperparameters: $C = 2.8950$, $\sigma = 1.5342$, and $\varepsilon = 3.6100\times10^{-6}$, illustrate a model configuration that emphasizes smooth decision boundaries and flexibility. The relatively low C value suggests a focus on balancing error minimization with generalization, while the moderate σ ensures adaptability to data patterns without overfitting.

When applied with Leave-Many-Out Cross-Validation (LMO_CV), the FOA-SVR model delivered outstanding results, achieving an RMSE of 0.0020 and an $R^2 = 0.9993$, indicating near-perfect predictions. The updated hyperparameters ($C = 17.2937$, $\sigma = 1.6752$, $\varepsilon =$

3.7636×10^{-6}) further demonstrate the model's ability to generalize effectively while maintaining precision. The slightly increased C value enhances error reduction, while the adjusted σ and stable ε values allow for broader flexibility in capturing complex data relationships. These results highlight the FOA-SVR model's strength in achieving a harmonious balance between predictive accuracy and generalization, making it a reliable tool for modeling intricate thermal conductivity datasets.

3.3. Leave-M-Out Cross-Validation (LMO_CV) and Holdout Cross-Validation (H_CV): comparative Results

Figures 7.a and 7.b display Kernel Density Estimate (KDE) plots comparing the distributions of thermal conductivity (panel a) and dynamic viscosity (panel b) between the original dataset (black curve) and test data derived from two cross-validation methods: Holdout (red curve) and Leave-M-Out (LMO) (blue curve).



-a- **-b-**

Figure 7. Kernel Density Estimate (KDE) plots (a: thermal conductivity, b: dynamic viscosity).

The KDE plots illustrate that both Holdout and LMO test data closely mirror the original dataset's distribution, with minor discrepancies in the means and spread. In Figure 7.a, the thermal conductivity distribution peaks around 0.8 W/m.K, with the red curve showing slight deviations near the peak and tails, while the blue curve aligns more closely with the black curve, reflecting better generalization under LMO.

Similarly, Figure 7.b shows dynamic viscosity distributions peaking around 0.5 mPa.s, where the red curve underestimates density near the peak compared to the black curve, whereas the blue curve demonstrates a closer fit, particularly at higher viscosity values. These observations highlight that LMO-selected test data more accurately reflects the original dataset's distribution, especially for dynamic viscosity, explaining why LMO_CV

outperformed H_CV in predictive accuracy. The superior performance of LMO_CV combined with FOA-SVR underscores their reliability for modeling complex physical properties, guiding subsequent research efforts to focus on these methods for further optimization.

3.4. Compararison between FOA-SVR and DA-SVR models

The comparison between the DA-SVR and FOA-SVR models highlights notable differences in their strategies for achieving predictive accuracy and generalization. Both models delivered exceptional results, consistently achieving R^2 values above 0.999, but the FOA-SVR model outperformed DA-SVR with lower RMSE values, indicating superior error minimization. This advantage stems from FOA-SVR's selection of optimized hyperparameters, including significantly lower penalty parameters (C) and kernel width (σ), which facilitated smoother decision boundaries and reduced the risk of overfitting.

These characteristics enabled FOA-SVR to generalize more effectively, particularly under the Leave-M-Out Cross-Validation (LMO_CV) method. While DA-SVR exhibited noticeable improvements when transitioning from Holdout Cross-Validation (H_CV) to LMO_CV, FOA-SVR maintained strong and consistent performance across both methods. This robustness is attributed to the FOX-inspired optimization algorithm, which adeptly balances exploration and exploitation during hyperparameter tuning, ensuring reliable model behavior.

Overall, FOA-SVR's ability to generalize effectively across diverse datasets, coupled with its capacity to minimize bias and error metrics, makes it the preferred choice for predicting dynamic viscosity and thermal conductivity. The FOX-inspired optimization algorithm provides a refined approach to hyperparameter selection, making FOA-SVR a powerful tool for complex regression tasks that demand high precision and reliability.

Figures 8 and 9 provide regression plots that visually assess the predictive performance of the FOA-SVR-LMO_CV model for dynamic viscosity and thermal conductivity, respectively. These plots compare the predicted values against the actual (experimental) values for both the test dataset and the entire dataset.

The diagonal line in each plot represents the ideal fit where predicted values perfectly match actual values, indicating a perfect model fit. Data points closer to this line demonstrate higher predictive accuracy and better generalization capabilities.

In Figure 8, which focuses on dynamic viscosity, the FOA-SVR-LMO_CV model demonstrates a strong positive correlation between predicted and actual values. The majority of data points align closely with the diagonal line, confirming the model's high accuracy. The calculated R^2 value exceeding 0.999 further supports this observation, indicating an almost

perfect linear relationship between predicted and experimental viscosity values. The minimal spread of data points around the diagonal line highlights the model's ability to minimize error and maintain low bias, particularly for unseen test data. This performance underscores the effectiveness of the FOX-inspired optimization algorithm in fine-tuning hyperparameters to achieve precise predictions.

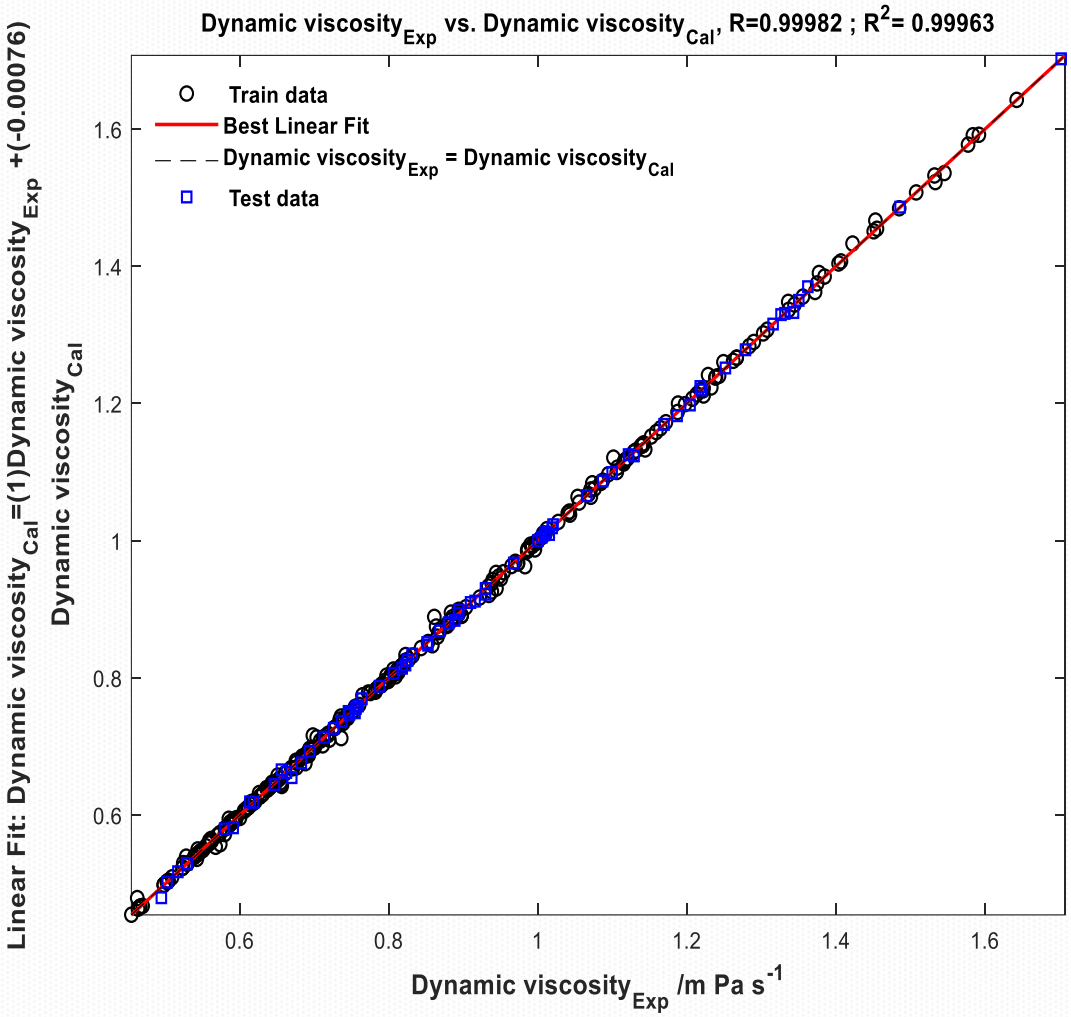


Figure 8. Regression plot showing the predicted versus actual values of dynamic viscosity for the test dataset and the entire dataset using the FOA-SVR-LMO_CV model.

Similarly, Figure 9 illustrates the regression plot for thermal conductivity, showing a similarly strong alignment between predicted and actual values. The FOA-SVR-LMO_CV model achieves an R^2 value of 0.99947, signifying exceptional predictive performance. The data points are tightly clustered around the diagonal line, reflecting minimal prediction errors across both the test dataset and the entire dataset. This tight clustering suggests that the model generalizes well across diverse data distributions, ensuring reliable predictions even for complex thermal conductivity datasets.

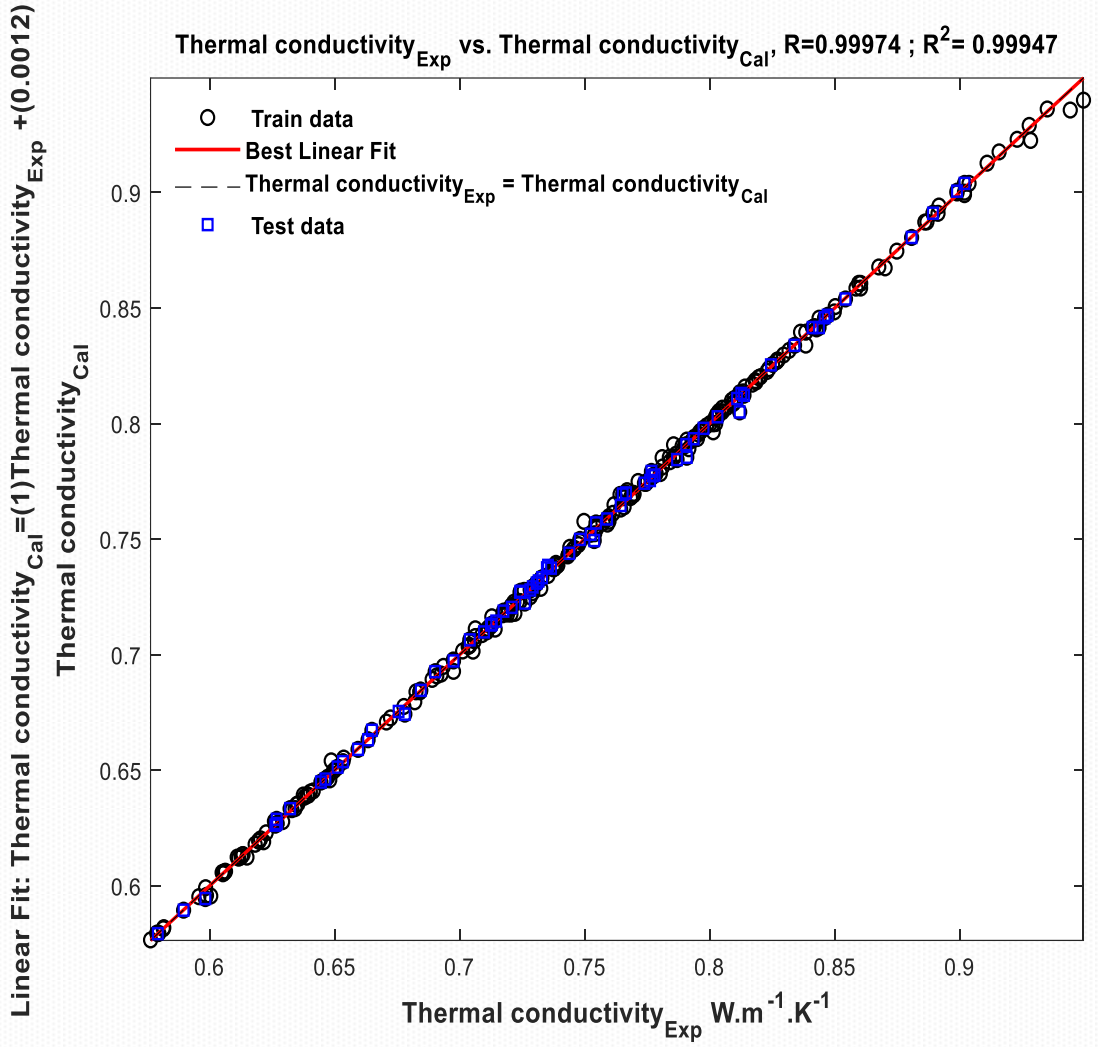


Figure 9. Regression plot showing the predicted versus actual values of the thermal conductivity for the test dataset and the entire dataset using the FOA-SVR-LMO_CV model.

Overall, these regression plots highlight the FOA-SVR-LMO_CV model's robustness in predicting dynamic viscosity and thermal conductivity with high accuracy. The FOX-inspired optimization algorithm's ability to balance exploration and exploitation during hyperparameter tuning plays a critical role in achieving such reliable performance across both datasets.

The regression plots in Figures 8 and 9 visually reinforce the FOA-SVR-LMO_CV model's robustness in predicting both dynamic viscosity and thermal conductivity. For dynamic viscosity, Figure 8 shows a strong positive correlation, with most data points closely following a diagonal line with a slope near 1, visually confirming the high R^2 values (>0.99) observed. Similarly, Figure 9 highlights equally strong predictive performance for thermal conductivity, with minimal dispersion of points around the ideal fit line. Together, these results validate the FOA-SVR-LMO_CV model as a powerful tool for accurately modeling complex physical properties while maintaining excellent generalization capabilities across datasets.

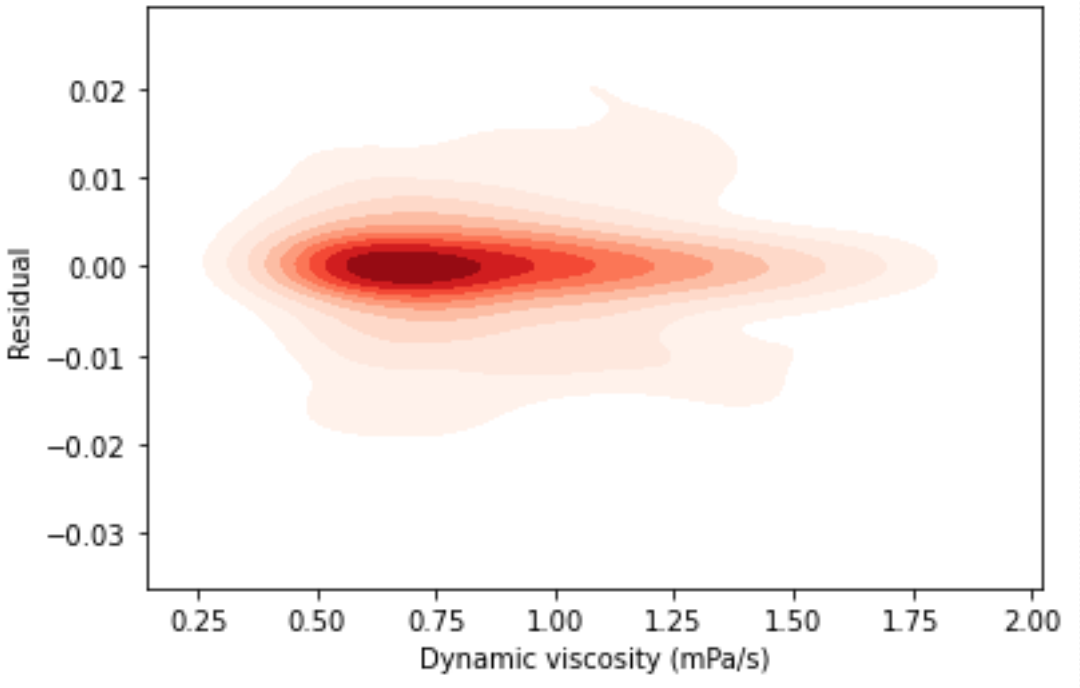


Figure 10. Kernel Density Estimate (KDE) plot of the residuals for dynamic viscosity predictions (mPa.s^{-1}) using the FOA-SVR-LMO_CV model.

Figure 10 presents the Kernel Density Estimate (KDE) plot for the residuals of dynamic viscosity predictions (measured in mPa.s^{-1}) using the FOA-SVR-LMO_CV model. The residuals represent the differences between the experimental and predicted values. The KDE plot illustrates the distribution of these prediction errors, with most residuals densely concentrated around zero. The density curve, shown in darker shades, highlights this central clustering.

This indicates that the FOA-SVR model provides highly accurate predictions, as minimal deviation exists between observed and predicted values. The reduced dispersion of residuals reflects the model's ability to generalize effectively across the dataset, minimizing overfitting while maintaining reliable predictions for dynamic viscosity.

Similarly, Figure 11 showcases the KDE plot for the residuals of thermal conductivity predictions obtained using the FOA-SVR-LMO_CV model. The residual values represent the differences between experimental measurements and model predictions for thermal conductivity. As observed in Figure 9, the residuals in Figure 10 are also tightly clustered around zero, with the density curve emphasizing this concentration.

This clustering suggests that the FOA-SVR model achieves high accuracy in predicting thermal conductivity values, with minimal error between predicted and actual results. The reduced spread of residuals further underscores the model's robustness and reliability in handling diverse datasets without overfitting.

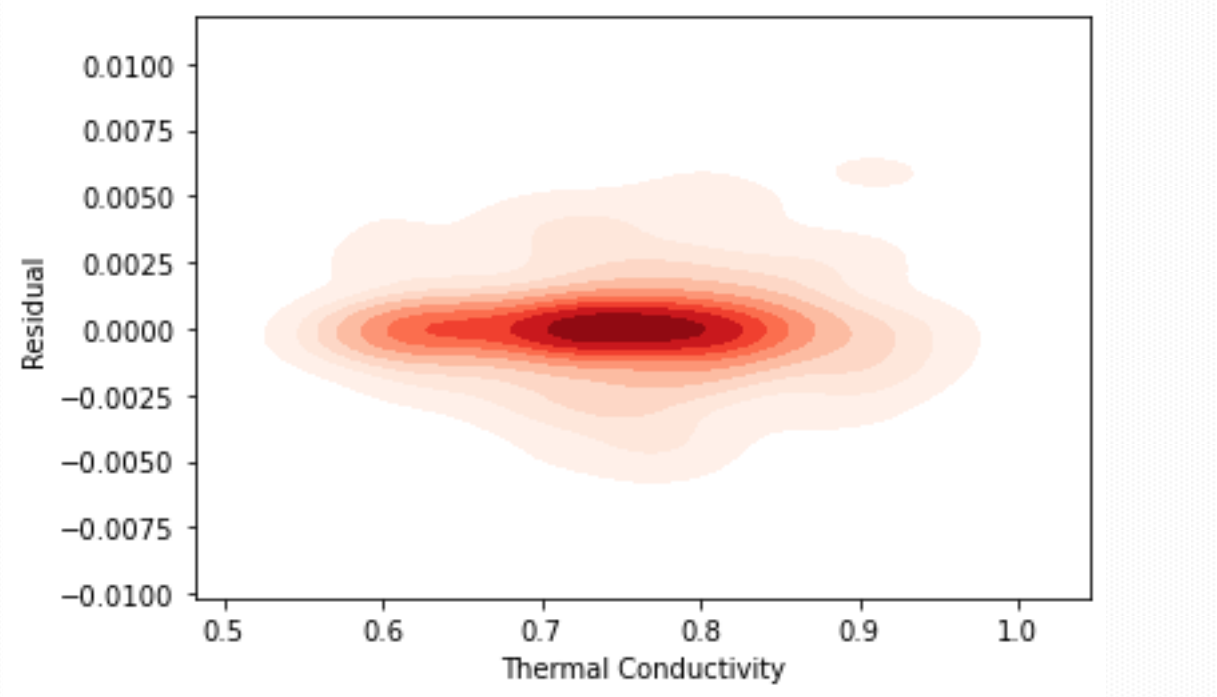


Figure 11. Kernel Density Estimate (KDE) plot of the residual values between the predicted and actual thermal conductivity using the FOA-SVR-LMO_CV model.

Figures 9 and 10 collectively demonstrate the exceptional predictive performance of the FOA-SVR-LMO_CV model for dynamic viscosity and thermal conductivity. The Kernel Density Estimate (KDE) plots highlight residuals, representing the differences between experimental and predicted values, are predominantly centered around zero, indicating minimal prediction error and high accuracy. The narrow dispersion of residuals reflects the model's ability to generalize effectively across diverse datasets, reducing overfitting and ensuring reliable predictions even for unseen data. These characteristics make the FOA-SVR model a valuable tool for applications requiring precise estimations of dynamic viscosity and thermal conductivity, offering industries the advantage of reduced experimental costs and improved computational efficiency. The findings reinforce confidence in the model's robustness and its suitability for scientific and industrial applications demanding accurate property predictions.

4. Comparison with previously published models

To evaluate the predictive capabilities of the developed models, their accuracy was compared with previously published models from the literature, as summarized in Table 5.

This table provides a comparative analysis of the predictive performance of different models for estimating thermophysical properties (thermal conductivity and dynamic viscosity) of hybrid ternary nanofluids (THNFs).

Table 5. Comparison of the Predictive Accuracy of the Developed DA-SVR Model for THNFs with Previously Published Models.

Ref.	Nanoparticles/Base fluid	Models	Data points	Inputs	Output	Statistical metrics		
						R/R^2	U^2	MSE/RMSE
[126]	MWCNT-TiO2-ZnO / DW	ANN	102	Nanofluid type, φand T	λ_{thnf}	0.9951	/	-2.0402×10^{-5} /
[127]	rGO-Fe_3O_4-TiO_2 / EG	BRT	1264	T and wt%	λ_{thnf}	0.9989 0.9978	0.0689	/ 0.0006
				T, γ, and wt%	μ	0.9979 0.9959	0.121	/ 0.0004
This study	CuO-$CaCO_3$-SiO_2 / DW	FOA-SVR	360	Nanofluid type, φand T	λ_{thnf}	0.9997 0.9995	3.91×10^{-5}	/ 0,0019
					μ	0,9998 0,9996	6.32×10^{-6}	/ 0,0053

Although the training and testing datasets used in this study differ from those in references 126 and 127, the findings suggest that the FOA-SVR and DA-SVR models achieve comparable levels of accuracy. While differences in datasets make a direct comparison less definitive, the low error metrics and high correlation coefficients obtained by our models highlight their effectiveness in predicting both thermal conductivity and dynamic viscosity for hybrid ternary nanofluids. The consistent performance across training, testing, and overall datasets emphasizes the robustness of our approach and aligns closely with prior studies. Future research could strengthen these conclusions by applying our models to the datasets used in references 43 and 44, enabling a more direct comparison of performance.

5. Conclusion

This study developed and evaluated four machine learning models: DA-SVR with H_CV, DA-SVR with LMO_CV, FOA-SVR with H_CV, and FOA-SVR with LMO_CV. All models demonstrated exceptional predictive capabilities, achieving R^2 values exceeding 0.999 across all datasets, underscoring their accuracy and reliability; moreover, a detailed comparison revealed the superior performance of the FOA-SVR models, which consistently outperformed DA-SVR models in terms of error minimization and generalization. The differences in performance can be attributed to the hyperparameter selection and the used optimization techniques. The FOX-inspired optimization algorithm employed in FOA-SVR allowed for the selection of lower penalty parameters (C) and sigma (σ) values, leading to smoother decision boundaries and better generalization to unseen data. In contrast, DA-SVR models, while robust,

exhibited a relatively rigid structure that limited their flexibility in certain scenarios; furthermore, the FOA-SVR models maintained consistent performance across both Holdout and LMO cross-validation methods, emphasizing their reliability and adaptability to various data splits. The role of cross-validation methods was also crucial in evaluating the models. The LMO_CV method proved to be more robust, consistently producing lower RMSE values and higher R^2 values compared to H_CV; this highlights the importance of using comprehensive validation techniques to ensure the reliability and generalizability of machine learning models.

The findings of this study have significant implications for the accurate modeling and prediction of thermophysical properties in advanced nanofluids. The FOA-SVR models' superior performance makes them valuable tools for industrial applications requiring precise and reliable predictions, such as in energy systems, thermal management, and advanced manufacturing. Future research could explore the integration of hybrid optimization techniques or the extension of these models to predict additional thermophysical properties, further enhancing their utility and applicability. Future work may explore the application of hybrid or multi-objective optimization techniques to further enhance the performance of these models in predicting other thermophysical properties of nanofluids.

CHAPTER IV :

CONTRIBUTION 02

Using Support vector machine optimized with Dragonfly Algorithm to predict water productivity of a nanofluid-based single-slope solar still

1. Introduction

The global water crisis is a pressing issue affecting billions of people worldwide. As of 2022, approximately 2.2 billion people lack access to safely managed drinking water, while 3.5 billion do not have access to safely managed sanitation. The situation is particularly dire in sub-Saharan Africa, where only 22-34% of populations in at least eight countries have access to safe water [128]. Agriculture accounts for about 70% of global freshwater withdrawals, followed by the industrial sector and the domestic uses which are responsible for 22% and 8% of that volume, respectively [129]. Therefore, it is clear that agriculture is the most water-intensive sector, thereby contributing extensively to freshwater scarcity [130,131]. Groundwater supplies roughly 25% of all water used for irrigation and half of the freshwater withdrawn for domestic purposes. Climate change exacerbates the problem, with droughts affecting more than 1.4 billion people between 2002 and 2021 [132]. By 2030, it is projected that almost half the world's population will be living in areas of high-water stress, and water scarcity could displace over 700 million people [133]. The United Nations predicts that by 2025, 1.8 billion people will be living in countries or regions with absolute water scarcity [134]. These statistics highlight the urgent need for sustainable water management practices and innovative solutions to address the global water crisis.

In response to the growing water scarcity in arid regions, a variety of methods have been developed to produce freshwater. Traditional techniques like distillation, Reverse Osmosis, Electrodialysis, and Vapor Compression are widely employed [135]. Desalination has emerged as a cost-effective water purification solution [136].

Renewable energy sources, particularly solar energy, offer simple and economical means of potable water production [137]. Solar power is extensively utilized for various thermal applications and power generation [138]. The integration of desalination systems with renewable energy sources is a key approach to reduce energy consumption and mitigate atmospheric pollution associated with fossil fuels [139].

Solar stills have proven to be an effective technology for desalinating brackish and saline water, especially in remote areas and islands. However, their primary drawback is low overall efficiency [140]. To address this limitation, researchers have investigated numerous designs and methods to improve the thermal efficiency and productivity of solar stills [141].

Solar distillation technology encompasses both passive and active systems, with passive designs relying exclusively on solar energy and achieving efficiencies between 14.9% and 21.8%, while active systems incorporate external heat sources for enhanced performance [142]. Innovative modifications have significantly improved these systems, including the use of

internal and external reflectors that can boost productivity by up to 165%, and the integration of latent heat storage with parabolic solar concentrators, which increases productivity by 45-65% depending on the season [143].

Over the past decade, nanofluid-based solar stills (NF-based SSs) have attracted significant attention compared to conventional solar stills (CSS). Figure 1 illustrates the number of articles published over the past decade that discuss various nanofluids (NFs). It is clear that the publication count has been consistently rising throughout the last ten years.

Nanofluids are great heat transfer carriers for collecting thermal energy in solar thermal applications, integrating nanofluids into desalination processes can significantly enhance efficiency, cost-effectiveness, and sustainability [144].

Using experimental data from a single-slope solar still, the research employs a Support Vector Regression-Dragonfly Algorithm (SVR-DA) to model and predict daily fresh water productivity, focusing on key control factors, particularly nanofluids. The integration of machine learning with nanofluid-enhanced solar desalination offers novel insights into heat transfer and efficiency improvements. By combining SVR-DA and nanofluid technology, the study optimizes solar still performance, addressing non-linear system challenges and demonstrating nanofluids' potential to boost productivity. The findings advance sustainable desalination technologies, providing solutions for global water scarcity and bridging machine learning with renewable energy for innovative engineering applications.

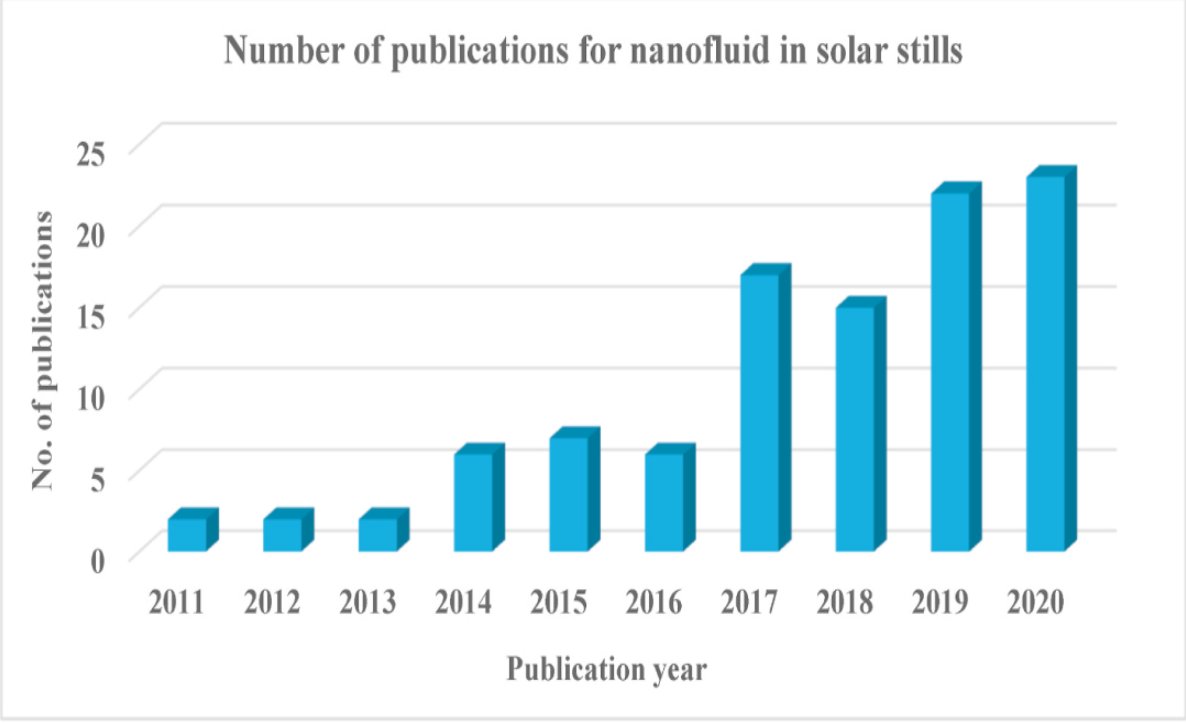


Figure 1. The number of research papers published between 2011 and 2020 according Google Scholar search containing the terms "solar still" and "nanofluid" [77].

2. Experimental setup and procedure

This study is based on experimental research conducted on a single-slope solar still (passive type) [145], oriented toward the south in Patiala, India. The experiment was performed on July 14, 2019, from 6:00 AM to 6:00 AM the following day, with hourly data recordings. The solar still's basin, constructed from stainless steel, featured a rectangular tray design with an evaporative surface area of 1 m^2.

The glass cover, inclined at 30° to the horizontal -approximately matching the latitude of the location- served a dual function: permitting incident solar radiation to enter while acting as a condensation surface. To prevent condensed distillate droplets from re-entering the evaporator surface, a rectangular plastic channel was attached to the lower edge of the glass cover, as illustrated in Figure 2 and 3. This design ensured efficient collection of distilled water while maintaining optimal system performance.

To enhance thermal efficiency, the tray's sides were wrapped in glass wool insulation. A 5 mm thick rubber-like material lined the basin, serving a dual purpose: maximizing solar energy absorption and effectively transferring that captured heat to the water within the basin. This design choice aims to optimize the solar still's performance by minimizing heat loss and maximizing energy utilization.

Also, it is noteworthy that different nanofluids are incorporated in the basin of the solar still: CuO, Al_2O_3, Ag, Fe_2O_3, and SiC-water nanofluids at several volume concentrations (0.02, 0.05, 0.08, 0.12, and 0.2). This analysis has been carried out at different water depths with an optimum of 0.02 m, and a comparison was made with a simple solar still without adding nanofluids. Daily production for Al_2O_3-water based nanofluid was found to be (14.22%) higher than simple solar still without nanofluid, followed by CuO (10.82%), Ag (8.11%), Fe_2O_3 (7.63%) and SiC (7.61%).

The water productivity of a new nanofluid-based solar still is modeled in terms of the solar radiation, ambient temperature, basin temperature, glass temperature, water depth, and nanoparticle properties including thermal conductivity, molecular mass, density, heat capacity, and concentration.

The performance of the model strongly depends on the input variables used to develop this model. The selection of appropriate input variables is an essential and indispensable step to be able to model the considered system reliably and improve the computational efficiency.



Figure 2. Experimental setup of single slope solar still [145].

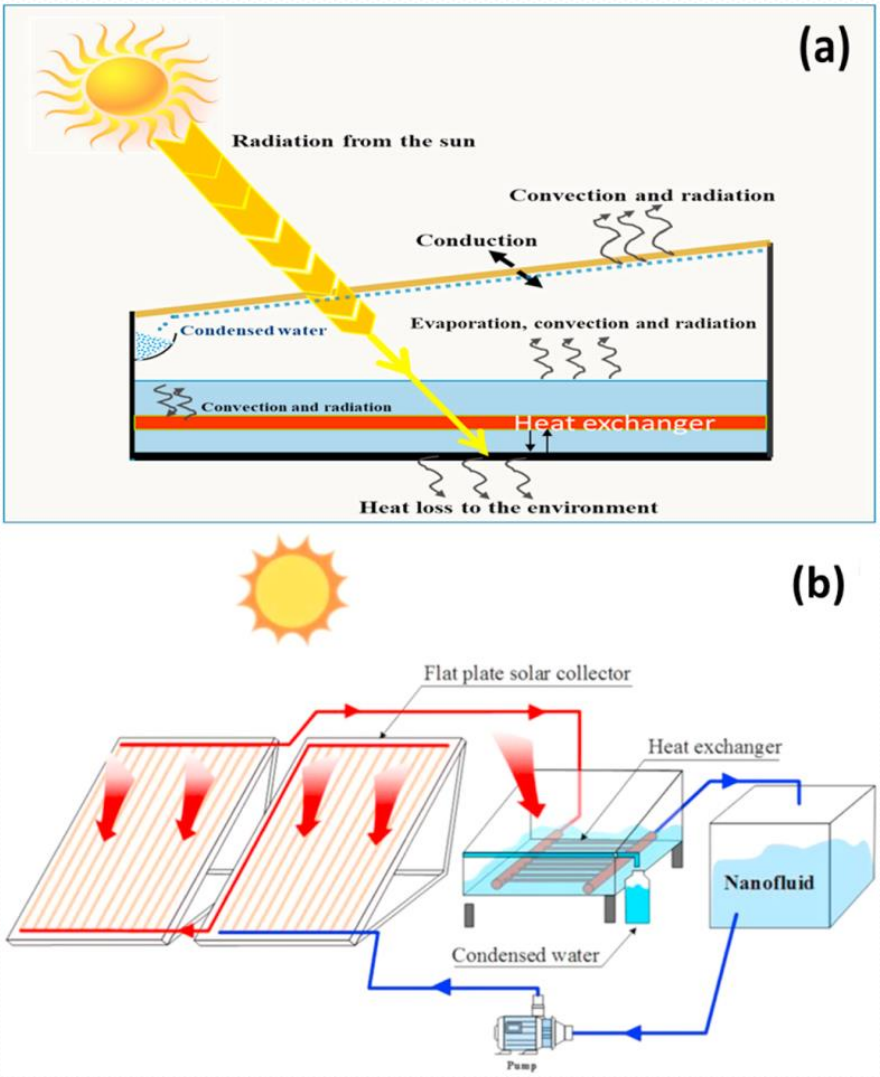


Figure 3. (a) Diagram illustrating the operation of a solar water desalination system, and (b) schematic representation of a solar still integrated with a heat exchanger.

3. Data collection

In this study, a comprehensive dataset comprising 251 data points has been collected from the previous work [145], with water productivity designated as the primary output variable. The dataset is utilized to assess the performance of a nanofluid-based solar still by investigating the influence of various input parameters on the water production process. The considered input variables include solar radiation, ambient temperature, basin temperature, glass temperature, and water depth, all of which represent key environmental and operational factors. Furthermore, the dataset incorporates nanoparticle properties such as thermal conductivity, molecular mass, density, heat capacity, and concentration, which are essential for evaluating the impact of the nanofluid on system efficiency. Solar radiation serves as the primary energy source for the system, while ambient and glass temperatures influence heat transfer and condensation rates. The basin temperature plays a crucial role in the evaporation process, whereas water depth affects the thermal mass and heat distribution within the system.

Table 1 presents the descriptive statistics of the collected dataset, offering a comprehensive overview of its key characteristics. It includes statistical measures such as the mean, median, standard deviation, minimum, and maximum values for each variable. These metrics provide insights into the central tendencies and variability within the dataset, facilitating a clearer understanding of the relationships between the input parameters and water productivity. This statistical summary serves as a fundamental reference for subsequent analyses, aiding in the identification of patterns and trends that may elucidate the effects of various factors on the performance of nanofluid-based solar stills.

4. Statistical description of the dataset

Based on the descriptive statistics provided in the table 1, we can offer an analysis of the dataset for the nanofluid-based solar still study as follows:

The dataset comprises 12 variables related potentially for solar desalination treatment system. The variables encompass aspects like volume concentration, time, solar radiation, ambient, basin, and glass temperatures, thickness, and the physical properties of nanoparticles (thermal conductivity, molecular mass, density, and heat capacity), and productivity as a unique output. The analysis focuses on descriptive statistics, providing insights into central tendency, dispersion, shape, and potential data issues.

The dataset reveals significant variability and unique distribution characteristics across its parameters, reflecting the complexity of the studied system. Volume concentration (%) demonstrates minimal values (Min: 0.0%, Max: 0.2%), with a low arithmetic mean (0.067%).

The positive kurtosis (1.716) suggests a leptokurtic distribution, and the skewness (0.79) indicates a slight positive skew. The low standard deviation (0.089) suggests low variability, but this is relative to the very small magnitudes. Time spans a full day, with an average of 11.28 hours and relatively low skewness (0.076), indicating a fairly uniform distribution. The standard deviation is 6.881 hours indicating the timing is recorded throughout the entire day. Solar radiation exhibits a broad range (Min: 1.005 W/m^2. Max: 831.762 W/m^2) and a substantial standard deviation (293.348 W/m2), signifying considerable variability, and pronounced skewness (0.882), highlighting diverse environmental conditions. The kurtosis (2.193) suggests a somewhat peaked distribution relative to a normal distribution. Temperature-related parameters, such as ambient, basin. and glass temperatures, are more stable, with mean values of 34.89°C, 46.66°C, and 42.59°C, respectively, and lower standard deviations (3.29°C to 14.32°C).

Table 1. Statistical analysis data

Measures	Min	Mean	Harm	Moment	Std
	Max	Geomean	Kurtosis	Skewness	Var
Volume concentration (%)	0.000	0.067	0.000	0.001	0.089
	0.200	0.000	1.716	0.790	0.008
Time (H)	0.000	11.280	0.000	24.482	6.881
	23.000	0.000	1.800	0.076	47.351
Solar radiation (W/m^2)	1.005	232.158	4.162	22137168.812	293.348
	831.76	31.877	2.193	0.882	86053.092
Ambient temperature (°C)	31.019	34.890	34.586	7.888	3.289
	41.051	34.737	1.676	0.223	10.820
Basin temperature (°C)	31.216	46.662	42.760	1555.435	14.316
	73.236	44.607	1.777	0.533	204.953
Glass temperature (°C)	28.976	42.587	39.552	1209.266	12.231
(°c)	66.949	40.978	1.959	0.665	149.594
Thickness (cm)	1.000	2.500	2.091	1.500	1.120
	5.000	2.283	3.176	1.073	1.255
Thermal conductivity (W/m °k)	0.000	60.124	0.000	7796514.749	145.220
	490.00	0.000	7.760	2.561	21088.826
Molecular mass (g/mol)	0.000	56.102	0.000	476019.440	72.326
	231.53	0.000	3.716	1.266	5231.046
Density (kg/m^3)	0.000	2906.000	0.000	36705506232.0	3438.891
	10490.	0.000	2.763	0.908	11825967.8
Heat capacity (J/k)	0.000	308.200	0.000	6417803.136	320.399
	773.00	0.000	1.242	0.196	102655.382
Productivity (mL/H.m^2)	0.540	145.996	13.253	2781899.409	155.360
	468.22	55.541	1.953	0.746	24136.656

Material properties like thickness, thermal conductivity, molecular mass, and density demonstrate broader ranges. Thickness varies from 1 to 5 cm (mean = 2.5 cm), while thermal

conductivity shows extreme variability (mean = 60.124 W/m.K, Std = 145.22). The high kurtosis and skewness observed in molecular mass and density suggest the presence of zero or near-zero values, which is attributed to instances where nanoparticles were not utilized in the experiment. Productivity (ml/hr.m²) spans from 0.54 to 468.23, with a mean of 145.99 and moderate variability (Std = 155.36). These statistical characteristics provide valuable insights into the heterogeneity of the system, laying the groundwork for robust modeling and predictive analyses.

The violin plots in Figure 4 provide a detailed visualization of the distribution of various experimental parameters influencing the performance of a solar still. Each plot combines a box plot and a kernel density estimation, offering insights into the spread, central tendency, and variability of the data. The width of each violin represents the density of data at different values, while the black and red lines indicate the mean and median, respectively.

Volume concentration shows a narrow distribution, indicating consistent impurity levels, while time exhibits moderate variability around its mean and median. Solar radiation displays significant skewness and a wide range, reflecting fluctuations in solar intensity. Ambient temperature is relatively stable with minimal skewness, whereas basin temperature shows higher variability due to direct exposure to solar radiation. Glass temperature has less variability, indicating stable thermal conditions for condensation. Thickness is uniform across measurements, while thermal conductivity reveals sparse data points and outliers. Molecular mass and density show moderate to high variability influenced by water composition and salinity. Heat capacity displays broad distribution, highlighting differences in thermal properties, while productivity varies significantly due to external factors like solar radiation and system efficiency.

Overall, these violin plots provide comprehensive insights into how different parameters behave and interact during solar still operation. They highlight areas of consistency (e.g., ambient temperature and thickness) as well as variability (e.g., solar radiation and productivity), offering valuable information for optimizing system design and performance.

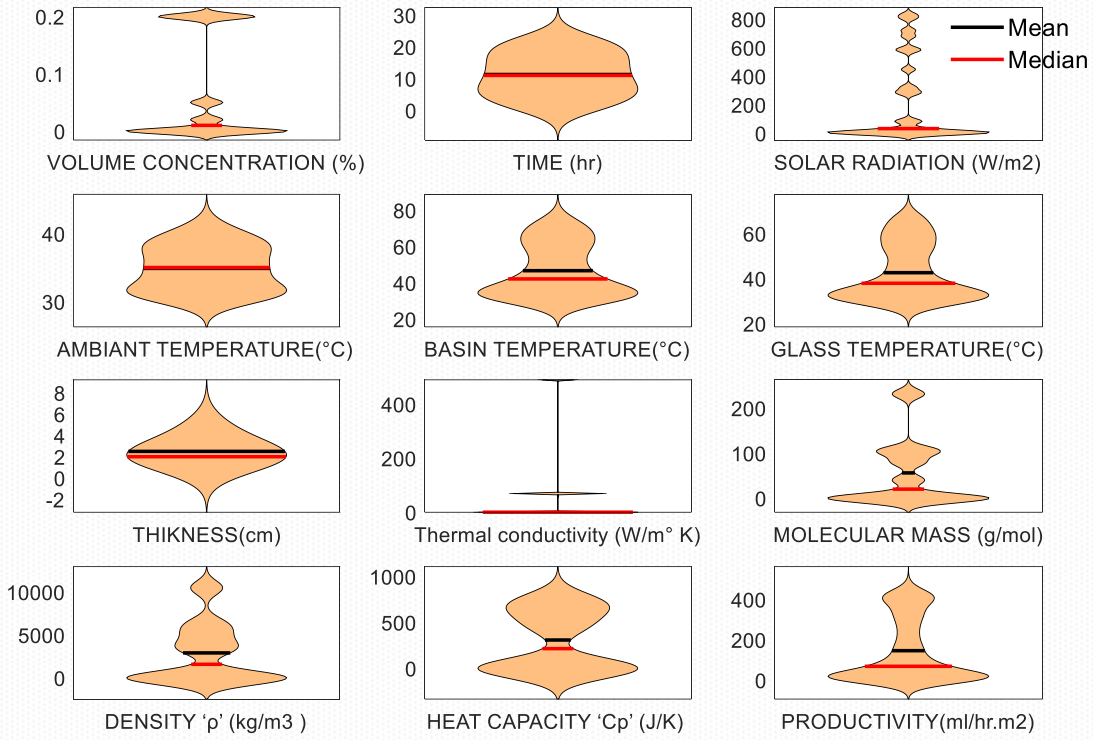


Figure 4. Visualization using violin plots to represent the distribution of various experimental parameters influencing the performance of a solar still.

5. Dragonfly Algorithm Optimization

The hybrid approach combining Support Vector Machines (SVM) with the Dragonfly Algorithm (DA) represents a powerful synergy in machine learning optimization. This method leverages the strengths of both algorithms to create a more robust and accurate model for regression and classification tasks [146,147].

Before applying the hybrid DA-SVM model. the dataset underwent several crucial preprocessing steps, the first one is the standardization, where all features were standardized to have zero mean and unit variance. This ensures that all variables contribute equally to the model and prevents features with larger scales from dominating the optimization process [148]. The dataset was divided into training (80%) and testing (20%) subsets. This split allows for model training on a significant portion of the data while reserving a separate set for unbiased evaluation of the model's performance [148].

The Dragonfly Algorithm (DA) is an innovative optimization technique within the field of swarm intelligence. This meta-heuristic approach draws inspiration from the natural swarming behaviors of dragonflies, both in their static and dynamic states. By mimicking these patterns, the algorithm has demonstrated remarkable efficiency and has outperformed many established meta-heuristic methods in comparative studies. Its unique approach to problem-solving has garnered attention in the optimization literature. showcasing its potential as a

powerful tool for tackling complex optimization challenges [149]. The Dragonfly Algorithm is employed to optimize the SVM hyperparameters. the optimization process focuses on three critical SVM parameters, the penalty parameter (C) that controls the trade-off between achieving a low training error and a low testing error [150], the Gaussian RBF Kernel parameter (σ) which defines the width of the Gaussian kernel, and epsilon (ϵ) which defines the width of the insensitive zone [148].

The optimization process was carried out using a population size of 50 search agents and a maximum of 500 iterations. The search space was defined with bounds set between a lower limit (lb) of 0.1 and an upper limit (ub) of 2000, ensuring a wide range for parameter exploration and fine-tuning.

6. DA-SVM model training

The DA optimization process iteratively adjusted the SVM hyperparameters to minimize the error on the training set. At each iteration. the DA algorithm generated new candidate solutions (hyperparameter combinations) based on the movement of dragonflies in the search space. These candidates were evaluated using cross-validation on the training data to assess their performance [151].

Based on the table 2 bellow, with using the final optimized parameters, the SVM model was trained on the entire training dataset. The resulting model utilized 200 support vectors. which are the critical data points that define the decision boundary or regression function [148].

Table 2. Optimization Parameters for DA-SVMr Model

Model	Penalty parameter C > 0	Sigma σ	Size of the insensitive zone (ε)	Kernel function	Quantity of support vectors
DA-SVMr	372.9428	1.2590	72.4209	Gaussian RBF	200

7. Model evaluation and performance

The trained DA-SVM model was then evaluated on the held-out test set to assess its generalization performance. This evaluation typically involves calculating metrics such as Mean Squared Error (MSE) for regression tasks or accuracy, precision, and recall for classification tasks [147]. The use of 200 support vectors suggests a balance between model complexity and generalization. A moderate number of support vectors indicates that the model has captured the underlying patterns in the data without overfitting to noise or outliers [148].

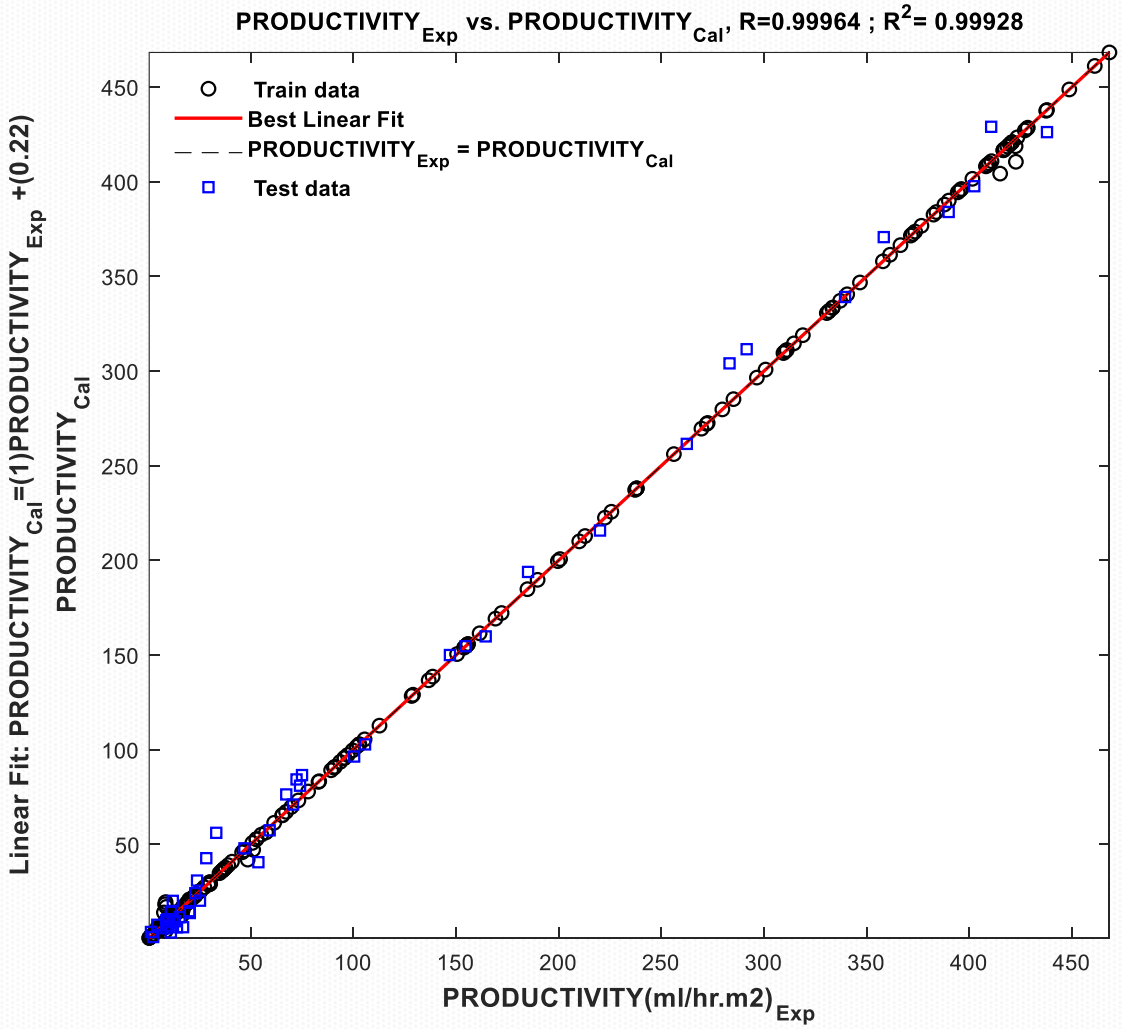


Figure 5. Comparison of Experimental and Predicted Productivity with Linear Fit Analysis.

This hybrid DA-SVM approach demonstrates the potential for metaheuristic algorithms like DA to enhance traditional machine learning techniques. By optimizing critical hyperparameters. the model can achieve improved accuracy and robustness compared to standard SVM implementations with manually tuned parameters[146,147].

Figure 5 illustrates the relationship between experimentally measured productivity and calculated productivity for a solar still system, showcasing the accuracy of the predictive model. The correlation coefficient (R = 0.99964) and coefficient of determination (R^2 = 0.99928) signify an almost perfect linear relationship, confirming the model's high predictive accuracy. Both training and test data closely follow the linear fit with minimal deviation from the ideal line, indicating that the model reliably predicts solar still productivity under varying experimental conditions. This visualization highlights the effectiveness of the model in capturing and predicting solar still performance metrics with exceptional precision.

Table 3 summarizes the statistical metrics used to evaluate the performance of a predictive model for solar still productivity across training, testing, and combined datasets. The Root Mean Square Error (RMSEb) measures the average error between predicted and experimental values, with the training data showing the lowest error (1.8987), indicating the model's strong accuracy during development.

Table 3. Statistical metrics for training, testing, and combined data sets in solar still productivity analysis

Data	RMSEb	R^2	r	b	slope	AARD	MAPE	MRPE	MAE	RSDD
Train	1.8987	0.9999	0.9999	0.2241	0.9981	4.1124	4.1124	168.6392	0.4846	1.2131
Test	8.5100	0.9958	0.9980	-0.0928	1.0122	33.0670	33.0670	249.5973	6.3981	8.3992
All	4.1675	0.9993	0.9996	0.2195	0.9997	9.9033	9.9033	249.5973	1.6673	2.8603

The Coefficient of Determination (R^2) and Correlation Coefficient (r) are near-perfect for all datasets, with values close to 1, confirming an excellent fit and strong linear relationship between predicted and experimental productivity. The Intercept (b) and Slope further validate the model's reliability, with slopes close to 1 across all datasets, indicating accurate predictions.

Relative error metrics such as AARD (Average Absolute Relative Deviation) and MAPE (Mean Absolute Percentage Error) are lowest for training data (4.1124), while test data exhibits higher variability with AARD and MAPE at 33.0670. The MRPE (Mean Relative Percentage Error) highlights larger errors in test data compared to training data, reflecting external influences during validation. Similarly, the Mean Absolute Error (MAE) and Relative Standard Deviation Difference (RSDD) are smallest in training data, indicating minimal deviation in predictions. Overall, the table 3 demonstrates that the model performs exceptionally well during training, with slightly reduced accuracy on test data due to higher variability, but maintains reliable performance across all datasets combined.

In summary. the model shows excellent performance with some room for improvement in handling unseen data and extreme cases. The high accuracy on both training and testing data suggests that it could be a valuable tool for its intended application, pending further validation and potential refinements to address the identified areas for improvement.

8. Residual Error distribution Analysis for the DA-SVMr Model

Figure 6 illustrate the residual error distribution for the DA-SVMr model, providing valuable insights into its predictive performance and reliability.

Figure 6(a) displays the residual error distribution as a scatter plot, where the residuals are randomly dispersed around the zero line. This randomness signifies that the errors are

unbiased and evenly distributed, indicating that the DA-SVMr model successfully captures the underlying relationships in the dataset without overfitting or underfitting. The majority of residuals lie within a narrow range, suggesting minimal deviations between observed and predicted values, which further highlights the model's accuracy. Additionally, the absence of discernible systematic patterns in the residuals reinforces the robustness and reliability of the model's predictions.

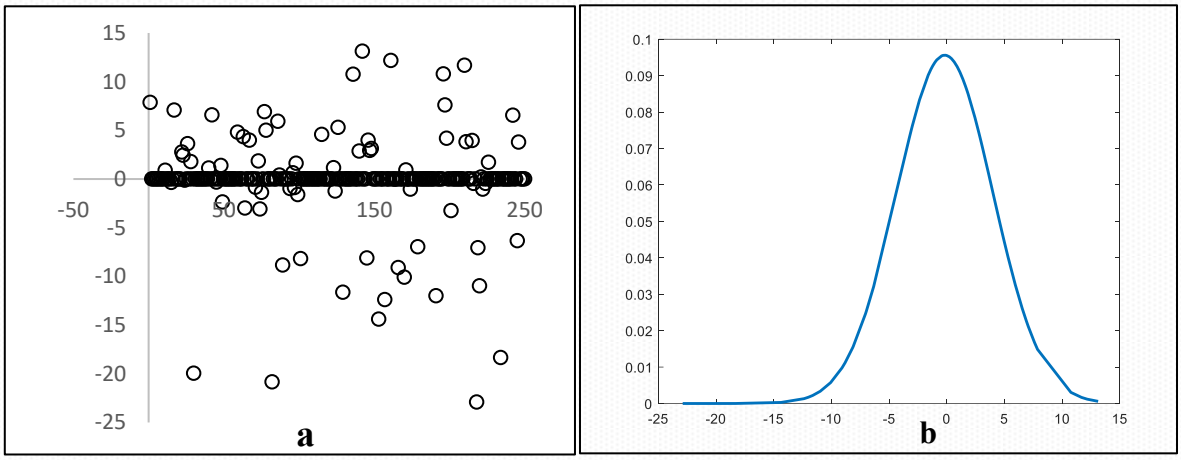


Figure 6. (a) Residual error distribution, (b) Normal distribution residual error.

On the other hand, Figure 6(b) presents a curve resembling a normal distribution, illustrating that the residual errors are symmetrically distributed around zero. This symmetry confirms that the DA-SVMr model provides unbiased estimates and accurately predicts outcomes. The bell-shaped curve further supports the notion that the residuals follow a normal distribution, which is often indicative of a well-performing predictive model. Together, these figures validate the effectiveness of the DA-SVMr model in delivering reliable and unbiased predictions, showcasing its ability to generalize well across different data points while maintaining high accuracy and robustness in its estimations.

In conclusion. the residual error distribution provides strong evidence for the effectiveness and reliability of the DA-SVMr model in capturing the complexities of the single slope solar still distillation process. This analysis reinforces confidence in the model's predictions and its potential utility for optimizing solar still design and operation.

9. Statistical Validation Using One-Way ANOVA

The results of the one-way ANOVA test between the actual and predicted values, using an F-distribution, indicate that the null hypothesis (H_0) is accepted, as the p-value (0.7937) exceeds the significance level (α=0.05). This suggests that the difference between the sample averages of the actual and predicted values is not statistically significant. The test statistic F is

0.0684, which lies within the 95% acceptance region [0, 3.8508], supporting the equality of group means. The observed effect size (f=0.0083f = 0.0083f=0.0083) and $\eta 2$ value (0.000069) indicate a negligible magnitude of variance explained by the group, reinforcing that the differences between the groups are minimal. Tukey's HSD test further confirms no significant differences between any pairwise means. Validation metrics, including a priori power of 1 and Levene's test (p-value = 0.794), affirm equal variances across groups. Additionally, the normality assumption, verified via the Shapiro-Wilk test, is satisfied due to the large sample size. These findings underscore the robustness of the predictive model and the similarity between actual and predicted values.

Table 4. One-way ANOVA test between the actual and predicted values.

Pair	Difference	SE	Q	Lower CI	Upper CI	Critical Mean	p-value
x_1-x_2	2844281.12	7689617.57	0.3699	-18495740.12	24184302.36	21340021.24	0.7937

10. Comparative Analysis with Related Studies

This section provides a comprehensive comparison of our study's findings with other relevant research in the field of solar still desalination, particularly focusing on the use of nanofluids to enhance performance.

In comparison with nanofluid-enhanced solar stills, our study's focus on using various nanofluids in a single-slope solar still which aligns with several recent investigations in the field. Sathyamurthy et al. (2019) investigated the use of MgO and TiO_2 nanofluids in stepped solar stills. They reported productivity increases of 45.8% and 33.33% for MgO nanofluids at 0.2% and 0.1% concentrations, respectively [152]. While our study focused on different nanoparticles, the significant productivity enhancements align with our findings, highlighting the potential of nanofluids in solar still applications.

Khelifi et al. (2024) explored the performance of hemispherical solar stills (HSS) enhanced with date and olive kernels as heat storage materials. Their study reported productivity rates of 8 kg/m²/day for HSS with olive kernels (13.54% increase) and 6.66 kg/m²/day for HSS with date kernels (10.87% increase) [153]. While our study focused on a single-slope design, the use of natural materials for heat storage presents an interesting avenue for future research in combination with nanofluids.

Sailash and Sakthivel (2024) conducted a comparative analysis of conventional solar stills and those enhanced with ZnO nanofluids. They reported a maximum daily output of 843 ml/day using ZnO nanofluid, compared to 500 ml/day without nanoparticles [154]. This 68.6% increase

in productivity is comparable to our findings with other nanofluids, reinforcing the effectiveness of nanoparticle addition in solar still systems.

A study by Abu-Zeid (2024) investigated the performance enhancement of solar still units using v-corrugated basins, internal reflecting mirrors, flat-plate solar collectors, and nanofluids. They reported productivity increases of up to 104.13% when using Al_2O_3 water-based nanofluid in the solar collector [155]. While our study focused on a simpler single-slope design, these results highlight the potential for further improvements by combining nanofluid enhancement with other design modifications.

Sharshir et al. (2018) conducted an energy and exergy analysis of solar stills with micro/nano particles. They reported daytime energy efficiencies of 41.18% and 38.61% for graphite/water and copper oxide/water mixtures, respectively, compared to 29.17% for a classical still. The daytime exergy efficiencies were 4.32%, 3.78%, and 2.63% for graphite, copper oxide nanofluid-based stills, and classical stills, respectively [156] [157]. While our study did not focus on exergy analysis, these findings complement our results by providing insights into the thermodynamic improvements offered by nanofluid addition.

When doing machine learning approaches comparison, our study's use of the DA-SVMr model for predicting solar still productivity represents a novel approach in the field. This model developed in the current study demonstrates excellent performance, with an R^2 value of 0.99928 and correlation coefficient of 0.99964. This indicates a very strong fit between predicted and experimental values, outperforming most other recent modeling approaches.

This exceptional accuracy achieved surpasses that of many traditional modeling techniques. For instance, Sohani et al. (2021) [158] and Bahiraei et al. (2020) [159] used various Artificial Neural Network (ANN) types, which, while effective, did not achieve the same level of accuracy as our DA-SVMr model.

The table 5 below summarizes some performance metrics of the current DA-SVMr model with other recent modeling studies for solar still productivity prediction.

The integration of the Dragonfly Algorithm for optimization of the SVM parameters also demonstrates an innovative approach compared to other studies. For example, Bahiraei et al. (2021) [160] used Particle Swarm Optimization (PSO) with ANFIS, achieving an R^2 of 0.9884, which is slightly lower than our model's performance.

Wang et al.'s Random Forest and ANN models optimized with Bayesian algorithm show comparable but slightly lower R^2 values [161]. Mashaly et al.'s ANN model achieved similar R^2 ranges during training, but lower values during testing, suggesting the DA-SVMr may have better generalization [162].

Table 5. Performance comparison of DA-SVMr model and recent modeling studies for solar still productivity prediction.

Study	Model Type	Performance Metrics
Current study (DA-SVMr)	Support Vector Regression with Dragonfly Algorithm	R^2 = 0.99928, r = 0.99964, RMSE = 1.8987 (training)
Wang et al. (2021) [163]	Random Forest with Bayesian Optimization	R^2 = 0.9964
Wang et al. (2021) [163]	Artificial Neural Network with Bayesian Optimization	R^2 = 0.9977
Mashaly et al. (2015) [164]	Artificial Neural Network	R^2 = 0.991-0.99 (training), 0.94-0.98 (testing)
Nazari et al. (2020) [165]	ANN optimized with Imperialist Competition Algorithm	RMSE = 15.77 (water productivity)
Sohani et al. (2022) [158]	Feedforward Neural Network	Average monthly error < 5%

The ANN-ICA model by Nazari et al. reported RMSE rather than R^2, making direct comparison difficult. However, their RMSE of 15.77 for water productivity is notably higher than the RMSE of 1.8987 achieved by the DA-SVMr model during training [166].

Sohani et al.'s Feedforward Neural Network demonstrated good performance with average monthly errors below 5%, but the DA-SVMr model's higher R^2 value suggests potentially better accuracy [167].

Overall, the DA-SVMr model shows superior or comparable performance to other recent modeling approaches, demonstrating its effectiveness in predicting solar still productivity. Its high accuracy and strong generalization make it a valuable tool for optimizing solar still design and operation.

In conclusion, our study's combination of nanofluid enhancement in solar stills with advanced machine learning techniques for performance prediction represents a significant contribution to the field. The DA-SVMr model's high accuracy and the substantial productivity increases observed with nanofluid addition, particularly Al_2O_3, align with and often surpass the findings of related studies. This comprehensive approach, integrating experimental design with sophisticated predictive modeling, offers a robust framework for future research and optimization in solar still technology.

11. Conclusions

This study successfully demonstrates the effectiveness of a hybrid Dragonfly Algorithm-optimized Support Vector Machine for regression (DA-SVMr) model in predicting the performance of a nanofluid-based single-slope solar still. The model leverages a comprehensive dataset of 251 data points, encompassing key parameters such as solar radiation, ambient and

basin temperatures, water depth, and nanofluid properties, to accurately model the non-linear relationship with daily freshwater productivity.

The DA-SVMr model achieves exceptional predictive accuracy, as evidenced by high R^2 and r values on both training (R^2 = 0.9999, r = 0.9999) and testing datasets (R^2 = 0.9958, r = 0.9980). This indicates the model's strong ability to capture the complex interactions between various influencing factors and the resulting water productivity. While some degree of overfitting is observed based on the differences in RMSE, AARD., and MAE between the training and testing sets, the model's performance on unseen data remains robust and reliable. This suggests that the model has effectively generalized the underlying patterns and relationships, even with limited data.

Residual analysis provides further validation of the model's reliability. The residuals are randomly distributed around zero, indicating that the errors are unbiased and evenly distributed. This randomness confirms that the DA-SVMr model accurately captures the underlying relationships within the dataset, without systematic over- or underestimation. The distribution of errors closely resembles a normal distribution, which supports the validity of statistical inferences based on the model.

Statistical validation via ANOVA testing confirms that there is no significant difference between the actual and predicted values. The high p-value (0.7937) and the location of the F-statistic within the acceptance region strongly support this conclusion. This underscores the accuracy and reliability of the DA-SVMr model in simulating the behavior of the solar still system. The findings from the Levene's and Shapiro-Wilk tests indicate the validity of assumptions of equal variances and normality, reinforcing the robustness of the ANOVA analysis. The negligible effect size and η2 value highlight the minimal variance explained by group differences, further confirming the model's accurate reflection of real-world behavior. Tukey's HSD test further supports the absence of significant pairwise mean differences, solidifying the model's consistent and accurate performance across all data points.

By integrating advanced machine learning techniques with nanofluid-enhanced solar desalination, this study offers new insights into the benefits of nanofluids for improved heat transfer in solar thermal applications. The DA-SVMr model can be used as a valuable tool for optimizing solar still design and operation. The optimized parameters obtained through the Dragonfly Algorithm (C=372.9428. σ=1.2590. ϵ=72.4209) provides insights into the ideal settings for this model to optimize the prediction. The model can be used to explore the impact of various design modifications, operating conditions, and nanofluid properties on water productivity, ultimately leading to more efficient and cost-effective solar desalination systems.

These findings have significant implications for addressing the global water crisis, particularly in arid and remote regions. The DA-SVMr model provides a powerful tool for designing and optimizing single-slope solar stills, enabling efficient freshwater production from brackish or saline water sources. This technology can contribute to sustainable water management practices and improve access to clean water for communities facing water scarcity. The success of this study also highlights the potential of advanced machine learning techniques to address complex engineering challenges in the field of renewable energy. Further research should focus on validating the model with additional datasets. exploring the application of other optimization algorithms, and investigating the long-term performance and economic viability of nanofluid-enhanced solar stills.

GENERAL CONCLUSION

Based on the comprehensive research presented, nanofluids have emerged as a significant advancement in thermal and energy transport systems, offering enhanced performance, efficiency and stability compared to conventional fluids. Their superior efficiency opens up applications across various industrial sectors, particularly in renewable energy and thermal management. while nanofluids have already proven their significance, hybrid nanofluids represent a remarkable leap forward. These advanced fluids offer superior thermal conductivity, stability, and efficiency, making them invaluable for applications in renewable energy, water desalination, and industrial cooling systems. Tri-hybrid nanofluids, in particular, demonstrate exceptional performance due to the synergistic interactions of three distinct nanoparticles, enabling accelerated energy transport and improved thermal management.

The implications of these advancements extend beyond the immediate scope of the studies. The ability to accurately predict and optimize nanofluid behavior opens up possibilities for addressing global challenges such as water scarcity and sustainable energy production. For instance, the improved efficiency of nanofluid-based solar stills could contribute to more effective water desalination processes in water-scarce regions. Similarly, the enhanced thermal management capabilities of nanofluids could lead to more efficient cooling systems in various industries, potentially reducing energy consumption and environmental impact.

The synergy between nanofluid technology and machine learning techniques has proven to be a powerful approach to optimizing thermal management and energy systems. Various machine learning algorithms, including Support Vector Regression (SVR) models optimized with Fox Optimization Algorithm (FOA) and Dragonfly Algorithm (DA), have demonstrated exceptional accuracy in predicting nanofluid properties and system performance.

The first contribution of my research developed and evaluated four machine learning models: DA-SVR with H_CV, DA-SVR with LMO_CV, FOA-SVR with H_CV, and FOA-SVR with LMO_CV. All models demonstrated exceptional predictive capabilities, achieving R^2 values exceeding 0.999 across all datasets, underscoring their accuracy and reliability. For dynamic viscosity prediction, the FOA-SVR model with LMO_CV achieved an RMSE of 0.0044 and an R^2 of 0.9997, while for thermal conductivity, it achieved an RMSE of 0.0020 and an R^2 of 0.99931. A detailed comparison revealed the superior performance of the FOA-SVR models, which consistently outperformed DA-SVR models in terms of error minimization and generalization.

The differences in performance can be attributed to the hyperparameter selection and the used optimization techniques. The FOX-inspired optimization algorithm employed in FOA-SVR allowed for the selection of lower penalty parameters (C) and sigma (σ) values, leading to

smoother decision boundaries and better generalization to unseen data. For instance, in predicting thermal conductivity, the FOA-SVR model with LMO_CV used hyperparameters C = 17.2937, σ = 1.6752, and ε = 3.7636×10^{-6}, which provided a balance between error reduction and model flexibility. In contrast, DA-SVR models, while robust, exhibited a relatively rigid structure that limited their flexibility in certain scenarios.

Furthermore, the FOA-SVR models maintained consistent performance across both Holdout and LMO cross-validation methods, emphasizing their reliability and adaptability to various data splits. The role of cross-validation methods was also crucial in evaluating the models. The LMO_CV method proved to be more robust, consistently producing lower RMSE values and higher R^2 values compared to H_CV. For example, in predicting dynamic viscosity, the FOA-SVR model improved from an RMSE of 0.0077 with H_CV to 0.0044 with LMO_CV1. This highlights the importance of using comprehensive validation techniques to ensure the reliability and generalizability of machine learning models.

The findings of this study have significant implications for the accurate modeling and prediction of thermophysical properties in advanced nanofluids. The FOA-SVR models' superior performance makes them valuable tools for industrial applications requiring precise and reliable predictions, such as in energy systems, thermal management, and advanced manufacturing. The models' ability to predict both dynamic viscosity and thermal conductivity with high accuracy ($R^2 > 0.999$) across a range of temperatures (15 to 60 °C) and nanoparticle concentrations (0.1 to 0.5 vol%) demonstrates their potential for practical applications.

The second contribution successfully demonstrates the effectiveness of a hybrid Dragonfly Algorithm-optimized Support Vector Machine for regression (DA-SVMr) model in predicting the performance of a nanofluid-based single-slope solar still. The model leverages a comprehensive dataset of 251 data points, encompassing key parameters such as solar radiation, ambient and basin temperatures, water depth, and nanofluid properties, to accurately model the non-linear relationship with daily freshwater productivity. The DA-SVMr model achieves exceptional predictive accuracy, with high R^2 and r values on both training ($R^2 = 0.9999$, $r = 0.9999$) and testing datasets ($R^2 = 0.9958$, $r = 0.9980$), indicating its strong ability to capture complex interactions between various influencing factors and resulting water productivity.

Residual analysis further validates the model's reliability, with errors randomly distributed around zero and closely resembling a normal distribution. This confirms that the DA-SVMr model accurately captures underlying relationships within the dataset without systematic over- or underestimation. Statistical validation via ANOVA testing corroborates these findings, with a high p-value (0.7937) and the F-statistic within the acceptance region,

indicating no significant difference between actual and predicted values. The Levene's and Shapiro-Wilk tests support the validity of equal variances and normality assumptions, while Tukey's HSD test confirms the absence of significant pairwise mean differences.

The integration of advanced machine learning techniques with nanofluid-enhanced solar desalination offers new insights into the benefits of nanofluids for improved heat transfer in solar thermal applications. The optimized parameters obtained through the Dragonfly Algorithm (C=372.9428, σ=1.2590, ϵ=72.4209) provide ideal settings for model prediction optimization. The DA-SVMr model serves as a valuable tool for exploring the impact of various design modifications, operating conditions, and nanofluid properties on water productivity, potentially leading to more efficient and cost-effective solar desalination systems.

These findings have significant implications for addressing the global water crisis, particularly in arid and remote regions. The DA-SVMr model provides a powerful tool for designing and optimizing single-slope solar stills, enabling efficient freshwater production from brackish or saline water sources. This technology can contribute to sustainable water management practices and improve access to clean water for communities facing water scarcity. The success of this study also highlights the potential of advanced machine learning techniques to address complex engineering challenges in the field of renewable energy.

In comparison with related studies, the DA-SVMr model demonstrates superior or comparable performance to other recent modeling approaches. Its high accuracy and strong generalization make it a valuable tool for optimizing solar still design and operation. The study's combination of nanofluid enhancement in solar stills with advanced machine learning techniques for performance prediction represents a significant contribution to the field, often surpassing the findings of related studies.

Future research directions should focus on validating the model with additional datasets, exploring the application of other optimization algorithms, and investigating the long-term performance and economic viability of nanofluid-enhanced solar stills. Additionally, the integration of hybrid optimization techniques or the extension of these models to predict additional thermophysical properties could further enhance their utility and applicability in solar still technology.

Based on the promising results observed with tri-hybrid nanofluids in various thermal applications, it is strongly recommended to explore their potential in solar still systems. Researchers and engineers should prioritize the development and testing of tri-hybrid nanofluid formulations specifically tailored for solar desalination processes. These advanced nanofluids, combining three distinct nanoparticles, have demonstrated superior thermal conductivity

and heat transfer capabilities, which could significantly enhance the efficiency and productivity of solar stills.

To fully realize the benefits of tri-hybrid nanofluids in solar stills, it is recommended to conduct comprehensive experimental studies to determine the optimal combination and concentration of nanoparticles for solar still applications, investigate the long-term stability and performance of tri-hybrid nanofluids under typical solar still operating conditions, perform comparative analyses between conventional nanofluids, hybrid nanofluids, and tri-hybrid nanofluids to quantify the improvements in freshwater production rates and overall system efficiency, develop computational models to predict and optimize the performance of tri-hybrid nanofluid-enhanced solar stills under various environmental conditions, and finally assess the economic viability and environmental impact of implementing tri-hybrid nanofluids in large-scale solar desalination projects.

By pursuing these research directions, the scientific community can unlock the full potential of tri-hybrid nanofluids in solar still technology, potentially revolutionizing water desalination processes and addressing global water scarcity challenges more effectively.

REFERENCES

[1] K. V. Modi, P. R. Patel, & S. K. Patel, Applicability of mono-nanofluid and hybrid-nanofluid as a technique to improve the performance of solar still: A critical review. Journal of Cleaner Production, *387*, 135875 (2023). https://doi.org/10.1016/j.jclepro.2023.135875

[2] S.U.S. Choi, J.A. Eastman, Enhancing thermal conductivity of fluids with nanoparticles, Argonne National Lab.(ANL), Argonne, IL (United States), 1995.

[3] I. Razzaq, W. Xinhua, G. Rasool, T. Sun, A.S. Shflot, M.Y. Malik, K. Abbas, S. Ali, A. Ali, Nanofluids for Advanced Applications: A Comprehensive Review on Preparation Methods, Properties, and Environmental Impact, ACS Omega (2025). https://doi.org/10.1021/ACSOMEGA.4C10143/ASSET/IMAGES/LARGE/AO4C10143_0021.JPEG.

[4] T. Ma, Z. Guo, M. Lin, Q. Wang, Recent trends on nanofluid heat transfer machine learning research applied to renewable energy, Renewable and Sustainable Energy Reviews 138 (2021) 110494. https://doi.org/10.1016/J.RSER.2020.110494.

[5] A.K. Hamzat, M.I. Omisanya, A.Z. Sahin, O. Ropo Oyetunji, N. Abolade Olaitan, Application of nanofluid in solar energy harvesting devices: A comprehensive review, Energy Convers Manag 266 (2022) 115790. https://doi.org/10.1016/J.ENCONMAN.2022.115790.

[6] S.S. Khaleduzzaman, M.R. Sohel, R. Saidur, J. Selvaraj, Stability of Al2O3-water Nanofluid for Electronics Cooling System, Procedia Eng 105 (2015) 406–411. https://doi.org/10.1016/J.PROENG.2015.05.026.

[7] M.R. Sohel, R. Saidur, S.S. Khaleduzzaman, T.A. Ibrahim, Cooling performance investigation of electronics cooling system using Al2O3–H2O nanofluid, International Communications in Heat and Mass Transfer 65 (2015) 89–93. https://doi.org/10.1016/J.ICHEATMASSTRANSFER.2015.04.015.

[8] M.B. Bigdeli, M. Fasano, A. Cardellini, E. Chiavazzo, P. Asinari, A review on the heat and mass transfer phenomena in nanofluid coolants with special focus on automotive applications, Renewable and Sustainable Energy Reviews 60 (2016) 1615–1633. https://doi.org/10.1016/J.RSER.2016.03.027.

[9] F. Abbas, H.M. Ali, T.R. Shah, H. Babar, M.M. Janjua, U. Sajjad, M. Amer, Nanofluid: Potential evaluation in automotive radiator, J Mol Liq 297 (2020) 112014. https://doi.org/10.1016/J.MOLLIQ.2019.112014.

[10] S. Chandel, D. Sharma, Ternary nanofluid dynamics in stagnated flow with exponential heat and inclined magnetic field: Applications in advanced cooling and aerospace system, Int J Heat Fluid Flow 109 (2024) 109508. https://doi.org/10.1016/J.IJHEATFLUIDFLOW.2024.109508.

[11] H.B. Kulkarni, M.M. Nadakatti, S.C. Kulkarni, R.M. Kulkarni, Investigations on effect of nanofluid based minimum quantity lubrication technique for surface milling of Al7075-T6 aerospace alloy, Mater Today Proc 27 (2020) 251–256. https://doi.org/10.1016/J.MATPR.2019.10.127.

[12] S. Akram, M. Athar, K. Saeed, A. Razia, T. Muhammad, H. Ahmed Alghamdi, Mathematical simulation of double diffusion convection on peristaltic pumping of Ellis nanofluid due to induced magnetic field in a non-uniform channel: Applications of magnetic nanoparticles in biomedical engineering, J Magn Magn Mater 569 (2023) 170408. https://doi.org/10.1016/J.JMMM.2023.170408.

[13] P. Chinnasamy, R. Sivajothi, S. Sathish, M. Abbas, V. Jeyakrishnan, R. Goel, M.S. Alqahtani, K. Loganathan, Peristaltic transport of Sutterby nanofluid flow in an inclined tapered channel with an artificial neural network model and biomedical engineering application, Scientific Reports 2024 14:1 14 (2024) 1–23. https://doi.org/10.1038/s41598-023-49480-9.

[14] J. Philip, P.D. Shima, Thermal properties of nanofluids, Adv Colloid Interface Sci 183–184 (2012) 30–45. https://doi.org/10.1016/J.CIS.2012.08.001.
[15] H. Khodadadi, S. Aghakhani, H. Majd, R. Kalbasi, S. Wongwises, M. Afrand, A comprehensive review on rheological behavior of mono and hybrid nanofluids: Effective parameters and predictive correlations, Int J Heat Mass Transf 127 (2018) 997–1012. https://doi.org/10.1016/J.IJHEATMASSTRANSFER.2018.07.103.
[16] J. Philip, J.M. Laskar, Optical Properties and Applications of Ferrofluids—A Review, Journal of Nanofluids 1 (2013) 3–20. https://doi.org/10.1166/JON.2012.1002.
[17] Z. Hedayatnasab, F. Abnisa, W.M.A.W. Daud, Review on magnetic nanoparticles for magnetic nanofluid hyperthermia application, Mater Des 123 (2017) 174–196. https://doi.org/10.1016/J.MATDES.2017.03.036.
[18] M. Kalteh, Investigating the effect of various nanoparticle and base liquid types on the nanofluids heat and fluid flow in a microchannel, Appl Math Model 37 (2013) 8600–8609. https://doi.org/10.1016/J.APM.2013.03.067.
[19] D. Yilmaz Aydin, M. Gürü, A. Sözen, E. Çiftçi, Investigation of the effects of base fluid type of the nanofluid on heat pipe performance, Proceedings of the Institution of Mechanical Engineers, Part A: Journal of Power and Energy 235 (2021) 124–138. https://doi.org/10.1177/0957650920916285.
[20] J.M. Munyalo, X. Zhang, Particle size effect on thermophysical properties of nanofluid and nanofluid based phase change materials: A review, J Mol Liq 265 (2018) 77–87. https://doi.org/10.1016/J.MOLLIQ.2018.05.129.
[21] A.M. Hussein, K. V. Sharma, R.A. Bakar, K. Kadirgama, The Effect of Nanofluid Volume Concentration on Heat Transfer and Friction Factor inside a Horizontal Tube, J Nanomater 2013 (2013) 859563. https://doi.org/10.1155/2013/859563.
[22] D.H. Prajitno, A. Maulana, D.G. Syarif, Effect of Surface Roughness on Contact Angle Measurement of Nanofluid on Surface of Stainless Steel 304 by Sessile Drop Method, J Phys Conf Ser 739 (2016) 012029. https://doi.org/10.1088/1742-6596/739/1/012029.
[23] A.K. Hamzat, M.I. Omisanya, A.Z. Sahin, O. Ropo Oyetunji, N. Abolade Olaitan, Application of nanofluid in solar energy harvesting devices: A comprehensive review, Energy Convers Manag 266 (2022) 115790. https://doi.org/10.1016/J.ENCONMAN.2022.115790.
[24] Y. Thakare, S. Dharaskar, A. Unnarkat, S.S. Sonawane, Nanofluid-based drug delivery systems, Applications of Nanofluids in Chemical and Bio-Medical Process Industry (2022) 303–334. https://doi.org/10.1016/B978-0-323-90564-0.00005-2.
[25] H. Chang, C.S. Jwo, P.S. Fan, S.H. Pai, Process optimization and material properties for nanofluid manufacturing, International Journal of Advanced Manufacturing Technology 34 (2007) 300–306. https://doi.org/10.1007/S00170-006-0597-0/METRICS.
[26] S. Suneetha, K. Subbarayudu, P. Bala Anki Reddy, Hybrid nanofluids development and benefits: A comprehensive review, Journal of Thermal Engineering 8 (2022) 445–455. https://doi.org/10.18186/THERMAL.1117455.
[27] S.K. Gupta, S. Pradhan, A review of recent advances and the role of nanofluid in solar photovoltaic thermal (PV/T) system, Mater Today Proc 44 (2021) 782–791. https://doi.org/10.1016/J.MATPR.2020.10.708.
[28] S.K. Verma, A.K. Tiwari, Progress of nanofluid application in solar collectors: A review, Energy Convers Manag 100 (2015) 324–346. https://doi.org/10.1016/J.ENCONMAN.2015.04.071.
[29] N.A.C. Sidik, T.H. Kean, H.K. Chow, A. Rajaandra, S. Rahman, J. Kaur, Performance enhancement of cold thermal energy storage system using nanofluid phase change materials: A review, International Communications in Heat and Mass Transfer 94 (2018) 85–95. https://doi.org/10.1016/J.ICHEATMASSTRANSFER.2018.03.024.

[30] F.L. Rashid, M.A. Al-Obaidi, H.I. Mohammed, H. Togun, S. Ahmad, A. Ameen, A review of the current situation and prospects for nanofluids to improve solar still performance, J Therm Anal Calorim 149 (2024) 13511–13531. https://doi.org/10.1007/S10973-024-13465-1/TABLES/7.

[31] B. Bhaumik, S. Chaturvedi, S. Changdar, S. De, A unique physics-aided deep learning model for predicting viscosity of nanofluids, International Journal for Computational Methods in Engineering Science and Mechanics 24 (2023) 167–181. https://doi.org/10.1080/15502287.2022.2120441.

[32] P.K. Kanti, P. Paramasivam, V.V. Wanatasanappan, S. Dhanasekaran, P. Sharma, Experimental and explainable machine learning approach on thermal conductivity and viscosity of water based graphene oxide based mono and hybrid nanofluids, Scientific Reports 2024 14:1 14 (2024) 1–16. https://doi.org/10.1038/s41598-024-81955-1.

[33] M. Bahiraei, L.K. Foong, S. Hosseini, N. Mazaheri, Predicting heat transfer rate of a ribbed triple-tube heat exchanger working with nanofluid using neural network enhanced by advanced optimization algorithms, Powder Technol 381 (2021) 459–476. https://doi.org/10.1016/J.POWTEC.2020.12.003.

[34] K. Venkateswarlu, K.P.V.K. Varma, U.K. Nutakki, Synthesis, characterization and application of mono-, hybrid and ternary nanofluids in hybrid photovoltaic thermal (PV/T) solar systems—a review, Journal of the Brazilian Society of Mechanical Sciences and Engineering 2022 44:11 44 (2022) 1–21. https://doi.org/10.1007/S40430-022-03864-6.

[35] Y. Meraihi, A. Ramdane-Cherif, D. Acheli, M. Mahseur, Dragonfly algorithm: a comprehensive review and applications, Neural Comput Appl 32 (2020) 16625–16646. https://doi.org/10.1007/S00521-020-04866-Y/METRICS.

[36] H. Mohammed, T. Rashid, FOX: a FOX-inspired optimization algorithm, Applied Intelligence 53 (2023) 1030–1050. https://doi.org/10.1007/S10489-022-03533-0/METRICS.

[37] S. Margoum, B. Hajji, S. Aneli, G.M. Tina, A. Gagliano, Optimizing Nanofluid Hybrid Solar Collectors through Artificial Intelligence Models, Energies 2024, Vol. 17, Page 2307 17 (2024) 2307. https://doi.org/10.3390/EN17102307.

[38] C. Kamsuwan, X. Wang, L.P. Seng, C.K. Xian, R. Piemjaiswang, P. Piumsomboon, Y. Pratumwal, S. Otarawanna, B. Chalermsinsuwan, Simulation of nanofluid micro-channel heat exchanger using computational fluid dynamics integrated with artificial neural network, Energy Reports 9 (2023) 239–247. https://doi.org/10.1016/J.EGYR.2022.10.412.

[39] S.K. Pathak, R. Kumar, V. Goel, A.K. Pandey, V. V. Tyagi, Recent advancements in thermal performance of nano-fluids charged heat pipes used for thermal management applications: A comprehensive review, Appl Therm Eng 216 (2022) 119023. https://doi.org/10.1016/J.APPLTHERMALENG.2022.119023.

[40] A. Arshad, M. Jabbal, Y. Yan, D. Reay, A review on graphene based nanofluids: Preparation, characterization and applications, J Mol Liq 279 (2019) 444–484. https://doi.org/10.1016/j.molliq.2019.01.153.

[41] S.M.S. Murshed, P. Estellé, A state of the art review on viscosity of nanofluids, Renewable and Sustainable Energy Reviews 76 (2017) 1134–1152. https://doi.org/10.1016/j.rser.2017.03.113.

[42] M.A. Rahman, S.M.M. Hasnain, S. Pandey, A. Tapalova, N. Akylbekov, R. Zairov, Review on nanofluids: preparation, properties, stability, and thermal performance augmentation in heat transfer applications, ACS Omega (2024). https://doi.org/10.1021/acsomega.4c03279.

[43] Y. Xuan, Q. Li, Heat transfer enhancement of nanofluids, Int J Heat Fluid Flow 21 (2000) 58–64.
[44] T. Ambreen, M.-H. Kim, Influence of particle size on the effective thermal conductivity of nanofluids: A critical review, Appl Energy 264 (2020) 114684.
[45] O. Mahian, L. Kolsi, M. Amani, P. Estellé, G. Ahmadi, C. Kleinstreuer, J.S. Marshall, M. Siavashi, R.A. Taylor, H. Niazmand, others, Recent advances in modeling and simulation of nanofluid flows-Part I: Fundamentals and theory, Phys Rep 790 (2019) 1–48.
[46] M.L.G. Ho, C.S. Oon, L.-L. Tan, Y. Wang, Y.M. Hung, A review on nanofluids coupled with extended surfaces for heat transfer enhancement, Results in Engineering 17 (2023) 100957.
[47] J.C. Maxwell, A treatise on electricity and magnetism, Clarendon press, 1873.
[48] W. Yu, Choi, SUS, The role of interfacial layers in the enhanced thermal conductivity of nanofluids: a renovated Maxwell model, Journal of Nanoparticle Research 5 (2003) 167–171.
[49] R.L. Hamilton, O.K. Crosser, Thermal conductivity of heterogeneous two-component systems, Industrial \& Engineering Chemistry Fundamentals 1 (1962) 187–191.
[50] J. Wohld, J. Beck, K. Inman, M. Palmer, M. Cummings, R. Fulmer, S. Vafaei, Hybrid Nanofluid Thermal Conductivity and Optimization: Original Approach and Background, Nanomaterials 12 (2022). https://doi.org/10.3390/nano12162847.
[51] A.O. Borode, N.A. Ahmed, P.A. Olubambi, M. Sharifpur, J.P. Meyer, Investigation of the thermal conductivity, viscosity, and thermal performance of graphene nanoplatelet-alumina hybrid nanofluid in a differentially heated cavity, Front Energy Res 9 (2021) 737915.
[52] Z. Mahmood, S.M. Eldin, K. Rafique, U. Khan, Numerical analysis of MHD tri-hybrid nanofluid over a nonlinear stretching/shrinking sheet with heat generation/absorption and slip conditions, Alexandria Engineering Journal 76 (2023) 799–819. https://doi.org/10.1016/j.aej.2023.06.081.
[53] H. Adun, D. Kavaz, M. Dagbasi, Review of ternary hybrid nanofluid: Synthesis, stability, thermophysical properties, heat transfer applications, and environmental effects, J Clean Prod 328 (2021) 129525. https://doi.org/https://doi.org/10.1016/j.jclepro.2021.129525.
[54] S. Chinchanikar, S.S. Kore, P. Hujare, A review on nanofluids in minimum quantity lubrication machining, J Manuf Process 68 (2021) 56–70. https://doi.org/https://doi.org/10.1016/j.jmapro.2021.05.028.
[55] J. Li, X. Zhang, B. Xu, M. Yuan, Nanofluid research and applications: A review, International Communications in Heat and Mass Transfer 127 (2021) 105543. https://doi.org/https://doi.org/10.1016/j.icheatmasstransfer.2021.105543.
[56] T. Kitano, T. Kataoka, T. Shirota, An empirical equation of the relative viscosity of polymer melts filled with various inorganic fillers, Rheol Acta 20 (1981) 207–209.
[57] H.C. Brinkman, The viscosity of concentrated suspensions and solutions, Journal of Chemical Physics 20 (1952) 571.
[58] D.G. Thomas, Transport characteristics of suspension: VIII. A note on the viscosity of Newtonian suspensions of uniform spherical particles, J Colloid Sci 20 (1965) 267–277. https://doi.org/https://doi.org/10.1016/0095-8522(65)90016-4.
[59] I.M. Krieger, T.J. Dougherty, A mechanism for non-Newtonian flow in suspensions of rigid spheres, Trans. Soc. Rheol 3 (1959) 137–152.
[60] H. Chen, Y. Ding, C. Tan, Rheological behaviour of nanofluids, New J Phys 9 (2007) 367.

[61] C. Ezekwem, A recent review of viscosity models for nanofluids, Energy Sources, Part A: Recovery, Utilization, and Environmental Effects 44 (2022) 1250–1315. https://doi.org/10.1080/15567036.2021.1993469.
[62] L.S. Sundar, K. V. Sharma, M.T. Naik, M.K. Singh, Empirical and theoretical correlations on viscosity of nanofluids: A review, Renewable and Sustainable Energy Reviews 25 (2013) 670–686. https://doi.org/10.1016/j.rser.2013.04.003.
[63] B.C. Pak, Y.I. Cho, Hydrodynamic and heat transfer study of dispersed fluids with submicron metallic oxide particles, Experimental Heat Transfer 11 (1998) 151–170. https://doi.org/10.1080/08916159808946559.
[64] Y. Xuan, W. Roetzel, Conceptions for heat transfer correlation of nanofluids, Int J Heat Mass Transf 43 (2000) 3701–3707. https://doi.org/https://doi.org/10.1016/S0017-9310(99)00369-5.
[65] I.L. Animasaun, N.A. Shah, A. Wakif, B. Mahanthesh, R. Sivaraj, O.K. Koriko, Ratio of momentum diffusivity to thermal diffusivity: introduction, meta-analysis, and scrutinization, Chapman and Hall/CRC, 2022.
[66] L.S. Sundar, S.M.O. Tavares, A.M.B. Pereira, A.C.M. Sousa, Review on thermal efficiency augment of flat plate collector equipped with mono and hybrid nanofluids and with inserts, International Journal of Thermofluids 26 (2025) 101111. https://doi.org/https://doi.org/10.1016/j.ijft.2025.101111.
[67] J. Pereira, A. Moita, A. Moreira, An overview of the molten salt nanofluids as thermal energy storage media, Energies (Basel) 16 (2023) 1825.
[68] S. Shrestha, B. Wang, P. Dutta, Nanoparticle processing: Understanding and controlling aggregation, Adv Colloid Interface Sci 279 (2020) 102162.
[69] V.T. Nguyen, N.H. Pham, D. V Papavassiliou, Prediction of the aggregation rate of nanoparticles in porous media in the diffusion-controlled regime, Sci Rep 14 (2024) 1916.
[70] S. Şirin, Investigation of the performance of cermet tools in the turning of Haynes 25 superalloy under gaseous N2 and hybrid nanofluid cutting environments, J Manuf Process 76 (2022) 428–443.
[71] J. Wang, X. Yang, J.J. Klemeš, K. Tian, T. Ma, B. Sunden, A review on nanofluid stability: preparation and application, Renewable and Sustainable Energy Reviews 188 (2023) 113854.
[72] M.L.G. Ho, C.S. Oon, L.L. Tan, Y. Wang, Y.M. Hung, A review on nanofluids coupled with extended surfaces for heat transfer enhancement, Results in Engineering 17 (2023). https://doi.org/10.1016/j.rineng.2023.100957.
[73] T.P. Teng, C.M. Cheng, F.Y. Pai, Preparation and characterization of carbon nanofluid by a plasma arc nanoparticles synthesis system, Nanoscale Res Lett 6 (2011) 1–11. https://doi.org/10.1186/1556-276X-6-293.
[74] H. Akoh, Y. Tsukasaki, S. Yatsuya, A. Tasaki, Magnetic properties of ferromagnetic ultrafine particles prepared by vacuum evaporation on running oil substrate, J Cryst Growth 45 (1978) 495–500.
[75] B. Bakthavatchalam, K. Habib, R. Saidur, B.B. Saha, K. Irshad, Comprehensive study on nanofluid and ionanofluid for heat transfer enhancement: A review on current and future perspective, J Mol Liq 305 (2020) 112787.
[76] Z. Said, L.S. Sundar, A.K. Tiwari, H.M. Ali, M. Sheikholeslami, E. Bellos, H. Babar, Recent advances on the fundamental physical phenomena behind stability, dynamic motion, thermophysical properties, heat transport, applications, and challenges of nanofluids, Phys Rep 946 (2022) 1–94.

[77] A. Iqbal, M.S. Mahmoud, E.T. Sayed, K. Elsaid, M.A. Abdelkareem, H. Alawadhi, A.G. Olabi, Evaluation of the nanofluid-assisted desalination through solar stills in the last decade, J Environ Manage 277 (2021) 111415.
[78] J. He, C. Wang, H. Tang, Z. Sun, Prospective research on the tribological behavior of graphdiyne nanofluid and its machine learning performance prediction, Appl Surf Sci 696 (2025) 162954. https://doi.org/https://doi.org/10.1016/j.apsusc.2025.162954.
[79] T.W.B. Riyadi, S.G. Herawan, A. Tirta, Y.J. Ee, A.L. Hananto, P.A. Paristiawan, A.A. Yusuf, H. Venu, Irianto, I. Veza, Nanofluid heat transfer and machine learning: Insightful review of machine learning for nanofluid heat transfer enhancement in porous media and heat exchangers as sustainable and renewable energy solutions, Results in Engineering 24 (2024) 103002. https://doi.org/https://doi.org/10.1016/j.rineng.2024.103002.
[80] L. Snoussi, O. Fakhfakh, M.I. Khedher, G.A. Khouqeer, K. V Sharma, F. Hosni, M. Sallah, Comparative analysis of machine learning techniques for estimating dynamic viscosity in various nanofluids for improving the efficiency of thermal and radiative systems, J Radiat Res Appl Sci 18 (2025) 101205. https://doi.org/https://doi.org/10.1016/j.jrras.2024.101205.
[81] P. Dehury, S. Chaudhari, T. Banerjee, S. Kumar Das, Prediction of thermophysical properties of deep eutectic solvent-based organic nanofluids: A machine learning approach, J Mol Liq 411 (2024) 125809. https://doi.org/https://doi.org/10.1016/j.molliq.2024.125809.
[82] G. Li, H. Sun, D. Han, S. Cheng, G. Zhao, Y. Guo, Applying machine learning to reveal the microscopic heat transfer mechanism of nanofluids as coolants, Thermochim Acta 738 (2024) 179788. https://doi.org/https://doi.org/10.1016/j.tca.2024.179788.
[83] A. Banasiewicz, A Brief History of Learning with Data, in: Organizational Learning in the Age of Data, Springer International Publishing, Cham, 2021: pp. 87–102. https://doi.org/10.1007/978-3-030-74866-1_4.
[84] O. Koteluk, A. Wartecki, S. Mazurek, I. Kołodziejczak, A. Mackiewicz, How do machines learn? artificial intelligence as a new era in medicine, J Pers Med 11 (2021) 32.
[85] I.H. Sarker, Machine learning: Algorithms, real-world applications and research directions, SN Comput Sci 2 (2021) 160.
[86] N. Cummins, A. Baird, B.W. Schuller, Speech analysis for health: Current state-of-the-art and the increasing impact of deep learning, Methods 151 (2018) 41–54.
[87] S. Hegde, S. Shetty, S. Rai, T. Dodderi, A survey on machine learning approaches for automatic detection of voice disorders, Journal of Voice 33 (2019) 947--e11.
[88] Y. Wang, I. V Tetko, M.A. Hall, E. Frank, A. Facius, K.F.X. Mayer, H.W. Mewes, Gene selection from microarray data for cancer classification—a machine learning approach, Comput Biol Chem 29 (2005) 37–46.
[89] A.W. Senior, R. Evans, J. Jumper, J. Kirkpatrick, L. Sifre, T. Green, C. Qin, A. Ž\'\idek, A.W.R. Nelson, A. Bridgland, others, Improved protein structure prediction using potentials from deep learning, Nature 577 (2020) 706–710.
[90] Y. Zoabi, S. Deri-Rozov, N. Shomron, Machine learning-based prediction of COVID-19 diagnosis based on symptoms, NPJ Digit Med 4 (2021) 1–5.
[91] A. Dey, others, Machine learning algorithms: a review, International Journal of Computer Science and Information Technologies 7 (2016) 1174–1179.
[92] S. Das, A. Dey, A. Pal, N. Roy, Applications of artificial intelligence in machine learning: review and prospect, Int J Comput Appl 115 (2015).
[93] J.L. Thenier-Villa, F.R. Martínez-Ricarte, M. Figueroa-Vezirian, F. Arikan-Abelló, Glioblastoma Pseudoprogression Discrimination Using Multiparametric Magnetic

Resonance Imaging, Principal Component Analysis, and Supervised and Unsupervised Machine Learning, World Neurosurg 183 (2024) e953–e962. https://doi.org/https://doi.org/10.1016/j.wneu.2024.01.074.

[94] S. Messaoud, A. Bradai, S.H.R. Bukhari, P.T.A. Quang, O. Ben Ahmed, M. Atri, A survey on machine learning in Internet of Things: Algorithms, strategies, and applications, Internet of Things (Netherlands) 12 (2020) 100314. https://doi.org/10.1016/j.iot.2020.100314.

[95] R.P. França, A.C. Borges Monteiro, R. Arthur, Y. Iano, Chapter 3 - An overview of deep learning in big data, image, and signal processing in the modern digital age, in: V. Piuri, S. Raj, A. Genovese, R. Srivastava (Eds.), Trends in Deep Learning Methodologies, Academic Press, 2021: pp. 63–87. https://doi.org/https://doi.org/10.1016/B978-0-12-822226-3.00003-9.

[96] S. Raghavendra, P.C. Deka, Support vector machine applications in the field of hydrology: A review, Appl Soft Comput 19 (2014) 372–386. https://doi.org/10.1016/J.ASOC.2014.02.002.

[97] V. Vapnik, The nature of statistical learning theory, Springer science & business media, 1999.

[98] V. Vapnik, S. Golowich, A. Smola, Support Vector Method for Function Approximation, Regression Estimation and Signal Processing, Adv Neural Inf Process Syst 9 (1996).

[99] R. Collobert collober, R.C. Williamson, SVMTorch: Support Vector Machines for Large-Scale Regression Problems, Journal of Machine Learning Research 1 (2001) 143–160. www.idiap.chhlearninggSVMTorch.html. (accessed March 21, 2025).

[100] Y. Ccoicca, Applications of support vector machines in the exploratory phase of petroleum and natural gas: a survey, International Journal of Engineering & Technology 2 (2013) 113.

[101] C. Cortes, V. Vapnik, L. Saitta, Support-vector networks, Machine Learning 1995 20:3 20 (1995) 273–297. https://doi.org/10.1007/BF00994018.

[102] C.J.C. Burges, A tutorial on support vector machines for pattern recognition, Data Min Knowl Discov 2 (1998) 121–167. https://doi.org/10.1023/A:1009715923555/METRICS.

[103] V. Vapnik, The nature of statistical learning theory, Springer science & business media, 2013.

[104] P.S. Yu, S.T. Chen, I.F. Chang, Support vector regression for real-time flood stage forecasting, J Hydrol (Amst) 328 (2006) 704–716. https://doi.org/10.1016/J.JHYDROL.2006.01.021.

[105] S.T. Chen, P.S. Yu, Pruning of support vector networks on flood forecasting, J Hydrol (Amst) 347 (2007) 67–78. https://doi.org/10.1016/J.JHYDROL.2007.08.029.

[106] Y. Dai, H. Wang, M. Yang, G. Li, X. Lv, A machine learning workflow for classifying and predicting the annual climatic status of cotton in Xinjiang, China, Ind Crops Prod 226 (2025) 120623. https://doi.org/https://doi.org/10.1016/j.indcrop.2025.120623.

[107] Z. Liu, Z. Gu, P. Liu, Chapter 5 - Machine learning basics, in: Z. Liu, Z. Gu, P. Liu (Eds.), Transportation Big Data, Elsevier, 2025: pp. 129–175. https://doi.org/https://doi.org/10.1016/B978-0-443-33891-5.00005-3.

[108] M. Mousavi, A. Pouranfard, P. Darvishi, Experimental study and modeling of thermal and rheological characteristics of water-based CuO/CaCO3/SiO2 ternary hybrid nanofluid, Colloids Surf A Physicochem Eng Asp 686 (2024) 133367. https://doi.org/10.1016/J.COLSURFA.2024.133367.

[109] Multicollinearity in Regression Analysis: Problems, Detection, and Solutions - Statistics By Jim, (n.d.). https://statisticsbyjim.com/regression/multicollinearity-in-regression-analysis/ (accessed March 13, 2025).

[110] Multicollinearity in Regression Analysis: Problems, Detection, and Solutions - DataScienceCentral.com, (n.d.). https://www.datasciencecentral.com/multicollinearity-in-regression-analysis-problems-detection-and/ (accessed March 13, 2025).
[111] K.P. Vatcheva, M. Lee, J.B. McCormick, M.H. Rahbar, Multicollinearity in Regression Analyses Conducted in Epidemiologic Studies, Epidemiology (Sunnyvale) 6 (2016) 227. https://doi.org/10.4172/2161-1165.1000227.
[112] R. Rodríguez-Pérez, J. Bajorath, Evolution of Support Vector Machine and Regression Modeling in Chemoinformatics and Drug Discovery, J Comput Aided Mol Des 36 (2022) 355. https://doi.org/10.1007/S10822-022-00442-9.
[113] What Is Support Vector Regression in Machine Learning?, (n.d.). https://learninglabb.com/support-vector-regression-in-machine-learning/ (accessed March 13, 2025).
[114] S. Alrefaee, … S.A.B.-I.J. of, undefined 2022, Hyperparameters optimization of support vector regression using black hole algorithm, Ijnaa.Semnan.Ac.IrSD Alrefaee, SM Al Bakal, ZY AlgamalInternational Journal of Nonlinear Analysis and Applications, 2022•ijnaa.Semnan.Ac.Ir 13 (2022) 2008–6822. https://doi.org/10.22075/ijnaa.2022.6107.
[115] M.A. Jumaah, Y.H. Ali, T.A. Rashid, S. Vimal, FOXANN: A Method for Boosting Neural Network Performance, (2024). http://arxiv.org/abs/2407.03369 (accessed March 16, 2025).
[116] B. Aamirah, S. Emambocus, M. Basheer Jasser, A. Mustapha, A. Amphawan, N. Cennamo, M.J. Deen, S. Morais, S. Mukhopadhyay, J. Lee, A.A.) My, Dragonfly Algorithm and Its Hybrids: A Survey on Performance, Objectives and Applications, Sensors 2021, Vol. 21, Page 7542 21 (2021) 7542. https://doi.org/10.3390/S21227542.
[117] M. Priya, S. Sujatha, A survey on Dragonfly heuristic optimization algorithm, applications, and challenges, Psvpec.InMR Priya, S Sujathapsvpec.In 7 (2024). https://www.psvpec.in/jcres/2024_1/91.pdf (accessed March 16, 2025).
[118] M. Khishe, A. Safari, Classification of Sonar Targets Using an MLP Neural Network Trained by Dragonfly Algorithm, Wirel Pers Commun 108 (2019) 2241–2260. https://doi.org/10.1007/S11277-019-06520-W.
[119] H. Mohammed, T. Rashid, FOX: a FOX-inspired optimization algorithm, Applied Intelligence 53 (2023) 1030–1050. https://doi.org/10.1007/S10489-022-03533-0.
[120] M.R. Apriyadi, D.P. Rini, Hyperparameter optimization of support vector regression algorithm using metaheuristic algorithm for student performance prediction, International Journal of Advanced Computer Science and Applications 14 (2023).
[121] H. Moussa, F. Dahmoune, M. Hentabli, H. Remini, L. Mouni, Optimization of ultrasound-assisted extraction of phenolic-saponin content from Carthamus caeruleus L. rhizome and predictive model based on support vector regression optimized by dragonfly algorithm, Chemometrics and Intelligent Laboratory Systems 222 (2022) 104493. https://doi.org/10.1016/J.CHEMOLAB.2022.104493.
[122] R. Rostamzadeh-Renani, M. Baghoolizadeh, S. Mohammad Sajadi, M. Pirmoradian, M. Rostamzadeh-Renani, S. Baghaei, S. Salahshour, Prediction of the thermal behavior of multi-walled carbon nanotubes-CuO-CeO2 (20-40-40)/water hybrid nanofluid using different types of regressors and evolutionary algorithms for designing the best artificial neural network modeling, Alexandria Engineering Journal 84 (2023) 184–203. https://doi.org/10.1016/J.AEJ.2023.10.059.
[123] M. Hemmat Esfe, S. Saedodin, An experimental investigation and new correlation of viscosity of ZnO–EG nanofluid at various temperatures and different solid volume fractions, Exp Therm Fluid Sci 55 (2014) 1–5. https://doi.org/10.1016/J.EXPTHERMFLUSCI.2014.02.011.

[124] M. Umar, Z. Sabir, M.A.Z. Raja, Y.G. Sánchez, A stochastic numerical computing heuristic of SIR nonlinear model based on dengue fever, Results Phys 19 (2020) 103585. https://doi.org/10.1016/J.RINP.2020.103585.
[125] Z. Said, N.K. Cakmak, P. Sharma, L.S. Sundar, A. Inayat, O. Keklikcioglu, C. Li, Synthesis, stability, density, viscosity of ethylene glycol-based ternary hybrid nanofluids: Experimental investigations and model -prediction using modern machine learning techniques, Powder Technol 400 (2022) 117190. https://doi.org/10.1016/J.POWTEC.2022.117190.
[126] X. Yang, A. Boroomandpour, S. Wen, D. Toghraie, F. Soltani, Applying Artificial Neural Networks (ANNs) for prediction of the thermal characteristics of water/ethylene glycol-based mono, binary and ternary nanofluids containing MWCNTs, titania, and zinc oxide, Powder Technol 388 (2021) 418–424. https://doi.org/10.1016/J.POWTEC.2021.04.093.
[127] Z. Said, N.K. Cakmak, P. Sharma, L.S. Sundar, A. Inayat, O. Keklikcioglu, C. Li, Synthesis, stability, density, viscosity of ethylene glycol-based ternary hybrid nanofluids: Experimental investigations and model -prediction using modern machine learning techniques, Powder Technol 400 (2022) 117190. https://doi.org/10.1016/J.POWTEC.2022.117190.
[128] S. Mbiankeu Nguea, Uncovering the linkage between sustainable development goals for access to electricity and access to safely managed drinking water and sanitation services, Soc Sci Med 345 (2024) 116687. https://doi.org/10.1016/J.SOCSCIMED.2024.116687.
[129] E. Aivazidou, N. Tsolakis, E. Iakovou, D. Vlachos, The emerging role of water footprint in supply chain management: A critical literature synthesis and a hierarchical decision-making framework, J Clean Prod 137 (2016) 1018–1037.
[130] L. Lamastra, N.A. Suciu, E. Novelli, M. Trevisan, A new approach to assessing the water footprint of wine: An Italian case study, Science of the Total Environment 490 (2014) 748–756.
[131] G. Pellegrini, C. Ingrao, S. Camposeo, C. Tricase, F. Conto, D. Huisingh, Application of water footprint to olive growing systems in the Apulia region: a comparative assessment, J Clean Prod 112 (2016) 2407–2418.
[132] C. Salvador, R. Nieto, S.M. Vicente-Serrano, R. García-Herrera, L. Gimeno, A.M. Vicedo-Cabrera, Public health implications of drought in a climate change context: a critical review, Annu Rev Public Health 44 (2023) 213–232.
[133] G.E. Eckstein, Water scarcity, conflict, and security in a climate change world: challenges and opportunities for international law and policy, Wis. Int'l LJ 27 (2009) 409.
[134] A. Mahato, S. Upadhyay, D. Sharma, Global water scarcity due to climate change and its conservation strategies with special reference to India: a review., Plant Archives (09725210) 22 (2022).
[135] B. Menin, Innovative Technologies for Large-Scale Water Production in Arid Regions: Strategies for Sustainable Development, Journal of Applied Mathematics and Physics 12 (2024) 2506–2558.
[136] A. Subramani, J.G. Jacangelo, Emerging desalination technologies for water treatment: a critical review, Water Res 75 (2015) 164–187.
[137] S.A. Kalogirou, Seawater desalination using renewable energy sources, Prog Energy Combust Sci 31 (2005) 242–281.
[138] J. Khan, M.H. Arsalan, Solar power technologies for sustainable electricity generation–A review, Renewable and Sustainable Energy Reviews 55 (2016) 414–425.

[139] M.A.M. Khan, S. Rehman, F.A. Al-Sulaiman, A hybrid renewable energy system as a potential energy source for water desalination using reverse osmosis: A review, Renewable and Sustainable Energy Reviews 97 (2018) 456–477.
[140] A. Samuel, J. Brizuela, K.-C. Chang, C.-T. Lin, Design and Investigation of an Effective Solar Still Applicable to Remote Islands, Water (Basel) 14 (2022) 703.
[141] J. Wiener, M.Z. Khan, K. Shah, Performance enhancement of the solar still using textiles and polyurethane rollers, Sci Rep 14 (2024) 5202.
[142] A.M. Tayeb, Performance study of some designs of solar stills, Energy Convers Manag 33 (1992) 889–898.
[143] A.E. Kabeel, M. Elkelawy, H.A. El Din, A. Alghrubah, Investigation of exergy and yield of a passive solar water desalination system with a parabolic concentrator incorporated with latent heat storage medium, Energy Convers Manag 145 (2017) 10–19.
[144] P.K. Nagarajan, J. Subramani, S. Suyambazhahan, R. Sathyamurthy, Nanofluids for solar collector applications: a review, Energy Procedia 61 (2014) 2416–2434.
[145] G.S. Dhindsa, V. Kumar, M.K. Mittal, G.S. Sokhal, N. Khalilpoor, M. Sharifpur, A. Issakhov, R. Tonk, Performance comparison of single-slope solar still loaded with various nanofluids, Energy Sci Eng 10 (2022) 4318–4331.
[146] C.M. Rahman, T.A. Rashid, Dragonfly algorithm and its applications in applied science survey, Comput Intell Neurosci 2019 (2019) 9293617.
[147] A. Bilal, A. Alkhathlan, F.A. Kateb, A. Tahir, M. Shafiq, H. Long, A quantum-optimized approach for breast cancer detection using SqueezeNet-SVM, Sci Rep 15 (2025) 3254.
[148] M. Hentabli, A.-E. Belhadj, F. Dahmoune, Dragonfly support vector machine modelling of the adsorption phenomenon of certain phenols by activated carbon fibres, Kemija u Industriji: Časopis Kemičara i Kemijskih Inženjera Hrvatske 70 (2021) 501–508.
[149] Y. Meraihi, A. Ramdane-Cherif, D. Acheli, M. Mahseur, Dragonfly algorithm: a comprehensive review and applications, Neural Comput Appl 32 (2020) 16625–16646.
[150] A. Bilal, A. Alkhathlan, F.A. Kateb, A. Tahir, M. Shafiq, H. Long, A quantum-optimized approach for breast cancer detection using SqueezeNet-SVM, Sci Rep 15 (2025) 3254.
[151] J. Zhao, D. Zhang, Q. He, L. Li, A hybrid-strategy-improved dragonfly algorithm for the parameter identification of an SDM, Sustainability 15 (2023) 11791.
[152] R. Sathyamurthy, A.E. Kabeel, E.S. El-Agouz, Ds. Rufus, H. Panchal, T. Arunkumar, A.M. Manokar, D.G.P. Winston, Experimental investigation on the effect of MgO and TiO2 nanoparticles in stepped solar still, Int J Energy Res 43 (2019) 3295–3305. https://doi.org/10.1002/ER.4460.
[153] R. Khelifi, T. Chekifi, A. Belaid, M. Guermoui, A. Rabehi, F. Khaled, M. Adouane, A. Al-Qattan, T.F. Agajie, Comparative performance analysis of hemispherical solar stills using date and olive kernels as heat storage material, Scientific Reports 2025 15:1 15 (2025) 1–15. https://doi.org/10.1038/s41598-025-87448-z.
[154] N. Sailash, T.S.-E.W. of Conferences, undefined 2024, Comparative Performance Analysis of Novel Single-Slope Conventional Solar Still and Solar Still with ZnO Water Nanofluids through Experimental Investigation, E3s-Conferences.Org (n.d.). https://www.e3s-conferences.org/articles/e3sconf/abs/2024/21/e3sconf_icecs2024_01024/e3sconf_icecs2024_01024.html (accessed March 20, 2025).
[155] M.A.E.R. Abu-Zeid, Y. Elhenawy, M. Toderaș, M. Bassyouni, T. Majozi, O.A. Al-Qabandi, S.S. Kishk, Performance Enhancement of Solar Still Unit Using v-Corrugated Basin, Internal Reflecting Mirror, Flat-Plate Solar Collector and Nanofluids, Sustainability 2024, Vol. 16, Page 655 16 (2024) 655. https://doi.org/10.3390/SU16020655.

[156] S.W. Sharshir, G. Peng, A.H. Elsheikh, E.M.A. Edreis, M.A. Eltawil, T. Abdelhamid, A.E. Kabeel, J. Zang, N. Yang, Energy and exergy analysis of solar stills with micro/nano particles: A comparative study, Energy Convers Manag 177 (2018) 363–375. https://doi.org/10.1016/J.ENCONMAN.2018.09.074.

[157] S. Sharshir, G. Peng, A. Elsheikh, … E.E.-E. conversion and, undefined 2018, Energy and exergy analysis of solar stills with micro/nano particles: a comparative study, Elsevier (n.d.). https://www.sciencedirect.com/science/article/pii/S019689041831077X (accessed March 20, 2025).

[158] A. Sohani, S. Hoseinzadeh, S. Samiezadeh, I. Verhaert, Machine learning prediction approach for dynamic performance modeling of an enhanced solar still desalination system, J Therm Anal Calorim 147 (2022) 3919–3930. https://doi.org/10.1007/S10973-021-10744-Z/METRICS.

[159] M. Bahiraei, S. Nazari, H. Moayedi, H. Safarzadeh, Using neural network optimized by imperialist competition method and genetic algorithm to predict water productivity of a nanofluid-based solar still equipped with thermoelectric modules, Powder Technol 366 (2020) 571–586. https://doi.org/10.1016/J.POWTEC.2020.02.055.

[160] M. Bahiraei, S. Nazari, H. Safarzadeh, Modeling of energy efficiency for a solar still fitted with thermoelectric modules by ANFIS and PSO-enhanced neural network: A nanofluid application, Powder Technol 385 (2021) 185–198. https://doi.org/10.1016/J.POWTEC.2021.03.001.

[161] Y. Wang, A.W. Kandeal, A. Swidan, S.W. Sharshir, G.B. Abdelaziz, M.A. Halim, A.E. Kabeel, N. Yang, Prediction of tubular solar still performance by machine learning integrated with Bayesian optimization algorithm, Appl Therm Eng 184 (2021) 116233. https://doi.org/10.1016/J.APPLTHERMALENG.2020.116233.

[162] A.F. Mashaly, A.A. Alazba, Comparative investigation of artificial neural network learning algorithms for modeling solar still production, Journal of Water Reuse and Desalination 5 (2015) 480–493. https://doi.org/10.2166/WRD.2015.009.

[163] Y. Wang, A.W. Kandeal, A. Swidan, S.W. Sharshir, G.B. Abdelaziz, M.A. Halim, A.E. Kabeel, N. Yang, Prediction of tubular solar still performance by machine learning integrated with Bayesian optimization algorithm, Appl Therm Eng 184 (2021) 116233. https://doi.org/10.1016/J.APPLTHERMALENG.2020.116233.

[164] A.F. Mashaly, A.A. Alazba, Comparative investigation of artificial neural network learning algorithms for modeling solar still production, Journal of Water Reuse and Desalination 5 (2015) 480–493. https://doi.org/10.2166/WRD.2015.009.

[165] S. Nazari, M. Bahiraei, H. Moayedi, H. Safarzadeh, A proper model to predict energy efficiency, exergy efficiency, and water productivity of a solar still via optimized neural network, J Clean Prod 277 (2020) 123232. https://doi.org/10.1016/J.JCLEPRO.2020.123232.

[166] S. Nazari, M. Bahiraei, H. Moayedi, H. Safarzadeh, A proper model to predict energy efficiency, exergy efficiency, and water productivity of a solar still via optimized neural network, J Clean Prod 277 (2020) 123232. https://doi.org/10.1016/J.JCLEPRO.2020.123232.

[167] A. Sohani, S. Hoseinzadeh, S. Samiezadeh, I. Verhaert, Machine learning prediction approach for dynamic performance modeling of an enhanced solar still desalination system, J Therm Anal Calorim 147 (2022) 3919–3930. https://doi.org/10.1007/S10973-021-10744-Z/METRICS.